UNIVERSITY OF CALFORNIA SAN DIEGO

Transparent polycrystalline Er and Er, Cr co-doped Al_2O_3 as potential gain media for lasers with an eye safe,1.5 μm emission

A dissertation submitted in partial satisfaction of the requirements for the degree of

Doctor of Philosophy

in

Material Science and Engineering

by

Matthew Adalberto Duarte

Dissertation Committee:

Professor Javier E. Garay, Chairperson

Professor Renkun Chen

Professor Olivia Graeve

Professor Jian Luo

Professor Vitali Nesterenko

2020

The dissertation of Matthew Adalberto Duarte is approved, and it is acceptable in quality and form for publication on microfilm and electronically:

_____

_____

_____

_____

_____

Chair

University of California San Diego

2020

Table of Contents

List of Figures

Chapter 1. Introduction and Motivation

Chapter 2. Previous Work on Erbium and Er co-doped Gain Media

List of Tables

Acknowledgements

There are numerous people I would like to give my thanks and appreciation for during this chapter of my life.

I would like to thank my advisor, Professor Javier Garay, for allowing me to work in his lab as an undergraduate and then continue to the end of my graduate studies. It was an experience to be a part of his lab, I have learned so much throughout my time here. I am grateful to him for the opportunity to work and the patience he displayed to me while teaching material science.

I would also like to thank Dr. Yasuhiro Kodera for his mentorship he provided to me since the days of undergrad. We have worked together so many times during my master's studies and for that I am truly grateful. You indirectly taught me a new level of patience from the beginning because every time we had a discussion; it always started off with long stories and I never interrupted you. Your contributions to our culinary discussions as well were appreciated.

Special thanks go to Professor Vitali Nesterenko, Professor Jian Luo, Professor Renkun Chen and Professor Olivia Graeve for serving on my committee.

The help of my undergraduate researchers, Jed Tadios, Kevin Tan, Kelli Iwamoto, Jonathon Lee, Christian Nino, Richard Escadeja and Alyysa Penamora, in assisting in the assigned tasks and letting me bounce ideas off all of you was invaluable.

To my close friends that stuck with me through this adventure, Dr. Elias Penilla, you have mentored me and given me various opportunities to advance myself inside and out of work. I enjoyed working alongside you and hope to further

our friendship. Nicholas Adame, you made my time in San Diego much more pleasant, I will always enjoy our daily banter and lunches. Daniel Quach, your knowledge on San Diego's past and present was always fun to listen to, our food hangouts were also enjoyable. Lastly, Sahan Ranawera and Hasandeep Saini, I appreciated all the good times we had, those are the moments I will never forget.

Also, without the many knowledgeable members of AMPS Lab, the completion of my research and studies would not have been possible. There are far too many people in this lab to mention individually that have truly helped me, you all know who you are, I appreciate all your insight.

I also want to thank my father for supporting me the best way he could and not questioning my career path. And a final thanks to my brothers, Richard, and Dennis for also supporting me and being there for the family during my absence at home. Without the love and support from my family, I would not have been the best version of myself as a scholar and more importantly, as a man. I want to thank Shannon Lutterloh, Cesar Ordaz, Ruben Ordaz and Javier Reyes for the support during the end stages of my work, your help was vital.

Lastly, I would like to dedicate this work to my mother, Irene Duarte and my loving girlfriend, Brenda 'Babu' Ordaz. To my mother, I am thankful for her unconditional support throughout my academic career. To my babu, I am thankful to her because despite the years and long distance away from home, she stuck with me and accepted this unrealistic lifestyle. She also encouraged me and never let me stray from the path I chose to follow. I will always greatly appreciate the strong woman in my life.

We gratefully acknowledge the funding of this work by a multidisciplinary research initiative (MRI) from the High Energy Lasers – Joint Technology Office (HEL-JTO) administered by the Army Research Office.

Chapter 3, in part is currently being prepared for submission for publication of the material. Chapter 3 is coauthored with Elias Penilla, Matthew Wingert, Yasuhiro Kodera, and Javier Garay. The dissertation author was the primary investigator and author of this material.

Chapter 4, in part is unpublished material. Chapter 4 is coauthored with Elias Penilla, Matthew Wingert, Yasuhiro Kodera, and Javier Garay. The dissertation author was the primary investigator and author of this material.

Vita

2014 Bachelor of Science, University of California Riverside

2016 Master of Science, University of California Riverside

2020 Doctor of Philosophy, University of California San Diego

PUBLICATIONS

Penilla, E.H., Devia-Cruz, L.F., Duarte, M.A. *et al.* Gain in polycrystalline Nd-doped alumina: leveraging length scales to create a new class of high-energy, short pulse, tunable laser materials. *Light Sci Appl* **7,** 33 (2018).

Penilla, E., Sellappan, P., Duarte, M., Wieg, A., Wingert, M., & Garay, J. (2020). Bulk polycrystalline ceria–doped Al_2O_3 and YAG ceramics for high-power density laser-driven solid-state white lighting: Effects of crystallinity and extreme temperatures - CORRIGENDUM. *Journal of Materials Research, 35*(8), 1121-1122.

Abstract of the Dissertation

Transparent polycrystalline Er and Er, Cr co-doped Al_2O_3 as potential gain media for lasers with an eye safe, 1.5 μm emission

By

Matthew Adalberto Duarte

Doctor of Philosophy in Materials Science and Engineering

University of California San Diego, 2020

Professor Javier E. Garay, Chair

The development of solid-state lasers with emission in the eye safe region of 1.5 μm is interesting for scientific and industrial purposes including laser cutting/manufacturing, communications and surgery. In this work I present the processing and characterization of erbium ($Er:Al_2O_3$) and erbium, chromium co-doped ($Er:Cr:Al_2O_3$) bulk aluminum oxide for laser gain media applications. These new gain media have excellent thermomechanical properties and are promising for laser power scaling.

In the first portion of this dissertation **C**urrent **A**ctivated **P**ressure **A**ssisted **D**ensification (CAPAD) is implemented to process and consolidate transparent bulk polycrystalline $Er:Al_2O_3$ ceramics via a simultaneous solid-state mixing and densification route. The materials have high transparency at the emission wavelength, and absorption lines characteristic of Er^{3+}. Room temperature

photoluminescence reveal broad emission peaks in the expected range of ~ 1.5 μm corresponding to intra-4f transitions in Er^{3+}. The emission peaks are narrower at cryogenic temperatures (down to 10 K) revealing thermally broadened emission. In addition, ~ 1.5 μm emission has relatively long lifetimes that do not vary across a broad emission spectrum (1.5 - 1.6 μm), suggesting similar local environment of optically active Er ions responsible for the broad emission.

In the second portion of this dissertation, chromium ions are co-doped with erbium into the alumina matrix, as a sensitizer in order to increase the absorption cross-sections. The ~ 1.5 μm emission corresponding to Er^{3+} can be accessed through the broad and deep chromium absorption bands. The result is improved absorption and longer emission lifetimes compared to the singly doped Er alumina materials. The Cr:Er:Al_2O_3 is promising as a tunable near infrared laser gain material that can be pumped with 0.532 μm, a wavelength commonly used for pumping Ti:Sapphire, the most successful tunable short pulsed laser. A common theme of this work is the interplay between material processing, the material properties, and the development of optical devices using bulk polycrystalline transparent ceramics.

Chapter 1. Introduction and Motivation

1.1. Motivation

The development of erbium (Er) doped gain media has been extensively studied over the last few decades because of the many benefits of light sources in the 1.5 – 1.6 μm range. Light emission in this wavelength range is less harmful to the eye and thus considered 'eye-safe'. In addition, this region of the near IR is extraordinarily important in communications [1], medical applications [2] and industrial [3] applications such as laser cutting and welding. The most commercially successful Er host materials have been Er doped fibers/glasses [3, 4] and single crystal hosts such as yttrium aluminum garnet (YAG) [5]. In order to satisfy the ever-increasing need for high-power solid-state lasers, there has also been considerable interest in Er doped ceramic media because ceramics have benefits for dimension scaling and mechanical properties [6 - 10].

Development of ceramic gain media has emerged as an active research area because of the numerous advantages of ceramics over single crystals. First, polycrystalline ceramics can be produced in large volumes, which makes them attractive for high power laser generation. Second, they can made into composite laser media with complicated structures that would otherwise be difficult to fabricate using single crystals. Third, ceramics can be heavily and homogeneously doped with laser-active ions when compared with single crystals. Furthermore, the use of ceramics enables mass production, which may lead to low cost commercial production of lasers or the production of lasers with customized special functions.

A particularly interesting gain media is rare earth (RE) doped α-Al_2O_3 (corundum) because it has significantly higher thermal conductivity and fracture strength than stat of the art gain media and can thus can potentially be used to significantly increase laser power [8,11,12]. Despite the benefits there are steep challenges to achieving high quality Er doped alumina. There are two main challenges. First, alumina is birefringent which causes scattering loss in polycrystalline materials with randomly oriented grains. Second, the low Er solubility of alumina makes it difficult to achieving dopant levels sufficient for lasing. In this dissertation, I present a processing method that can successfully achieve high transparency in Er and Er co-doped alumina. In addition, I present the optical property characterization in order to demonstrates the materials' promise as laser gain materials.

1.2. Overview of the Dissertation

This dissertation is structured into 5 chapters. Chapter one presents the background and gives the motivation of this study. Chapters two is dedicated to the background and properties of erbium doped media and chromium-erbium co-doped media. Chapter three and four are dedicated to experimental method, results and discussions on erbium doped Al_2O_3 and co-doped Al_2O_3, with an emphasis to understand the spectroscopy to further develop a functional solid state laser. Chapter five summarizes and concludes the entire work and presents some suggestions on improving the experimental method and also future directions.

1.3. Introduction to Laser Gain Media

There are many types of lasers, but the four that have had the most commercial success are: gas, dye, semiconductor and solid-state lasers. Fiber lasers are an important sub-class of solid-state lasers. In this section, the characteristics of each type will be briefly described, with the main focus being on solid-state lasers.

Gas Lasers use a gas or a mixture of gases within a tube as gain media. The most common gas laser uses a mixture of helium and neon (HeNe), with a primary output of 632.8 nm. It was first developed in 1961 and has proved to be the forerunner of a whole family of gas lasers. They function by applying an electric current which is discharged through a gas to produce coherent light [13].

Dye Lasers use a laser medium that is usually a complex organic dye in liquid solution or suspension. The most striking feature of these lasers is their “tunability.” Proper choice of the dye and its concentration allows the production of laser light over a broad range of wavelengths in or near the visible spectrum. Dye lasers commonly employ optical pumping although some types have used chemical reaction pumping. The most commonly used dye is Rhodamine 6G which provides tunability over 200 nm bandwidth in the red portion (620 nm) of the spectrum [14].

Semiconductor Lasers (often referred to as diode lasers) are not to be confused with solid state lasers. Semiconductor devices consist of two layers of semiconductor material sandwiched together. Light is generated by flowing the forward electrical current to this p-n junction. These lasers are generally very small physically, and individually of only modest power. However, they may be built into

larger arrays that together can deliver very large powers. One of the most common diode lasers is the Gallium Arsenide diode laser with a central emission of 840 nm [15]. Another popular diode laser wavelength is 970 – 980 nm. These have become extremely useful as pump sources for emission at ~ 1500 nm, a commonly used telecommunication wavelength.

The main components of solid-state lasers are the gain media, a pump source and various cavities depending of the design the laser.

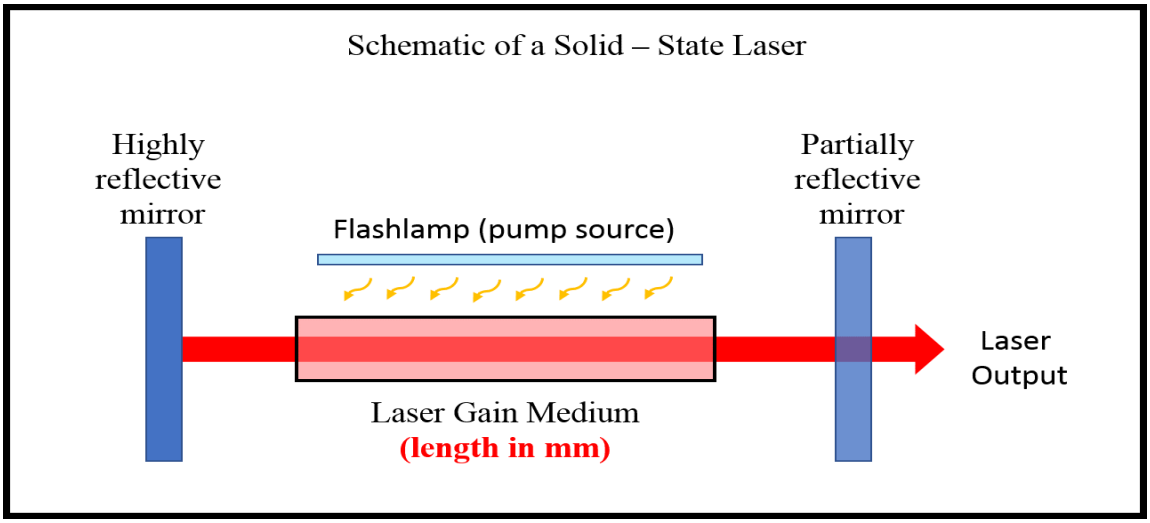

Figure 1.1. Basic schematic of a solid-state laser design.

One very common solid-state laser design involves a set of two mirrors that form an optical cavity in which light from the gain medium can resonate, as shown schematically in Figure 1.1. The gain medium is typically an inorganic solid that serves as a host for optically active dopant ions. Many different gain media geometries are used including, rods and slabs. The sub-class of fiber lasers uses long glass fibers as the gain media.

The pump source is often a flash lamp or a laser diode that when absorbed by active ions in the laser gain media, excites electrons in the active ions to an energy state above their ground state. A population inversion, which is necessary for lasing, occurs when more electrons in the active ions have been excited than those remaining at the ground state [16]. When these excited electrons return to their ground state, they emit photons either by spontaneous emission or stimulated emission. In addition to the desired light emission, the process also involved heat generation which is essentially waste heat that must be managed.

The absorption-emission process depends on the active dopant and usually occurs through either a three or four level process as described schematically in Figure 1.2.

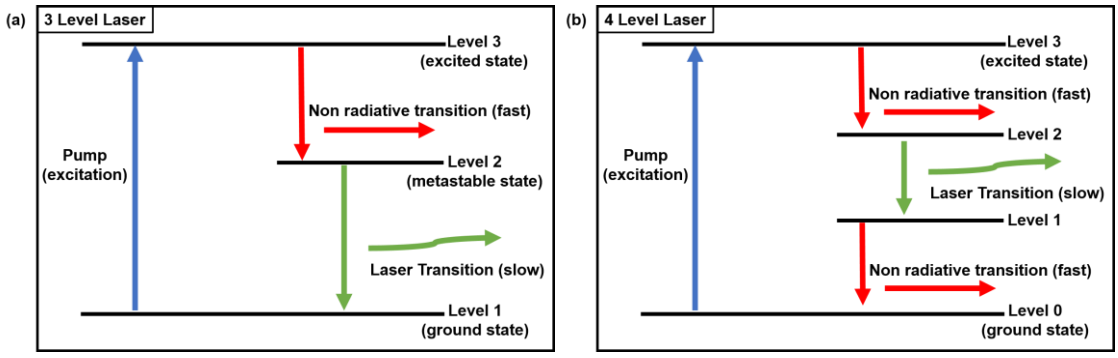

Figure 1.2. Schematic energy levels and transitions for (a) a 3 level laser process and (b) a 4 level laser process.

In a three-level system, the laser transition ends on the ground state. The unpumped gain medium exhibits strong absorption on the laser transition
A population inversion and consequently net gain result only when more than half of the ions are pumped into the upper laser level; the threshold pump power is thus relatively high compared to a 4-level system as discussion below.

A lower threshold pump power can be achieved with a four-level laser medium, where the lower laser level is well above the ground state and is quickly depopulated e.g. by multi-phonon transitions. Ideally, no appreciable population density in the lower laser level can occur even during laser operation. In that way, reabsorption of the laser radiation is avoided (provided that there is no absorption on other transitions). This means that there is no absorption of the gain medium in the unpumped state, and the gain usually rises linearly with the absorbed pump power.

1.4. State of the art Polycrystalline Solid-State Laser Gain Media

Currently, rare-earth (RE) element-doped YAG, ($Y_3Al_5O_{12}$), is still the most extensively studied and widely used ceramic for lasers [17]. Ikesue and Aung [18] have reviewed the progress of polycrystalline Nd:YAG ceramic for laser application. Advanced processing has led to ceramics with an almost pore-free microstructure. The optical quality of the pore-free polycrystalline Nd- and Yb-doped ceramics was extremely high leading to laser conversion efficiency, the so-called slope efficiency were comparable with that of high quality commercial Nd:YAG single crystals, as shown in Figure 1.3.

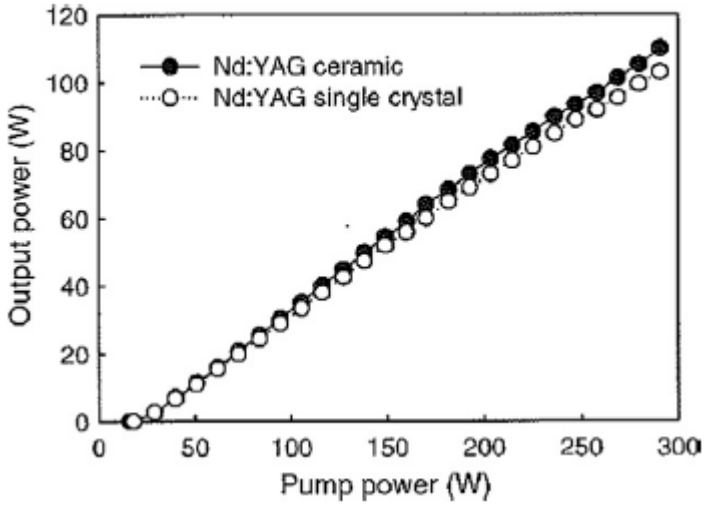

Figure 1.3. Input–output curve of ceramic and single crystal 0.6% Nd^{3+}-doped YAG rod lasers. This compares the effectiveness of the ceramic alongside the single crystal. [19]

Nd:YAG is an extremely successful gain media, but it does have limitations. Recent studies indicated that YAG is not the best host material for high power laser systems due to its relatively low thermal conductivity and high thermal expansion coefficient. One method of comparing the thermal loading tolerance of different materials has been described by Koechner [20], where the amount of power deliverable by a laser scales directly with thermal conductivity κ, and the fracture stress σ_F and is represented by the thermal shock figure of:

$$R_s = \frac{k(1-v)}{\alpha E} * \sigma_f \qquad \text{(Eq.1.1)}$$

where, κ is the thermal conductivity, v is the Poisson's ratio, α is the thermal expansion coefficient, E is the elastic modulus, and σ_F is the fracture stress. The result is a laser gain medium with a thermo-mechanical figure of merit of Rs~800 W/m for Nd:YAG [12].

Sesquioxides, such as Sc_2O_3,Y_2O_3, and Lu_2O_3, have been shown to be very promising host materials for high power laser applications, mainly due to their high thermal conductivity and high absorption and emission cross-sections of trivalent RE ions [21]. Alumina that is discussed in detail in Chapter 1.5 has also been considered. The advantages of Al_2O_3 as an optical gain media over state of the art gain materials such as YAG, sesquioxides and laser glasses are significant; it has higher thermal conductivity, chemical inertness and higher mechanical toughness, all attributes that could lead to more stable, more powerful lasers.

1.5. Alumina as a Solid-State Laser Gain Medium

Alumina has a long history as a gain medium. In 1960, Theordore Maiman of Hughes Research Laboratories produced the world's 1st laser ever using crystal ruby as a gain medium. Ruby, a α-Al_2O_3 single crystal doped with chromium ions, Cr^{3+}, doped in at a typical concentration of ~0.05 – 0.35% by weight [22]. α-Al_2O_3, single crystals doped with Ti (Ti:Sapphire) is another extremely successful gain medium. In fact, Ti:Sapphire based lasers are perhaps the most pervasive short pulsed, tunable lasers today.

The crystal structure of α-Al_2O_3, the corundum structure, consists of close packed planes (A and B planes) of large oxygen anions (radius 0.14 nm) stacked in the sequence, shown in Figure 1.4. The aluminum cations (radius 0.053 nm) have valence of +3 and oxygen anions have valence of –2 so that there are two Al^{3+} ions for every three O^{2-} ions to maintain electrical neutrality [23].

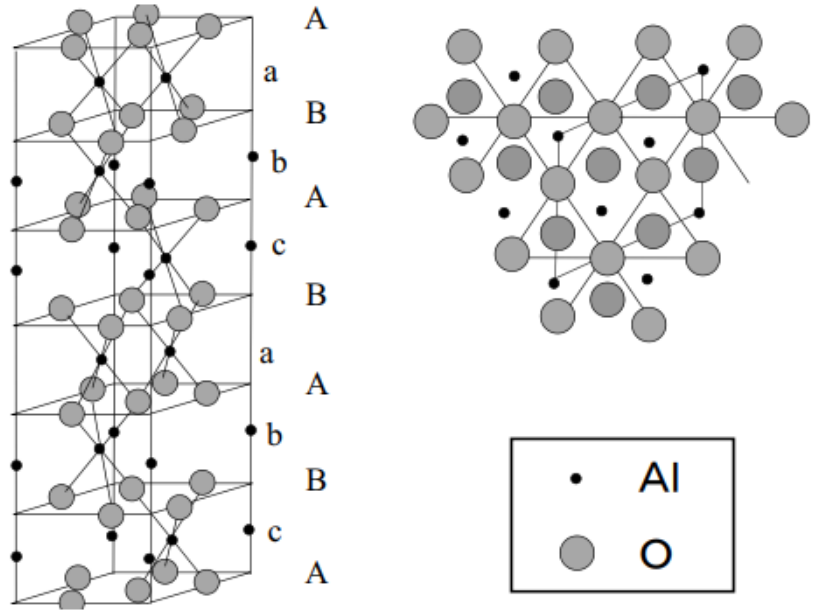

Figure 1.4. Corundum structure of α-Al_2O_3 [Figure from reference 23].

Thus, the cations occupy only two-thirds of the octahedral sites of the basic array. This placement forms three different types of aluminum cation layers, named a, b, and c stacked between the anion layers as shown in Figure 1.4.

The radius of Cr^{3+} ions (0.064 nm) and ti3+ ions (0.069 nm), the optically active dopants in ruby and Ti:Sapphire are similar to Al^{3+} so that there is a wide range of solubility of these ions in the α-Al_2O_3 lattice. On the other hand, when considering using Al_2O_3 as a host material for rare earth ions, we have to consider the significant ionic radius mismatch between the rare earth ions and the aluminum ion; (Er is ~ 1.8 times larger than). Thus, rare earth elements exhibit very low solubility within the crystal structure. This solubility is too low for efficient lasing as discussed in Chapter 1.X. Another major obstacle arises due to uniaxial crystal structure α-Al_2O_3. Because of birefringence, laser quality transparency was believed

to be unachievable in polycrystalline α-Al_2O_3 unless some technique of ceramic grain alignment, like magnetic alignment [8], is used. To overcome these processing challenges, our group used a non-equilibrium processing technique called CAPAD.

The processing method called ***C***urrent ***A***ctivated ***P***ressure ***A***ssisted ***D***ensification (CAPAD), commonly known as Spark Plasma Sintering, (SPS), has been implemented to process and consolidate transparent bulk polycrystalline Al_2O_3 ceramics. CAPAD has emerged as a versatile powder consolidation method. This materials processing method involves the use of large electric currents and high pressures to densify materials more quickly and at lower temperatures than conventional sintering [24]. A considerable number of materials have already been processed using the CAPAD technique [25]. This process is particularly exceptional at producing nanocrystalline ceramics [26]. Fully dense materials with grain sizes less than 20nm are even possible using this technique [27]. This capability of creating a fully dense ceramic with relatively nanocrystalline grains is imperative for Al_2O_3. In Figure 1.2, an undoped Al_2O_3 is displayed as a representation of the level of transparency that can be achieved from the CAPAD process.

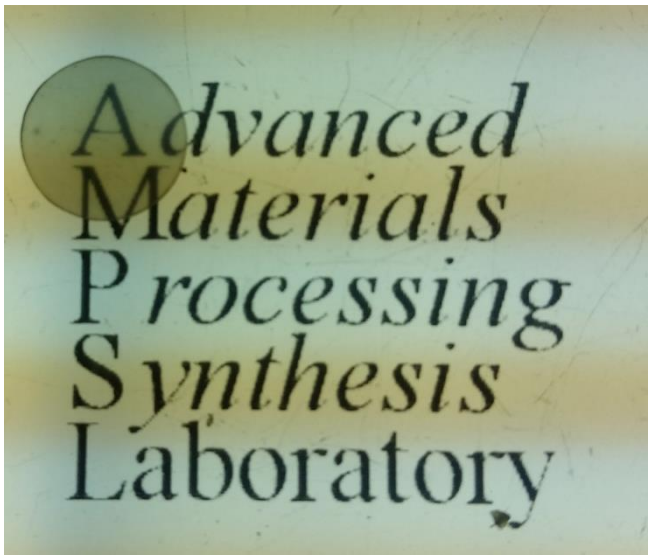

Figure 1.5. Backlit image of undoped Al_2O_3 after CAPAD processing.

Penilla et al [11] presented a method to successfully incorporate Tb^{3+} ions up to a concentration of 0.5 at% into a dense alumina matrix, achieving a transparent light-emitting ceramic. They used sub-micrometer alumina and nanometric RE oxide powders are simultaneously densified and reacted using current-activated, pressure-assisted densification (CAPAD). These doped ceramics have a high transmission. They also display PL characteristic of Tb^{3+} emission that are centered in the visible at 485 nm and 543 nm. Additionally, the luminescent lifetimes are long and compare favorably with lifetimes of other laser ceramics.

In subsequent work, we used reaction/densification in CAPAD to produce Nd doped alumina [12]. We presented the first bulk polycrystalline Nd:Al_2O_3 ceramics that exhibit stimulated emission and optical gain. Importantly, we demonstrate that gain can be achieved without single sight doping, *i.e.,* with some Nd segregated to the grain boundaries.

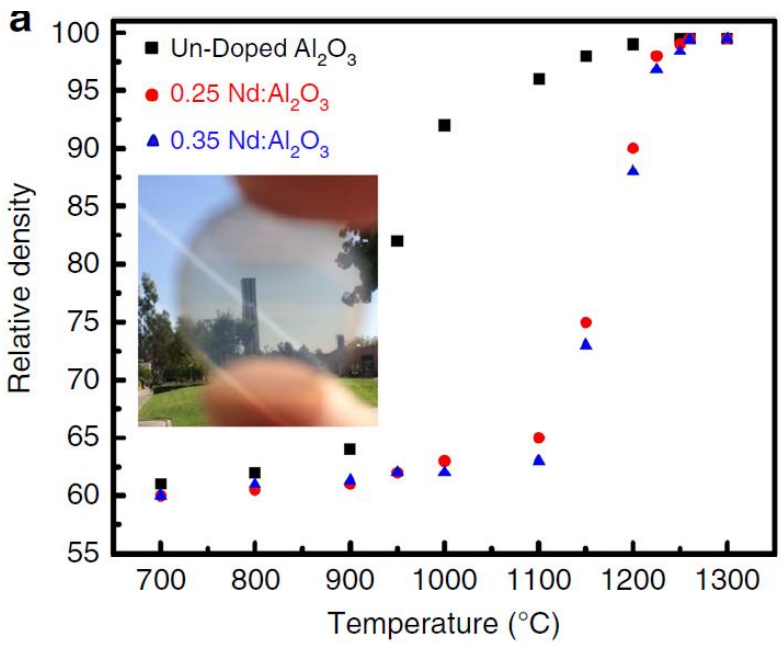

Figure 1.6. Physical and microstructural characterization of Nd:Al_2O_3 (a) the effect of CAPAD temperature on the relative density of un-doped and samples doped with 0.25 and 0.35 at.% Nd [12].

We demonstrated the effects of processing temperature on the relatively density of the Nd:Al_2O_3 ceramic as shown in Figure 1.6. As expected, the density of the ceramics increases with temperature. A cross play with processing temperatures, dopant concentrations and various other factors lead to fabricating a transparent bulk ceramic as seen in the inset of Figure 1.6.

1.6. Important Gain Material Properties and Parameters

Photoluminescence (PL) and PL Measurements of Optically Active Materials

Photoluminescence (PL) measurements are essential for characterizing the light emission properties of luminescent materials. In a PL measurement, a sample is exposed to radiation in the form of light, often in the ultra-violet (UV), visible spectrum or near infrared (near-IR). This radiation causes electrons in the sample to enter an excited state, as described in Figure 1.2. When the atoms return to a lower energy

state, they emit radiation, which is measured by a detector, as shown in Figure 1.7. The emitted radiation contains a lot of information about the electronic structure of the sample. Photoluminescence properties, including emission spectra, excitation spectra, emission intensity, absorption, quantum efficiency, and thermal quenching, are significantly influenced by the composition of the host lattice, the dopant ions and their concentrations. PL properties can also be significantly affected by impurities and other defect in the materials such as vacancies and groups of point defects.

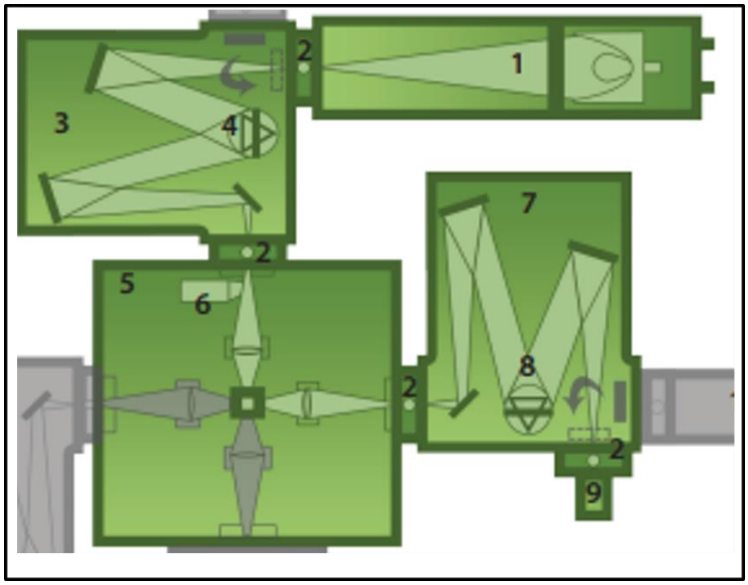

Figure 1.7. Photoluminescence experimental setup used, schematic from HORIBA.

Radiative transitions are defined as energy relaxation through the emission of photons whereas non-radiative transition occur through phonon processes. Since phonon energies are lower than electron energies, typically multiple phonons are involved in the relaxation process. Energy relaxation through phonon processes are often called ‘vibrational’ processes and energy levels that have similar energies are said to be in vibrational contact since they can be bridged by phonon.

Figure 1.8 is a simplified energy diagrams called a Jablonski diagram, depicting the radiative and non-radiative transitions that lead to the observation of photoluminescence.

When absorption of light occurs, an electron is promoted within 10^{-14}–10^{-15} seconds from the ground electronic state to an excited state. A variety of non-radiative and radiative processes occur following the absorption of light leading to the observation of emission of light.

Excitation usually occurs to a higher vibrational level of the intended excited state (E_2 according the Figure 1.8). Excited electrons then relax rapidly to the lowest vibrational level of the excited electronic state [28]. This non-radiative process is often called vibrational relaxation. Vibrational relaxation involves the relaxation of an excited-vibrational state to less energetic vibrational modes through the transfer of vibrational energy, typically in the form of heat. Vibrational relaxation processes occur within 10^{-14}–10^{-12} seconds, a time much shorter than typical luminescence lifetimes.

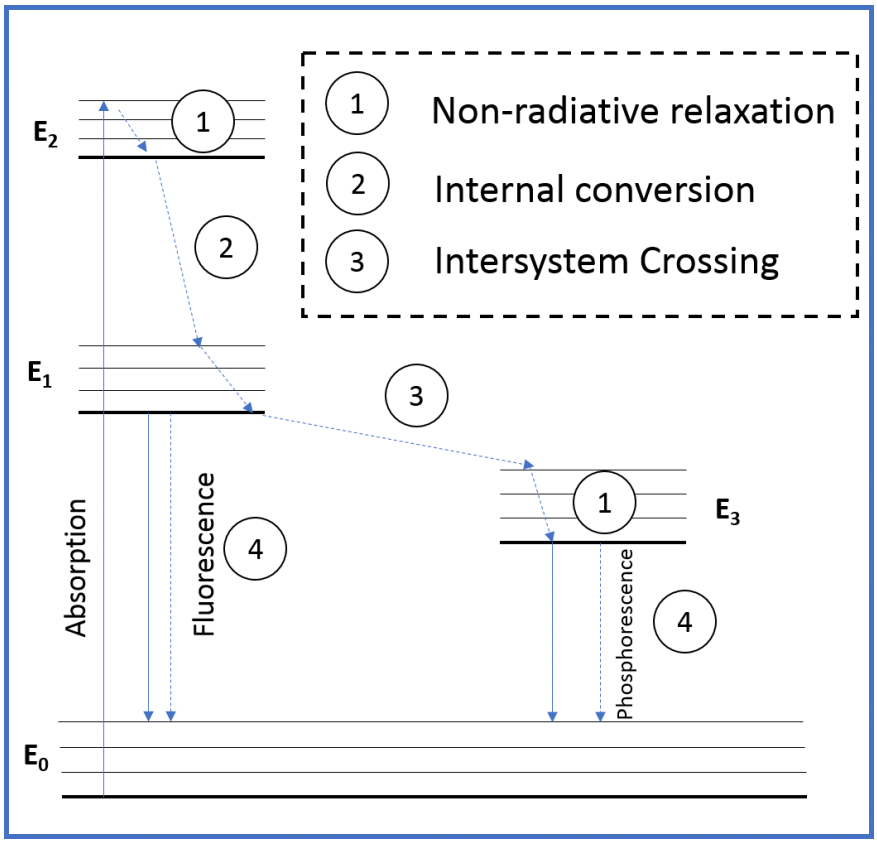

Figure 1.8. The Jablonski diagram. It illustrates the electronic states of an ion and the transitions between them [28].

If the electron is excited to a higher-energy excited state than E_1, a rapid non-radiative relaxation usually occurs to the lowest-energy singlet excited state (E_1). Relaxation processes between electronic states of like spin multiplicity such as E_1 and E_2 are called 'internal conversion'. These processes normally occur on a time scale of 10^{-12} s [28]. Non-radiative relaxation processes between different excited states are not limited to states with the same spin multiplicity. A process in which relaxation proceeds between excited states of different spin multiplicity is called 'intersystem crossing'. The relaxation from E_1 to E_3 in Figure 1.8, is an example of an intersystem crossing. Because of the lower probability for intersystem crossing

processes they occur more slowly (~10^{-8} s) than internal conversions [28]. The aforementioned non-radiative processes occur very rapidly and only release very small amounts of energy. The rest of the stored energy will be dissipated either radiatively, by emission of photons or non-radiatively, by the release of thermal energy.

Fluorescence refers to the emission of light associated with a radiative transition from an excited electronic state that has the same spin multiplicity as the ground electronic state. Fluorescence is depicted by the radiative transition $E_1 \rightarrow E_0$ in Figure 1.8. Since fluorescence transitions are spin-allowed, they occur very rapidly and the average lifetimes of the excited states responsible for fluorescence are typically <10^{-6} s [28].

Electronic transitions between states of different spin multiplicity are 'spin-forbidden' which means that they are less probable than spin-allowed transitions. The factors that increase the probability of phosphorescence are the same factors discussed above that increase the probability of intersystem crossing. Therefore, if the triplet excited state is populated by intersystem crossing then luminescence might occur from the triplet state to the ground state [28].

Phosphorescence refers to the emission of light associated with a radiative transition from an excited electronic state that has a different spin multiplicity from that of the ground electronic state. Phosphorescence is depicted by the radiative transition $E_3 \rightarrow E_0$ in Figure 1.8. Since phosphorescence transitions are spin-forbidden, they occur slowly and the average lifetime of the excited states

responsible for phosphorescence typically range from 10^{-6} s to several seconds. Luminescence refers to both fluorescence and phosphorescence [28].

Luminescence usually quenches when the doping level exceeds a critical value. This is due to concentration quenching arising from energy transfer between dopants and/or re-absorption of the emitting light. Therefore, the precise control of the dopant concentration is essential for achieving high luminescence. The optimal concentration is usually lower than 1 atomic %, depending on the host material [29, 30] and dopant ion. However, adding the required amount of dopant can lead to the formation of inclusions deteriorating the transparency, making the preparation of transparent ceramics with luminescence properties challenging [31].

The ionic size of cations (dopants) has a great effect on the photoluminescence properties by changing the crystal-field strength and the repulsion effect on dopants. The shifts of emission spectra have been seen upon substitutions between alkaline-earth or rare earths [32]. Much of the study on the PL of the erbium and chromium ions in Al_2O_3 will be discussed in the later chapters.

Radiative Lifetimes

The radiative lifetime of an excited electronic state in a laser gain medium is the lifetime which would be obtained if radiative decay via spontaneous emission were the only mechanism for depopulating this state.

The dynamic behavior of a laser can be described with reasonable precision by a set of coupled rate equations. We describe the system in terms of multiple energy levels, but of prime importance are the excited upper energy level and the lower energy level.

Under pulsed excitation, the transient photoluminescence intensity yields the lifetime of nonequilibrium states. The intensity of the emission after excitation of the electrons declines exponentially over time. The time between the start of the emission and when its intensity decreases to 1/*e* of its initial value is called the radiative lifetime. This important parameter characterizes how an electronic level is depopulated and the dynamic mechanism of this excitation. [28]

To better understand the absorption-emission process, consider an atom or ion at a ground state "X" that absorbs light and is excited to a state "X*". If the ion has a single pathway for decay, we can write an equation:

$$X^* \rightarrow X + h\nu\ (photon) \qquad \text{(Eq. 1.2)}$$

This is a first-order process whose rate can be expressed mathematically as:

$$\int -\frac{d[X^*]}{dt} = \int k_f[X^*] \qquad \text{(Eq. 1.3)}$$

where k_f is the rate constant of the fluorescence decay). The reciprocal of k_f is called the fluorescence lifetime τ_f. Integration of (Eq.1.4) gives:

$$[X^*] = [X_o] \exp\left[-\frac{t}{\tau_f}\right] \qquad \text{(Eq. 1.4)}$$

Therefore, a plot of ln[X*] vs. time gives us a straight line with the slope of $1/\tau_f$. The value of the [X*] intensity is gathered from the measurements of the fluorescence. Lifetimes on the order of microseconds and longer (milliseconds, seconds) are normally indicative of phosphorescence, while fluorescence lifetimes are normally on the sub-microsecond level (nanoseconds, picoseconds etc) [28].

Cryogenic Measurements.

Cryogenic spectroscopy is important for laser development for two reasons. First, laser performance is very temperature dependent and often improves at low temperature. Thus, there have been many schemes introduced over the years for cryogenic cooling of lasers. Second, cryogenic cooling of laser gain media has been, and is, routinely used for sorting out energy level assignments of rare earth and transition metal ions. It is well known that broadened spectral absorption lines at or near room temperature become significantly narrower and more intense as temperature is lowered.

Properties of particular interest are the temperature dependence of the thermal conductivity, thermal expansion coefficient, Poisson's ratio and Young's modulus with temperature because those quantities determine the magnitude of the thermal gradient and the resulting stresses and strain in solid-state materials [34]. In turn, the thermooptic effect (dn/dT) of the gain medium, determines the effect that the thermal gradient has on the refractive index, n and therefore the laser beam quality.

The RE emission spectrum depends on the host media. The peaks and valleys in the spectra have different shapes based on the precise location of the Stark levels, the intensities of the transitions between the Stark levels. Studies have been made of the line-broadening mechanisms for Er^{3+} in crystals and glasses. Experimental investigations have sought to determine the relative importance of homogeneous and inhomogeneous broadening in RE-doped media, and the exact value of the homogeneous and inhomogeneous line widths of various host media.

The homogeneous line width of a transition is temperature dependent since the nonradiative transition rate, as governed by multi-phonon emission, is temperature dependent. At low temperatures, the phonon population is very small and the nonradiative transition rates are commensurately lower. Thus, the overall line broadening at low temperature arises mostly from inhomogeneous or Stark splitting of the line. As the temperature is increased, the line width increases along with its homogeneous component.

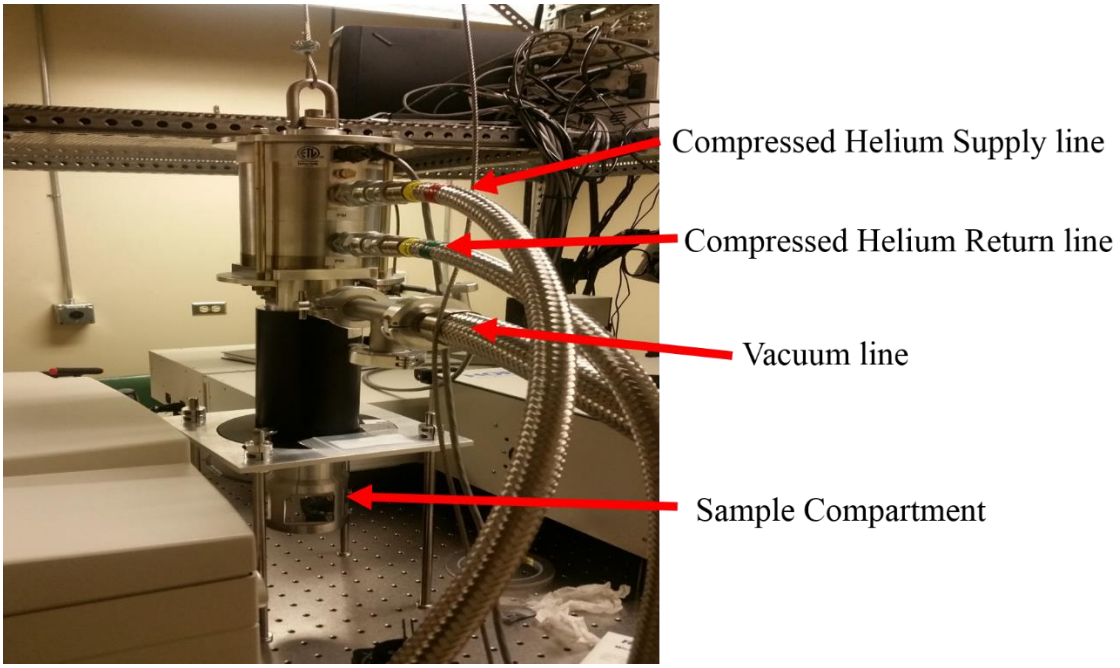

Figure 1.9. Cryostat set up. A closed-cycle helium cryostat from Advanced Research Systems, ARS-2HW, using a conductive cold finger.

Some of the reduction in lifetime with increasing temperature could be associated with an increased phonon induced radiative transition rate, but the rapid reduction in lifetime at high temperatures is characteristic of fluorescence quenching due to multi-phonon nonradiative decay [35].

Also, the non-radiative rate constant, k_f, decreases at lower temperatures. As the temperature T approaches absolute zero, τ_f approaches $1/k_f$. Therefore, the value of the fluorescence lifetime can be determined as $1/k_f$.

Our experimental setup for our cryogenic measurements is shown in Figure 1.9. Our spectrophotometer sample chamber was modified to integrate the closed-cycle helium cryostat from Advanced Research Systems, ARS-2HW, using a conductive cold finger where the sample is within a windowed housing that enabled measurements from 8 to 295 K. Briefly, we attached an optical breadboard onto the top of the sample chamber to provide additional mechanical support. A shaft collar was attached to the cryostat housing and then mounted onto the optical breadboard. With this design, vibrations due to helium pumping are significantly mitigated. It also improves the ability to adjust the angle of incidence for the sample.

Absorption and Emission Cross Sections

The optical gain is a parameter of great importance when designing a laser. It describes the fractional amplification of the light as it travels a certain distance in an active medium. It can be simply expressed as:

$$\gamma(\lambda) = N_2\sigma_{\mathrm{em}}(\lambda) - N_1\sigma_{\mathrm{abs}}(\lambda) \qquad \text{(Eq. 1.5)}$$

where $\gamma(\lambda)$ is the optical gain, N_1 and N_2 are the populations of the ground state and the excited state, respectively, σ_{em} and σ_{abs} are the stimulated emission and absorption cross sections. The cross section is a fundamental property of the atom in a particular environment and, in general terms is defined as a fictitious area within which the atom absorbs or emits electromagnetic field incident on it [36]. In (Eq. 1.5), the first term gives the amplification of light due to stimulated emission, and

the second one represents losses due to photons absorption. Stimulated emission and absorption of light are both induced processes, depending on the intensity of the incident radiation. The amount of light that can be amplified is directly related to the stimulated emission cross section of the particular atom or ion generating the emission [36].

Since there is a major advantage in knowing the cross sections in a given system, there are several theories available that allow cross section modeling. Ions with a large number of transitions for which absolute values of the absorption cross sections can be measured, can be further studied with the Judd-O'felt theory [37, 38]. This theory allows the prediction of the stimulated emission cross section peaks [39], [40] and integrated values for transitions between any levels. In the case of the REs, it assumes that the energy difference between the 4f and 5d levels is much larger than the energy spread of the 4f levels due to (L,S) coupling [41].

The main idea of the Judd-Ofelt theory is that the strength of any transition can be determined by a set of three parameters Ω_2, Ω_4 and Ω_6, that define the effect of the host on the radiative properties of the ion. These parameters are calculated by performing a least-square fit of the measured oscillator strengths to the theoretical ones, that contain the dependence on the reduced matrix elements U{2,4,6}. Once determined, they permit the calculation of the strength of any transition, and the integrated cross section [36]. The theory is limited to providing only transition intensities that have been extensively studied such as YAG crystals and various glass hosts. These parameters are not well studied for Al_2O_3 as a host crystal, the

oscillator strength between transitions isn't as available as YAG or other well studied material systems, therefore, use of this theory is limited for our work.

Another accepted theory is the McCumber theory [42] which generalizes the Einstein relations for broadband transitions, which are typical for rare earth ions in glassy or disordered environments. The theory shows that at any frequency, the absorption, spontaneous emission and stimulated emission spectra are uniquely related by simple relations. These relations are obtained in the context of narrow energy widths of the individual Stark levels and of thermal equilibrium between the impurity ions and the host [42]. It assumes that the width of the individual Stark level is small compared to k_BT (k_B is Boltzmann's constant and T is the temperature), and for ions in thermal equilibrium with the lattice, the two cross sections are connected by [42]:

$$\sigma_{em}(\nu) = \sigma_{abs}(\nu) \exp\left(\frac{\epsilon - h\nu}{k_B T}\right) \qquad \text{(Eq. 1.6)}$$

where ϵ is the excitation energy between the two levels. The theory of McCumber permits accurate calculations of one of the cross sections, when the other one is known from measurements. The McCumber relation connects the absorption cross section to the emission one at a particular wavelength. According to this, the absorption and emission cross section are uniquely related at any wavelength across the spectrum. This way, it provides absolute values, as well as spectral information. When the above conditions are not met, distortions from the actual value and spectral shape are seen. For the case of rare earth doped systems, the assumption that ions are in thermal equilibrium with the host holds very well, since the induced phonon

relaxations within a certain Stark manifold occur in a much shorter time than the lifetime of the manifold.

The other assumption however, regarding the narrow width of the individual Stark levels compared to k_BT, is doubted. We can obtain absorption cross section, σ_{abs} spectra by using the total RE concentration in the expression, $\sigma_{abs} = \alpha/N$, where σ_{abs} is the, α is the absorption coefficient, and N is the volumetric concentration of RE ions contributing to the absorption spectrum. The absorption coefficient was measured estimated using the transmission measurement and N was assumed to be the initially added concentration of RE. In order to not overestimate the absorption coefficient (and cross section values), we considered only absorption observable below the scattering envelope. Because of this underestimation of our absorption cross section measurements, the use of the McCumber Theory was not used.

Another accepted approach is based on the relationship between Einstein A and B coefficients, generalized for transitions with finite line width. This is the so called Einstein or Fuchtbauer-Ladenburg (FL) relation [36, 43-45], which relates the integrated absorption and the stimulated cross sections. In most general form, the FL relation can be written as [46]:

$$\sigma_{\mathrm{em}}(\lambda) = \frac{\eta\lambda^5 \mathrm{I}(\lambda)}{8\pi \mathrm{n}^2 \mathrm{c}\tau_{\mathrm{rad}} \int \lambda \mathrm{I}(\lambda)\mathrm{d}\lambda} \qquad \text{(Eq. 1.7)}$$

where σ_{em} is the emission cross section, η is the fluorescence quantum efficiency, λ is the fluorescence wavelength, $I(\lambda)$ is the fluorescence intensity, τ_{rad} is the radiative lifetime, n and c are the refractive index and the light velocity, respectively. In the literature however, there are various forms of the FL relation, but this is an exact relation and is a reliable way of determining the emission cross section from

fluorescence measurements for RE doped crystals. In integral form, the above relation can describe the emission cross section for transitions in host materials, between manifolds that are wide splitted by the crystal field of the host [37, 39],[47-51]. (Eq. 1.7) can lead to similar expressions allowing the stimulated emission cross section be calculated exactly in terms of the intensity of the fluorescence and the lifetime of the manifold [47, 52-57]. In these methods, the radiative lifetime of the manifold is assumed to be the same as the measured fluorescence lifetime, neglecting any other processes that may reduce the quantum efficiency of the transition.

In this study, analysis of the absorption cross section will be discussed from the transmission measurements taken of the ceramics. Analysis of the stimulated emission cross sections will be discussed using the FL theory, as seen in the later chapters, fluorescence and radiative lifetime measurements were taken and application of this theory was possible.

Sigma Tau product

The effective stimulated-emission cross section (σ_{em}) and radiative lifetime (τ_{rad}) are two important parameters for the assessment of a laser crystal. Knowledge of both σ_{em} and τ_{rad} is essential in evaluating laser system performance parameters such as saturation intensity and threshold pump power. For example, the threshold pump power is inversely proportional to the product of the effective emission cross section and the radiative lifetime of the lasing crystal [58, 59]. We can calculate the product $\sigma\tau$ at the peak lasing wavelength as determined by the measured emission

spectra of the differently doped media. If the emission cross section is calculated using F-L relation (Eq. 1.7) the product is given by:

$$\sigma_{em}\tau = \frac{\lambda^5 * I(\lambda)}{8\pi n^2 c * \int I(\lambda)\lambda d\lambda} \quad \text{(Eq. 1.8)}$$

In evaluating a laser gain media, we want a medium with a gain efficiency as high as possible. One can find that both σ and τ vary quite a lot between different materials, but their product varies much less: those crystals with high laser cross section tend to have a low upper-state lifetime or vice versa. The upper-state lifetime is limited by the rate of spontaneous emission, and the strength of that depends on the laser cross sections and the emission bandwidth.

In this study, the $\sigma_{em}\tau$ product is calculated for both material systems as a means of comparing its potential as a viable laser gain media. We understand there are various other factors to take into consideration when designing a laser system However, from a material science perspective, we study all the variables that make up the $\sigma\tau$ product and based our analysis from there.

1.7. References

[1] R.J. Mears, L. Reekie, I.M. Jauncey, D.N. Payne “Low-noise erbium-doped fibre amplifier operating at 1.54μm” Electronics letters 23 (1987) p. 1026-1028

[2] J. Šulc, H. Jelínková, “Solid state lasers for medical applications” in Lasers for Medical Applications (2013) p. 127-176 Woodhead Publishing Series in Electronic and Optical Materials

[3] L. V. Kotov, M. E. Likhachev, M. M. Bubnov, O. I. Medvedkov, M. V. Yashkov, A. N. Guryanov, J. Lhermite, S. Février, and E. Cormier “75 W 40% efficiency single-mode all-fiber erbium-doped laser cladding pumped at 976 nm” Optics Letters 38, (2013) 2230

[4] P. Babu, Hyo Jin Seo, C.R. Kesavulu, Kyoung Hyuk Jang, C.K. Jayasankar Thermal and optical properties of Er^{3+}-doped oxyfluorotellurite glasses. Journal of Luminescence 129 (2009) 444–448

[5] S. A. Payne, L. L. Chase, L. K. Smith, W. L. Kway, and W. F. Krupke Infrared Cross - Section Measurements for Crystals Doped with Er3+, Tm3+, and Ho3+, IEEE JOURNAL OF QUANTUM ELECTRONICS, (28) 1992 p. 2619

[6] C. Gheorghe, S. Georgescu, V. Lupei, A. Lupei, and A. Ikesue "Absorption intensities and emission cross section of in Sc_2O_3 transparent ceramics" J. Appl. Phys. **103**, 083116 (2008)

[7] T. Sanamyan, J. Simmons, M. Dubinskii, "Efficient cryo-cooled 2.7-μm Er3+:Y2O3 ceramic laser with direct diode pumping of the upper laser level" Laser Phys. Lett. 8 (2010) 569–572

[8] T.Sanamyana, R.Pavlacka G.Gilde M.Dubinskii "Spectroscopic properties of Er^{3+}-doped α-Al_2O_3". Optical Materials Volume 35, Issue 5, March 2013, Pages 821-826

[9] L. D. Merkle, A. C. Sutorik, T. Sanamyan, L. K. Hussey, G. Gilde, C. Cooper, and M. Dubinskii. "Fluorescence of Er^{3+}:AlN polycrystalline ceramic." January 2012/Vol. 2, No. 1/OPTICAL MATERIALS EXPRESS 78-91

[10]. A.T. Wieg, Y. Kodera, Z. Wang, T. Imai, C. Dames, and J. E. Garay, "Visible photoluminescence in polycrystalline aluminum nitride ceramics with high thermal conductivity" Applied Physics Letters (2012),101, 111903.

[11] E. H. Penilla, Y. Kodera, J.E. Garay, Blue-green emission in terbium-doped alumina (Tb:Al_2O_3) transparent ceramics, Adv. Funct. Mater. 23 (48) (2013) 6036–6043

[12] E. H. Penilla, L. F. Devia-Cruz, M. A. Duarte, C. L. Hardin, Y. Kodera, and J. E. Garay, "Gain in Polycrystalline Nd-doped Alumina: Leveraging Length Scales to Create a New Class of High-Energy, Short Pulse, Tunable Laser Materials" *Light: Science & Applications.* (2018)

[13] Halina Abramczyk, "Introduction to Laser Spectroscopy," Elsevier. May 6, 2005.

[14] F. P. Schafer, W. Schmidt, and J. Volze, "Organic Dye Laser," Appl. Phys. Letters **9**, 306 (1966).

[15] W. W. Chow and S. W. Koch, *Semiconductor-Laser Fundamentals*, Springer, Berlin (1999).

[16] R. L. Byer, “Diode laser-pumped solid-state lasers”, Science 239, 742 (1988).

[17] Kunio Yoshida, Akio Ikesue, and Yoshiaki Okamoto, “All Ceramic Composite with Layer by Layer and Clad-Core Structure by Advanced Ceramic Technology,” The Optical Society. Conference on Lasers and Electro-Optics. San Francisco, California United States. 16–21 May 2004.

[18] A. Ikesue, Y.L. Aung, “Synthesis and Performance of Advanced Ceramic Lasers,” Journal of the American Ceramic Society. Volume 89, Issue 6 June 2006, 1936-1644.

[19] J. Lu, H. Yagi, K. Takaichi, T. Uematsu, J.-F. Bisson, Y. Feng, A. Shirakawa, K.I. Ueda, T. Yanagitani, A.A. Kaminskii, Appl. Phys. B 79 (2004) 25.

[20] W. Koechner, *Solid-State Laser Engineering*, Springer, New York 2006.

[21] V. Peters, A. Bolz, K. Petermann, G. Huber, “Growth of high-melting sesuioxides by the heat exchanger method,” J. Cryst. Growth, (2002) 237-239, 879-883.
[22] William T. Silvfast, “Laser Fundamentals: Edition 2,” Cambridge University Press. July 21, 2008.

[23] Takashi Shirai, Hideo Watanabe, Masayoshi Fuji, Minoru Takahashi, “Structural properties and surface characteristics on aluminum oxide powders” Material Science (2009) Vol. 9, 23-31.

[24] J. E. Garay, “Current-Activated, Pressure-Assisted Densification of Materials,” *Annu. Rev. Mater. Res.*, vol. 40, no. 1, pp. 445–468, Jul. 2010.

[25] R. Orrù, R. Licheri, A. M. Locci, A. Cincotti, and G. Cao, “Consolidation/synthesis of materials by electric current activated/assisted sintering,” *Mater. Sci. Eng. R Reports*, vol. 63, no. 4–6, pp. 127–287, Feb. 2009.

[26] F. Maglia, I. G. Tredici, and U. Anselmi-Tamburini, “Densification and properties of bulk nanocrystalline functional ceramics with grain size below 50nm,” *J. Eur. Ceram. Soc.*, vol. 33, no. 6, pp. 1045–1066, Jun. 2013.

[27] U. Anselmi-Tamburini, J. E. Garay, and Z. A. Munir, “Fast low-temperature consolidation of bulk nanometric ceramic materials,” *Scr. Mater.*, vol. 54, no. 5, pp. 823–828, Mar. 2006.

[28] M.A. Omary, H.H. Patterson, “Luminescence, Theory,” University of Maine, Orono. Elsevier 2017.

[29] N. Hirosaki, R.-J. Xie, K. Kimoto, T. Sekiguchi, Y. Yamamoto, T. Suehiro, and M. Mitomo, “Characterization and Properties of Green-Emitting β-SiAlON:Eu^{2+} Powder Phosphors for White Light-Emitting Diodes,” Appl. Phys. Lett., 86, 211905, 3 pp (2005).

[30] K. Inoue, N. Hirosaki, R.-J. Xie, and T. Takeda, “Highly Efficient and Thermally Stable Blue-Emitting AlN:Eu2+ Phosphor for Ultraviolet White Light-Emitting Diodes,” J. Phys. Chem. C, 133, 9392–7 (2009).

[31] Rong-Jun Xie, Hubertus T. Hintzen “Optical Properties of (Oxy)Nitride Materials: A Review” J. Am. Ceram. Soc., 96 [3] 665–687 (2013).

[32] H. Watanabe, H. Wada, K. Seki, M. Itou, and N. Kijima, “Synthetic Method and Luminescence Properties of SrxCa1_xAlSiN3:Eu2+ Mixed Nitride Phosphors,” J. Electrochem. Soc., 155, F31–6 (2008).

[33] Schulz, P.A. Liquid-nitrogen-cooled Ti:Al2O3 laser. IEEE J. Quantum Electron. 1991, Volume 27, 1039–1047.

[34] Brown, D.C. Nonlinear Thermal Distortion in YAG Rod Amplifiers. IEEE J. Quantum Electron. 1998, Volume 33, 2383–2392.

[35] D.C. Brown, “The Promise of Cryogenic Solid-State Lasers” IEEE JOURNAL OF SELECTED TOPICS IN QUANTUM ELECTRONICS, VOL. 11, NO. 3, MAY/JUNE 2005.

[36] R.M. Martin, “Reciprocity between Emission and Absorption for Rare Earth Ions in Glass” WORCESTER POLYTECHNIC INSTITUTE. Dissertation April 25, 2006.

[37] B. R. Judd, ”Optical absorption intensities of rare earth ions”, Phys. Rev., 127, 750, (1962).

[38] [G. S. Ofelt, ”Intensities of crystal spectra o rare earth ions,” J. Chem. Phys., 37,511, (1962).

[39] W. F. Krupke, ”Induced-Emission Cross Sections in Neodymium Laser Glasses”, IEEE J. Quantum Electron., QE-10, 450, (1974).

[40] R. R. Petrin, M. L. Kliewer, J. T. Beasley, R. C. Powell, I. D. Aggarwal, R. C. Ginther, ”Spectroscopy and Laser Operation of Nd:ZBLAN Glass”, IEEE J. Quantum Electron., 27, 1031 (1991).

[41] Walsh B.M., “Judd-Ofelt theory: principles and practices,” (edtion) Advances in Spectroscopy for Lasers and Sensing. Springer, Dordrech (2006).

[42] D. E. McCumber, ”Einstein Relations Connecting Broadband Emission and Absorption Spectra”, Phys. Rev., 136, A954 (1964).

[43] P. H. Sarkies, J. N. Sandoe, and S. Parke, ”Variations of Nd3+ cross section for stimulated emission with glass composition”, J. Phys. D: Appl. Phys., 4, (1971).

[44] J. N. Sandoe, P. H. Sarkies and S. Parke, Variation of Er3+ cross section for stimulated emission with glass composition, J. Phys. D: Appl. Phys., 5, (1972).

[45] J. Wilson, and J. F. B. Hawkes, Optoelectronics: An Introduction, Pretience-Hall, p. 429, (1983).

[46] [W. J. Miniscalco, and R. S. Quimby, ”General procedure for the analysis of Er3+ cross sections”, Optics Letters, 16, 258, (1991).

[47] D. E. McCumber, ”Theory of Phonon-Terminated Optical Masers”, Phys. Rev., 134, A299 (1964).

[48] M. C. Williams, and R. T. Brundage, ”Stimulated-emission cross sections and nonradiative relaxation of the 5L6 state of trivalent americium in fluorozirconate glass”, Phys. Rev. B, 45, 4561 (1992).

[49] H. M. Pask, R. J. Carman, D. C. Hanna, A. C. Tropper, C. J. Mackechnie,

P. R. Barber, and J. M. Dawes, ”Ytterbium-Doped Silica Fiber Lasers: Versatile Sources for the 1-1.2 μm Region”, IEEE J. Sel.Topics Quant. Electron., 1, 2 (1995).

[50] C. Florea, K. A. Winick, ”Ytterbium-Doped Glass Waveguide Laser Fabricated by Ion Exchange”, J. Lightwave Technol., 17, 1593 (1999).

[51] D. J. Coleman, S. D. Jackson, P. Golding and T. A. King, ”Measurements of the spectroscopic and energy transfer parameters for Er3+-doped and Er3+, Pr3+-codoped PbO − Bi2O3 − Ga2O3 glasses”, J. Opt. Soc. Am. B, 19 (2002).

[52] B. F. Aull and H. P. Jenssen, ”Vibronic Interaction in Nd:YAG Resulting in Nonreciprocity of Absorption and Stimulated Emission Cross Sections”, IEEE J. Quantum Electron., Vol. QE-18, 925-930 (1982).

[53] T. Y. Fan, M. R. Kotka, ”End-Pumped Nd : LaF3 and Nd : LaMgAl11O19 Lasers”, IEEE J. Quantum Electron., 25, 1845 (1989)

[54] C. Huang, L. McCaughan and D. M. Gill, ”Evaluation of Absorption and Emission Cross Sections of Er-Doped LiNbO3 for Applications to Integrated Optic Amplifiers”, J. Lightwave Technol., 12, 803 (1994).

[55] T. Schweizer, D. W. Hewak, B. N. Samson and D. N. Payne, ”Spectroscopic data of the 1.8-, 2.9-, and 4.3-μm transitions in dysprosium-doped gallium lantnum sulfide glass”, Opt. Lett., 21, 1594 (1996)

[56] T. Schweizer and B. N. Samson, ”Infrared emission and ion-ion interaction in thulium- and terbium-doped gallium lanthanum sulfide glass” J. Opt. Soc. Am. B, 16, 308, (1999).

[57] J. F. Philipps, T. Topfer, H. Ebendorff-Heidepriem, D. Ehrt, R. Sauerbrey, ”Spectroscopic and lasing properties of Er3+ : Nd3+ -doped fluoride phosphate glasses”, Appl. Phys. B, 72, 399 (2001).

[58] T. Y. Fan and R. L. Byer, ‘‘Diode laser pumped solid-state laser,’’ IEEE J. Quantum Electron. **24**, 895–912 (1988).

[59] J. Dong, M. Bass, Y. Mao, P. Deng, and F. Gan, “Dependence of the Yb31 emission cross section and lifetime on temperature and concentration in yttrium aluminum garnet,” Vol. 20, No. 9/September 2003/J. Opt. Soc. Am. B 1979.

Chapter 2. Previous work on Er and Er co-doped Gain Media

Rare earth ions as dopant in laser gain media

Rare earth elements are some of the most useful dopants for solid state gain media. The key to the optical behavior of the rare earth elements is contained in their very particular atomic structure. The classic image of atoms is that of a nucleus surrounded by shells of electrons, which are gradually filled as one moves across the periodic table. In general, the successive shells have monotonically increasing radii. However, at the atomic number Z=57, an abrupt contraction takes place. The 5s and 5p shells ($5s^2 5p^6$) are filled and one adds next a 4f shell in which electrons are inserted [1]. Instead of having a larger radius than the 5s and 5p shells, the 4f shell actually contracts and becomes bounded by these shells. This was explained by Mayer by considering the effective radial potential (a form of Coulomb potential energy) of the electrons [2]:

$$v(r) = -\frac{e^2}{r}\left[1 + (Z-1)\varphi\left(\frac{r}{\mu}\right)\right] + \frac{h^2}{8\pi^2 m} * \frac{l(l+1)}{r^2} \qquad \text{(Eq. 2.1)}$$

where *e* is the electronic charge, *r* is the distance from the nucleus, *h* is the Planck's constant, *m* is the mass of the electron, *l* is the angular momentum quantum number of the electron, $\varphi\left(\frac{r}{\mu}\right)$ is called the Thomas-Fermi function. The Thomas-Fermi function provides a functional form for the kinetic energy of a non-interacting electron gas as a function of the density.

As we progress across the lanthanide series, the average radius of the 4f shell slowly decreases [3]. This lanthanide contraction is about 10% from the beginning to the end of the series. The 4f electrons are responsible for the rich array of optical

properties of the REs. This shielding of the 4f electron shell from its environment by the outermost 5s and 5p electrons is responsible for the rare earths' wide application in optical devices. Essentially the shielding causes the rare earth elements to behave similarly in different host lattices, making it relatively easy to engineer properties.

2.1. Properties of Erbium doped Media

Erbium (Er) is a chemical element in the lanthanide series of the rare earth metals that displays the interesting property in its electronic configuration due to the shielding discussed in Chapter 2.1. This shielding has the effect that the energy levels of this 4f shell are largely insensitive to the environment that they reside in. Due to these unique optical properties, erbium is often employed in a wide variety of host matrices primarily for use as an amplifying material [4]. When erbium is embedded in a solid, it generally assumes the trivalent Er^{3+} state, which has an electronic configuration [Xe]-$4f^{11}$. The 4f-shell of the Er^{3+} ion is not completely filled, which allows for different electronic configurations with different energies due to spin-spin and spin-orbit interactions. Radiative transitions between most of these energy levels are parity forbidden for free Er^{3+} ions. When Er^{3+} is incorporated in a solid, however, the surrounding material perturbs the 4f wave functions [3]. This has two important consequences. First, the host material can introduce odd-parity character in the Er^{3+} 4f wave functions, which makes radiative transitions weakly allowed. Second, the host material causes Stark-splitting of the various energy levels, which broadens the optical transitions. The energy levels of erbium, in increasing levels of energy are (according to Dieke) [5]: $^4I_{15/2}$, $^4I_{13/2}$, $^4I_{11/2}$, $^4I_{9/2}$, $^4F_{9/2}$, $^4S_{3/2}$, $^2H_{11/2}$, $^4F_{7/2}$, $^4F_{5/2}$, $^4F_{3/2}$, $^2G_{9/2}$, $^4G_{11/2}$, and $^4G_{9/2}$.

The most common laser transition is that from the $^4I_{13/2}$ manifold to the ground-state manifold $^4I_{15/2,}$ as shown in the simplest energy diagram in Figure 2.1. Laser oscillation, arising from these transitions was observed mainly in the wavelength region 1.53 to 1.66 μm.

Light sources in the vicinity of 1.53 to 1.66 μm are important, due to the absorption of aqueous humour rather than the cornea at this wavelength, it is safer for the eyes. Because that transition is a quasi-three-level transition, erbium-doped laser and amplifiers require a significant excitation density of the erbium ions, and erbium lasers typically exhibit a high threshold pump power.

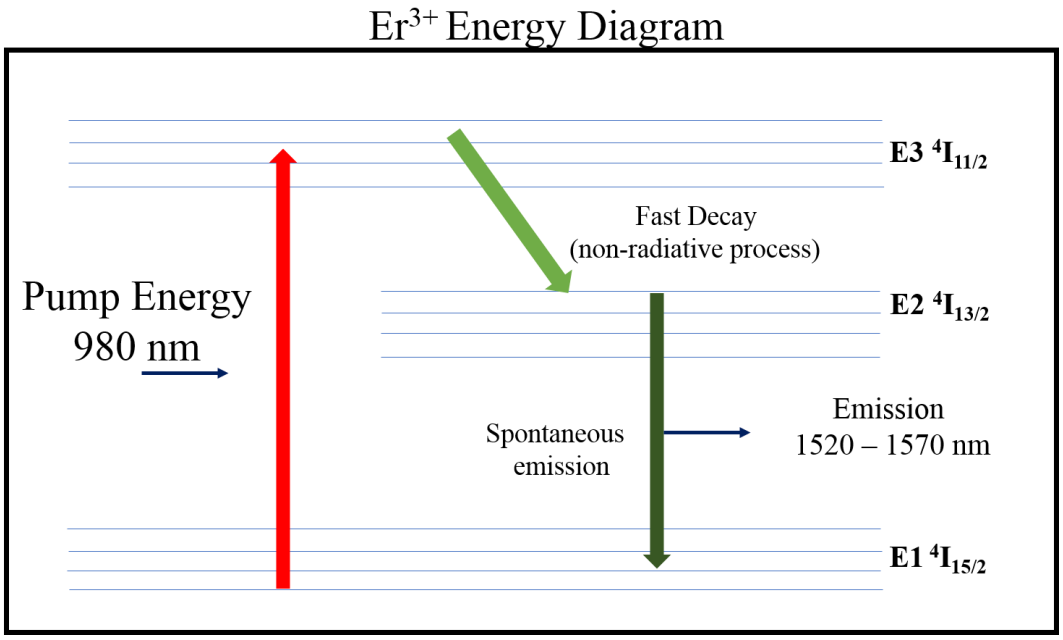

Figure 2.1. Simplified energy level structure of the $^4I_{15/2} \rightarrow {}^4I_{13/2}$ transition trivalent erbium ion.

The most common pump scheme is based on the transition $^4I_{13/2} \rightarrow {}^4I_{15/2}$ with a pumping wavelength around 0.9 – 1 μm, although in-band pumping ($^4I_{13/2} \rightarrow {}^4I_{15/2}$ e.g. at ~1.45 μm) is also possible and has been a growing interest due to the lower quantum defect, which causes less heat generation.

Emission in the ~2.8 μm [6] region, $^4I_{11/2} \rightarrow {}^4I_{13/2}$ transition, are particular interesting for medical applications [7, 8] thanks to the strong water absorption in this spectral region. As well as allowing for extremely precise cutting and ablation of water-containing tissues, light sources operating at 2.8 μm can reduce the burning of skin during surgery, decrease the use of anesthesia and shorten recovery time, especially in skin surgery and the cutting and removal of hard tissues such as tooth enamel and bone. Some examples of the lasing of erbium around 2.8 μm are found in [9, 10]. This emission at 2.8 μm is due to a cooperative upconversion process. This upconversion, due to an Er-Er interaction, occurs if the energy for a $^4I_{13/2} \rightarrow {}^4I_{9/2}$ transition is gained by a transition from the $^4I_{13/2}$ level to the ground state in a neighboring erbium ion. A rapid relaxation from the $^4I_{9/2}$ level populates the $^4I_{11/2}$ level. High erbium concentrations are a necessary condition for this process.

The green laser emission in erbium ($^4S_{3/2} \rightarrow {}^4I_{15/2}$) is also interesting for a wide range of applications, including color displays, optical data storage, biomedical diagnostics, sensors and undersea optical communications. The population of the $^4S_{3/2}$ level is achieved by up-conversion. In general, the up-conversion is achieved via the so-called frequency up-conversion mechanism first investigated by Auzel [11]. This process involves either sequential or multiphoton stepwise excitation and energy transfer between rare-earth ions in solids and the subsequent emission of photons with energies above those of the excitation photons [12, 13].

2.1.1. Erbium doped Thin Films

Erbium-doped thin films have been fabricated through various methods in order to incorporate them into optical waveguide amplifiers, operating as

telecommunication windows near 1.5 μm [14]. They are attractive due to their small size and potential integration as loss-compensating components with other optical devices, such as passive splitters [15] or combiners [16]. Ideally, these waveguide amplifiers should have high gain, small size, and require low pump power [17].

In an article released in 1993, Al_2O_3 films were fabricated on Si substrates which were then implanted with Er ions to peak concentrations ranging from 0.01 to 1 at. % [18]. Those samples have shown relatively broad photoluminescence emission spectra centered at λ_0= 1.533 μm, corresponding to intra-4f transitions in Er^{3+}.

In that study, they revealed that an optimum Er concentration of 0.23 at % along with post-implantation thermal annealing increased the PL intensity by a factor of ~40.

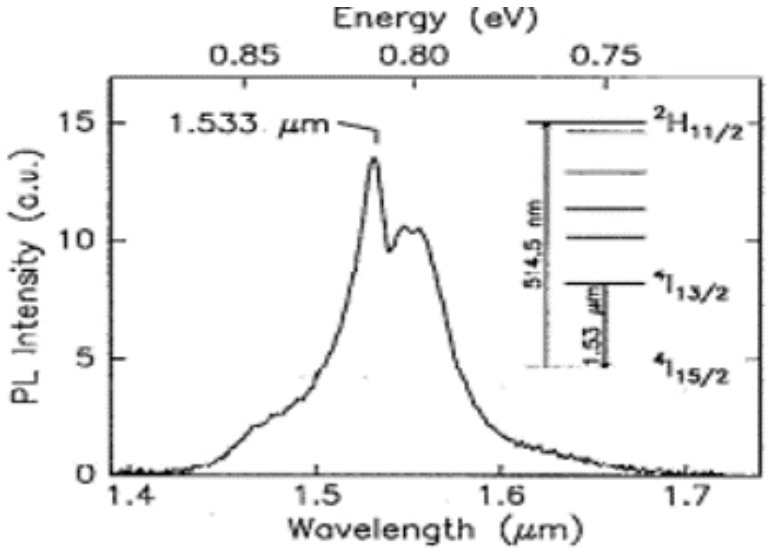

Figure 2.2. Room-temperature PL spectra of Er-implanted Al_2O_3 thin films. A 514.5 nm excitation source was used to show broad emission at 1533 nm [18].

At the higher concentrations, there were effects of concentration quenching. The Er ions in those thin films were excited using an Ar laser emitting at 514.5 nm (the $^2H_{11/2} \rightarrow {}^4I_{15/2}$ transition) , as shown in Figure 2.2. The broad PL emission spectra

is caused by the local electronic environment of the Er ions around the Al_2O_3 thin film. The peak structure of the spectrum is attributed to Stark splitting of the degenerate 4f levels, characteristic of Er^{3+} embedded in a solid, as discussed in Chapter 2.1. This, as well as homogeneous and inhomogeneous broadening in the broadness we see in Figure 2.2. This broadness in Er-implanted Al_2O_3 offers larger bandwidth for multiplexed signal amplification [18].

There are limitations to the application Er doped thin films. For instance, relatively high pump powers are required to reach net gain. This is due to the fact that at the high Er concentrations required to reach high gain per unit length, cooperative upconversion interactions between the closely spaced Er ions reduce the effective excited Er population for a given pump power [19]. In addition, the high pump powers required to overcome these interactions can cause excited state absorption (ESA) effects that also reduce the pump efficiency. Therefore, it is either important to develop new materials which show low upconversion, combined with a suitable waveguide technology or work with a different material system altogether, such as 3D materials, where we have more potential for high powered applications.

2.1.2. Erbium doped Glasses/Fibers

Erbium has been made to lase at 1.54 μm in both silicate and phosphate glasses. Because of the three-level behavior of erbium and the weak absorption of pump radiation co-doping with other rare earth ions is necessary to obtain satisfactory system efficiency.

An important use of erbium is its inclusion into laser gain media to form the erbium doped amplifiers. The amplifier has become a very important component in

optical fiber telecommunications as they are routinely used for signal boosting during long distance signal transmission to maintain signal quality.

Compared to other solid state lasers operating in this transition, fiber lasers offer favorable characteristics such as high beam quality and great reliability. They also have a greater potential for power scaling because of their high surface-to volume ratio. However, many issues still have to be addressed to increase their power level to several tens of watts while ensuring long-term stability [20]. The increase of the thermal load on all intracavity components needs to be considered, fusion splices are expected to become increasingly critical. This is especially challenging at wavelengths far from the peak gain of Er^{3+} ions where higher reflectivity output couplers are required to reduce the lasing threshold [20, 21].

2.1.3. Erbium doped Ceramics

The most commercially successful Er host materials have been Er doped fibers/glasses [22, 23], single crystal YAG. Er in polycrystalline hosts such as YAG [24], cubic- sesquioxides [25, 26] and birefringent oxides like Al_2O_3 [27, 28] has also been studied

In order to satisfy the ever-increasing need for high-power solid-state lasers, there has been considerable interest in Er doped ceramic media because ceramics have benefits for dimension scaling and mechanical properties [14, 29-32]; indeed, impressive laser performance has been reported in Er doped ceramics [33]. Lasing of erbium ions was first realized with highly doped Er:YAG crystals [34]. In that case, the laser transition is $^4I_{11/2} \rightarrow {}^4I_{13/2}$, with an emission wavelength around 2.9 μm.

For low doping concentrations, this laser transition would be self-terminating, as the lower level has a significantly longer lifetime than the upper level. For high erbium concentrations, however, complicated energy transfer processes change this situation. In this study, we won't be focusing on high erbium concentrations as the laser transition of interest is at ~1.5 μm. Er:YAG lasers can also be operated on the $^4I_{13/2} \rightarrow {}^4I_{15/2}$ transition, then emitting around 1.645 μm. Efficient operation can be achieved by in-band pumping e.g. with an erbium-doped fiber laser emitting at 1.53 μm.

Figure 2.3. Optical picture of the polished Er:YAG ceramic sample demonstrating the high transparency capable with this material system [35].

Cavalli et. al [35] synthesized 2 at.% of Er^{3+} YAG, with Y_2O_3, Al_2O_3,and Er_2O_3 powders mixed in proper stoichiometric ratios via ball milling for 72 hours. The

powder mixtures were then pressed into pellets in a metallic die. The pellets were then vacuum sintered and annealed and polished. The sample with composition 2% Er:YAG exhibits after sintering a regular pore-free microstructure with equiaxed grains ranging from 10 to 30 μm and confirmed by the high transmittance of the sample, as seen in Figure 2.3. Also, they revealed that excitation with ~980 nm light leads the to the $^4I_{13/2} \rightarrow {}^4I_{15/2}$ an emission transition as expected.

Other Er doped cubic- sesquioxides [25, 26] ceramics have been fabricated such as Er:Lu_2O_3, Er:Sc_2O_3 and Er:Y_2O_3 and display excellent spectroscopic properties. These oxide materials are promising laser host materials, but it is very difficult to grow single crystals of these oxides by the conventional melt-growth method because of their high melting temperature. However, modern sintering technology has enabled the fabrication of polycrystalline ceramic laser materials for use as laser gain media in solid-state lasers. This has opened the way to fabrication of high melting point materials and incongruently melting materials, which could not be produced by the conventional melt-growth technology [36]. Extensive analysis has been performed on all these materials, in an attempt to present each of these material systems as potential high power laser gain media. Generally, the fracture strength of ceramic materials is higher than that of single crystal counterparts if they have the same crystal structure.

Therefore, sesquioxide ceramic materials are expected to feature in the development of high power lasers in the future. Due to the cubic crystal systems of these sesquioxides and relatively similar ionic radii sizes to the erbium ion, these material systems display very sharp absorption and fluorescence lines which can

prove important in terms of designing a laser. A summary of the works is shown in Figure 2.4, where cryogenic measurements of the absorption and stimulated emission cross sections were calculated.

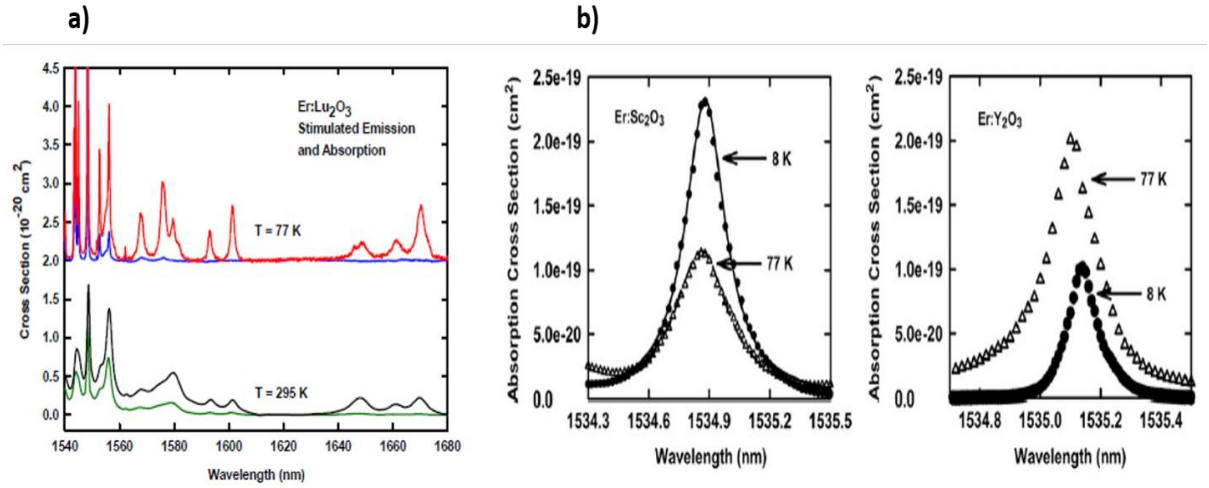

Figure 2.4. Plots of cross sections for the sesquioxides. a) Absorption and stimulated emission cross section spectra of Er:Lu_2O_3 [25] b) Absorption of Er:Sc_2O_3 and Er:Y_2O_3 in the zero line spectral region at two temperatures [26].

As mentioned in Chapter 1.5, a particularly interesting gain media has been rare earth (RE) doped α-Al_2O_3 (corundum) because it has significantly higher thermal conductivity and fracture strength and can thus can potentially be used to significantly increase laser power output [37].

Recently, there has been studies [27] that sufficient amounts of Er^{3+} ions have been incorporated into both highly crystalline α-Al_2O_3 powders and fully densified transparent α-Al_2O_3 ceramics. Their analysis of the ground state and the first three excited multiplets of Er^{3+} ions in α-Al_2O_3 host was the first ever presented. The bulk ceramic displayed remarkable spectroscopic properties of an erbium doped media. Their results of spectroscopic study of Er:Al_2O_3 was their 1st attempt toward

transparent bulk Er^{3+} doped sapphire composite laser gain material. Since then, significant progress has been made to improve the transparency of the Er:Al_2O_3 bulk ceramic through different processing methods [28] and even more spectroscopic analysis was shown displaying many of the known Er transitions.

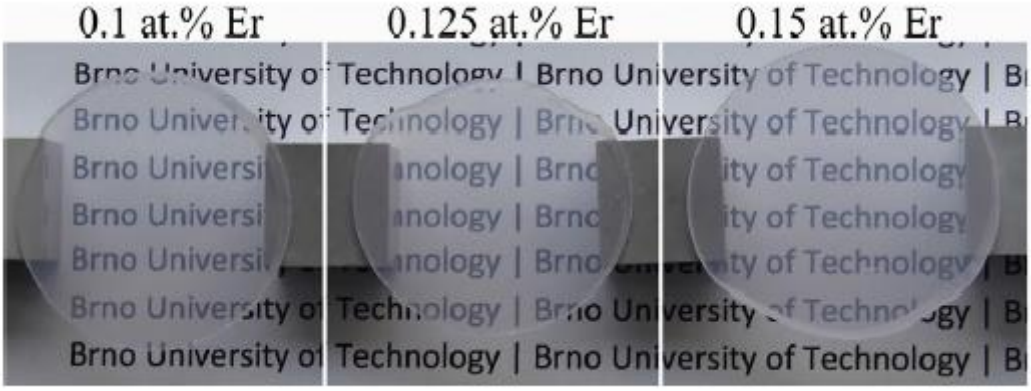

Figure 2.5. Transparent Er^{3+} doped alumina fabricated through the HIP-ing method [28].

Drdlíková *et al* [28] fabricated highly transparent ceramics with fine grain sizes by sintering followed by hot isostatic pressing (HIP). They proved that they incorporated Er^{3+} ions in the range of 0.1 to 0.17 at% through optical spectroscopy showing characteristic Er^{3+} absorption and emission. However, the measured emission lifetimes in the ceramics was relatively short, 1.61 μs, particularly at the $^4G_{11/2} \rightarrow {}^4I_{15/2}$ transition, which can increase the lasing threshold and likely preclude lasing in the ceramics. For both works, either the $^4G_{11/2} \rightarrow {}^4I_{15/2}$ or the $^4I_{13/2} \rightarrow {}^4I_{15/2}$ transition was employed as their excitation scheme. Their measured absorption cross section at $^4I_{11/2}$ this spectral region was likely too small for it to be an effective pumping band for lasing.

2.2. Properties of Erbium Co-doped Media

The idea of co-doping was introduced in 1963 [38] and were later used in other works. The research at the time aimed to determine the chemical mechanisms of growing and doping in materials such as alkaline earth halides (e.g., CaF_2, BaF_2, etc.) doped with rare earths for potential use in optically pumped lasers [38, 39]. In addition, optical energy transfer (ET) was investigated for chromium (Cr) and neodymium (Nd) doubly doped into (YAG) [40] and other Cr-doped materials [41].

Co-doping was mainly applied to describe the studies of absorption and luminescence properties. At the time, it was believed that all ET existed between activators and the sensitizer (or donor) ion in one of its excited states, while the activator (or acceptor) ion was in its ground state. The energy accumulated by the sensitizer is therefore transferred to the activator. This conventional ET explains sensitized fluorescence as well as concentration quenching. It was then proposed that ET promoting the acceptor ion in an excited state might be followed by ESA of the pump photon to promote the acceptor ion into a higher excited state [42]. Or that another type of ET might occur where both the sensitizer and activator ions are in one of their excited states prior to ET [43], thus also leading to possible fluorescence at a higher frequency than the excitation beam frequency.

The most common type of co-doping with erbium has been doping with ytterbium. Er^{3+}/Yb^{3+} co-doping has become an effective method for producing short, efficient lasers and amplifiers in the long haul telecommunications wavelength range. A 980 nm pumping scheme is proved to be an effective tool because of the high-Yb^{3+} absorption cross section and the additional pumping mechanism available at this wavelength. Ytterbium co-doping increases the pump absorption near 980 nm and

efficient energy transfer between the Yb^{3+} and the Er^{3+} ions enables the operation of long lasers with low Er^{3+} concentrations. This mechanism was first demonstrated by Snitzer and Woodcock in bulk glass [44]. More recently, Er^{3+}/Yb^{3+} co-doping fiber lasers [45, 46] and planar waveguide amplifiers based on phosphate glass [47] have been demonstrated.

2.2.1. Erbium Co-doped Fibers/Glasses

The first long-wavelength pumped (1.06-μm) Er/Yb co-doped fiber laser was reported in 1988 by a group from the University of Southampton [49]. The fiber host was an aluminosilicate glass with a relatively low concentration of Yb^{3+}. The optical conversion efficiency from 1.06 → 1.55 μm was reported to be only 4%. From their findings, they stated that the host glass compositions were critically important in controlling the back energy transfer [50, 51] from active ion to sensitizer ion. This is due to the high phonon energies that both phosphate glasses and fibers possess. It has been found that high phonon energies from these hosts are necessary to increase the nonradiative relaxation rate from the active ion compared with the back-transfer process from active ion to sensitizer [52]. Although, this is of a less concern for Al_2O_3, understanding of the back-transfer process and what controls it can lead us to fabricate a more energy efficient media.

The first optical fiber amplifier based on Er/Yb co-doped fibers and a diode-pumped Nd:YAG pump laser at 1064 nm was reported in 1991 [53]. To the best of our knowledge, there isn't reported literature on co-doping with Cr^{3+} in erbium fibers. Cr^{4+} doping is of great interest, particularly in fibers, due to the significantly less transmission and propagation losses achieved. The stable +4 oxidation state of Cr

ions has been found in aluminate, alumino-silicate, and gallate glasses, which results in the absorption spectrum at ranges of 600-1000 nm [54]. The emission peak of Cr^{4+} doping is roughly 1.6 μm, which is ideal for optical fiber telecommunications [55, 56], which would explain why there is little literature for Cr^{3+} co-doping.

2.2.2. Erbium Co-doped Ceramics

Particularly in bulk crystals efficient pump absorption on the $^4I_{15/2} \rightarrow {}^4I_{13/2}$ of the Er^{3+} transition is difficult to achieve, because the absorption cross sections are relatively small, and the doping concentration is limited by the need to avoid excessive quenching processes. The chromium sensitizer ions can efficiently absorb pump radiation and then transfer the energy to erbium ions in the ground-state manifold, bringing them into $^4I_{11/2}$. From that level, the ions are quickly transferred into the upper laser level $^4I_{13/2}$, so that energy transfer back to sensitizer ion is suppressed. There are various dopant concentration combination, between the erbium and chromium, that have been explored, which depend on the host material used as well as the erbium transition of interest. If the laser emission at ~2.8 μm is desired, heavily doped Er media is required, due to the upconversion process. For the ~1.5 um emission, a combination of low concentration Er and Cr would be ideal for the gain media.

M. Pokhrel et. al, [57] report the synthesis and spectroscopic characteristics of high Er^{3+} content (50%) transparent YAG ceramic co-doped with nominal 0.1% Cr^{3+}.The purpose of this study is to explore the near infrared emission mechanisms in Er^{3+} by pumping directly the Er^{3+} or by exciting the Cr^{3+} to its absorption band at 407 nm and utilize the purposed material as laser active medium. Introduction of Cr^{3+} was

found to have influence on the emission characteristics of Er^{3+} [58] by suitable energy transfer mechanism which is determined by the concentrations of Cr and the Er [58, 59].

Lundt et. al, [60] report on spectroscopic studies of Cr:Er:GGG in order to clarify how efficient the Cr^{3+} to Er^{3+} energy transfer is in this material, while pumping with a HeNe laser. They also studied the effects both erbium and chromium doping concentration had on the emission transitions. The growing emission intensities at both wavelengths for an increase of the erbium concentration can be explained by an improvement of the Cr^{3+} to Er^{3+} energy transfer efficiency. The decrease of the 1.6 μm emission at higher erbium concentrations, while the 2.8 μm emission further increases, is due to a cooperative upconversion process In Cr:Er:GGG the chromium'-emission decreases strongly with increasing erbium concentration. At an erbium concentration of 50 at.%, no chromium emission was detectable [61]. The decrease of this emission intensity indicates a Cr^{3+} to Er^{3+} energy transfer efficiency close to unity for high erbium concentrations. A similar level of efficiency has also been reported for **Cr:**Er: YSGG [61].

2.3. References

[1] P.M. Becker, A.A. Olsson, J.R. Simpson, "Erbium-Doped Fiber Amplifiers: Fundamentals and Technology" 1999.

[2] M.Mayer, Phys. Rev. 60, 184 (1941).

[3] S.Hufner, "Optical Spectra of Rare Earth Compounds" (Academic Press, New York, 1978).

[4] B.Denker, E. Shklovsky, "Handbook of Solid-State Lasers 1st Edition Materials, Systems and Applications" Woodhead Publishing. February (2013).

[5] G. H. Dieke and H. M. Crosswhite "The Spectra of the Doubly and Triply Ionized Rare Earths" Applied Optics Vol. 2, Issue 7, pp. 675-686 (1963).

[6] D.F. de Sousa, L.F. C. Zonetti, M.J.V. Bell, J.A. Sampaio, L.A.O. Nunes, M.L. Baesso, A.C. Bento and L.C.M. Miranda, Appl. Phys. Lett., 74, 908 (1999).

[7] R.M. Dwyer and M. Bass, Lasers in Medicine, Academic, New York, Vol, 3, p. 107. (1977).

[8] K. Kincade, Laser Focus World, 73, August (1996).

[9] G.J.Kintz, R. Allen and L. esterowitz, Appl. Phys. Lett., 50, 1553 (1987).

[10] S. A. Pollack and M. Robinson, Electron. Lett., 24, 320 (1988).

[11] F.E. Auzel, Proc. IEEE, 61, 758 (1973).

[12] P.E.A. Möbert. E. Heumann and G. Huber. Opt. Let., 22, 1412 (1997).

[13] T. Danger, J. Koetke, R. Brede, E. Heumann, G. Huber and B.H.T. Chai, J. Appl. Phys, 76, 1413 (1994).

[14] W. J. Miniscalco, "Erbium-doped glasses for fiber amplifiers at 1500 nm", IEEE J. Lightwave Technol. 9 (2), 234 (1991).

[15] P. Camy, J. E. Roman, F. W. Willems, M. Hempstead, J. C. van der Plaats, C. Prel, A. Beguin, A. M. J. Koonen, J. S. Wilkinson, and C. Lerminiaux, Electron. Lett. 32, 321 (1996).

[16] J. P. Delavaux, S. Granlund, O. Mizuhara, L. D. Tzeng, D. Barbier, M. Rattay, F. S. Andre, and A. Kevorkian, Proceedings of ECOC 96, p. 123 (1996).

[17] Y. C. Yan, A. J. Faber, H. de Waal P. G. Kik and A. Polman, "Erbium-doped phosphate glass waveguide on silicon with 4.1 dB/cm gain at 1.535 μm" Appl. Phys. Lett. 71, 2922 (1997).

[18] G. N. van den Hoven, E. Snoeks, and A. Polman, J. W. M. van Uffelen, Y. S. Oei, and M. K. Smit, “Photoluminescence characterization of Er-implanted Al203 films” Appl. Phys. Lett. 62, 3065 (1993).

[19] E. Snoeks, G. N. van den Hoven, A. Polman, B. Hendriksen, M. B. J. Diemeer, and F. Priolo, J. Opt. Soc. Am. B 12, 1468 (1995).

[20] V. Fortin, M. Bernier, S. T. Bah, AND R. Vallee, “30 W fluoride glass all-fiber laser at 2.94 μm,” Optics Letters Vol. 40, No. 12 2882-2885 (2015).

[21] D. Faucher, M. Bernier, N. Caron, and R. Vallée, Opt. Lett. 34, 3313 (2009).

[22] M. E. Fermann *et al.*, “Efficient operation of an Yb-sensitised Er fiber laser at 1.56 μm”, Electron. Lett. 24, 1135 (1988).

[23] F. Tong, W.P. Risk, R.M. Macfarlane., “551 nm diode-laser-pumped upconversion laser”, Electron. Lett. 25, 1389 (1989).

[24] Y.E. Young, S.D. Setzler, K.J. Snell, P.A. Budni, T.M. Pollak, and E.P. Chicklis, “Efficient 1645-nm Er:YAG laser”, Opt. Lett. 29 (10), 1075 (2004).

[25] L.D. Merkle, N. Ter-Gabrielyan, N.J. Kacik, T. Sanamyan, H. Zhang, H. Yu, J. Wang, and M. Dubinskii, "Er:Lu_2O_3 – Laser-related spectroscopy," Opt. Mater. Express 3, 1992-2002 (2013).

[26] L.D. Merkle and N.Ter-Gabrielyan ”Er^{3+} in Sc_2O_3 and Y_2O_3: Spectroscopy to elucidate laser behavior,” Journal of Luminescence Volume 133, January 2013, Pages 254-256.

[27] T.Sanamyan, R.Pavlacka, G.Gilde and M.Dubinskii, “Spectroscopic properties of Er^{3+}-doped α-Al_2O_3” Optical Materials Volume 35, Issue 5, March 2013, Pages 821-826.

[28] K. Drdlíková, R. Klement, D. Drdlík, T. Spusta, D. Galusek and K. Maca. “Luminescent Er^{3+}doped transparent alumina ceramics”. Journal of the European Ceramic Society 37 (2017) 2695–2703.

[29] T. Hebert, R. Wannemacher, W. Lenth, *and* R. M. Macfarlane., “Blue and green CW upconversion lasing in Er:$YLiF_4$”, Appl. Phys. Lett. 57, 1727 (1990).

[30] W.L. Barnes, R.I. Laming, E.J. Tarbox and P.R. Morkel., “Absorption and emission cross section of Er^{3+} doped silica fibers”, IEEE J. Quantum Electron. 27 (4), 1004 (1991).

[31] T.J. Whitley, C.A. Millar, R. Wyatt, M.C. Brierley and D. Szebesta., “Upconversion pumped green lasing in erbium doped fluorozirconate fibre”, Electron. Lett. 27 (20), 1785 (1991).

[32] S. Honkanen, T. Ohtsuki, S. Jiang; S.I. Najafi and N. Peyghambarian “High Er concentration phosphate glasses for planar waveguide amplifiers”, Proc. SPIE 2996, 32 (1997).

[33] Gary W. Burdick , John B. Gruber , Kelly L. Nash , Sreerenjini Chandra & Dhiraj K. Sardar, “Analyses of 4f11 Energy Levels and Transition Intensities Between Stark Levels of Er^{3+} in $Y_3Al_5O_{12}$” Spectroscopy Letters 43:406–422, 2010.

[34] E. V. Zharikov *et al.*, “Stimulated emission from Er^{3+} ions in yttrium aluminum garnet crystals at λ = 2.94 μm”, Sov. J. Quantum Electron. 4, 1039 (1975).

[35] E. Cavalli, L. Esposito, J. Hostaša and M. Pedroni, “Synthesis and optical spectroscopy of transparent YAG ceramics activated with Er^{3+},” Journal of the European Ceramic Society, Volume 33, Issue 8, August 2013, Pages 1425-1434.

[36] A. Ikesue, Y. L. Aung, V. Lupei *CERAMIC LASERS*., Cambridge University Press. (2013).

[37] E.H. Penilla, L.F.Devia-Cruz, M.A. Duarte, C.L Hardin, Y. Kodera, J.E. Garay, “Gain in Polycrystalline Nd-doped Alumina: Leveraging Length Scales to Create a New Class of High-Energy, Short Pulse, Tunable Laser Materials” Light Science Applications, April 2018.

[38] E. Mahlab, V. Volterra, W. Low, and A. Yariv, Orthorhombic electron spin resonance spectrum of U3 in CaF2, *Phys. Rev.* 131(3), 920 (1963).

[39] P. Weller and J. Scardefield, Doping of alkaline earth halide single crystals, *J. Electrochem. Soc.* 111(8), 1009 (1964).

[40] M. Taylor, An experimental study of the efficiency of optical energy transfer between Cr3 and Nd3 ions in yttrium aluminium garnet, *Proc. Phys. Soc.* 90(2), 487 (1967).

[41] G. Blasse and A. Bril, Energy transfer from trivalent rare earth ions to Cr3, *Phys. Lett. A* 25(1), 29 (1967).

[42] R. A. Hewes and J. F. Sarver, Infrared excitation processes for the visible luminescence of Er3, Ho3, and Tm3 in Yb3-sensitized rare-earth trifluorides, *Phys. Rev.* 182(2), 427 (1969).

[43] G. Ban and H. Hersh, Degradation of some IR upconverting phosphors by ionizing radiation, *J. Electron. Mater.* 1(2), 320 (1972).

[44] E. Snitzer and R. Woodcock, "Yb^{3+}-Er^{3+} glass laser", Appl. Phys. Lett. 6, 45, 1965.

[45] SNITZER. E., PO, H., HAKIMI, F., TUMMINELLI, R., and MCCOLLUM, B.c.: "Erbium fiber laser amplifier at 1.55~ with pump at 1.49~ and Yb sensitized Er oscillator". Conf. Optical Fiber Communications - OFC'88, New Orleans, Louisiana, USA, 1988, Paper PD2

[46] J.T. Kringlebotn, P.R. Morkel, L. Reekie, J.L. Archambault, D.N. Payne, "Efficient doped-pumped single-frequency erbium:ytterbium fiber laser", IEEE Photonics Technol. Lett., 1993, 5, (IO), pp. 1162-1164

[47] BARBIER. J.M., DELAVAUX, J.M., KEVORKIAN, A., GASTALDO, P., and JOUANNO, J.M : "Yb/Er integrated optics amplifiers on phosphate glass in single and double pass configurations". Conf. Optical Fiber Communications - OFC'95, San Diego, California, USA, 1995, Paper PD3-1

[48] P.K. Tawalare, V.B. Bhatkar, S.K. Omanwar, S.V. Moharil, "Cr^{3+} sensitized near infrared emission in Al2O3:Cr,Nd/Yb phosphors" Journal of Alloys and Compounds 790 (2019) 1192-1200.

[49] E. Snitter, H. Po, F. Hakimi, R. Tumminelli and B. C. McCollum, Optical Fiber Sensor Conference, 1988 Technical Digest Series, Vol. 1 (Optical Society of America, Washington, D.C. 19881, PD5.

[50] S. Hinojosa, M.A Meneses-Nava, O. Barbosa-García, L.A Díaz Torres, M.A Santoyo and J.F Mosiño, “Energy back transfer, migration and energy transfer (Yb-to-Er and Er-to-Yb) processes in Yb,Er:YAG” Journal of Luminescence. Volumes 102–103, May 2003, Pages 694-698.

[51] J.T. Vega-Durán, O. Barbosa-García, L.A. Diáz-Torres, *and* M.A. Meneses-Nava, “Effects of energy back transfer on the luminescence of Yb and Er ions in YAG” Appl. Phys. Lett. **76**, 2032 (2000).

[52] I.P. Kaminov, T.L. Koch, *Optical Fiber Telecommunications IIIB*. Elsevier 1997.

[53] J. D. Minelly et al., “Diode-array pumping of Er^{3+}/Yb^{3+} Co-doped fiber lasers and amplifiers,” IEEE Photonics Technology Letters **5**(3), 301–303 (1993).

[54] T. Murata, M. Torisaka, H. Takebe, and K. Morinaga, “Compositional dependence of the valency state of Cr ions in oxide glasses,” J. Non-Cryst. Solids 220, 139-146 (1997).

[55] Y. G. Choi, K. H. Kim, Y. S. Han, and J. Heo, “Oxidation state and local coordination of chromium dopant in soda-lime-silicate and calcium-aluminate glasses,” Chem. Phys. Lett. 329, 370-376 (2000).

[56] U. Hömmerich, H. Eilers, W. M. Yen, J. S. Hayden, and M. K. Aston, “Near infrared emission at 1.35 μm in Cr doped glass,” J. Lumin. 60 and 61, 119-122 (1994).

[57] M. Pokhrel, G. A. Kumar, P. Samuel, K. I. Ueda, T. Yanagitani, H. Yagi, and D. K. Sardar, "Infrared and upconversion spectroscopic studies of high Er^{3+}content transparent YAG ceramic," Opt. Mater. Express 1, 1272-1285 (2011).

[58] R. Gross, G. Huber, B. Struve, and E. W. Duczinski, “Cr^{3+}-sensitization of the 3 μm Er^{3+}:YAG laser,” J. Phys. Colloq. 1(7), C7.363–C7.366 (1991).

[59] T. Saiki, S. Motokoshi, K. Imasaki, H. Fujita, M. Nakatsuka, and C. Yamanaka, “Nd/Cr:YAG ceramic rod laser pumped using arc-metal-halide-lamp,” Jpn. J. Appl. Phys. 46(1), 156–160 (2007).

[60] H. Lundt and H. Weidner, “Photoluminescence properties of Cr:Er:GGG”, OPTICS COMMUNICATIONS, Volume 82, number 5,6 May (1991).

[61] E.V. Zharikov, N.N. Ilichev, S.P. Kalitin, V.V. Laptev, A.A. Malyutin, V.V. Osiko, P.P. Pashinin, A.M. Prokorov, Z.S. Saidov, V.A. Smimov, A.F. Umyskov and I.A. Shcherbakov, Sov. J. Quantum Electron. 16 (1986) 635.

Chapter 3. Synthesis of Large Emission Cross Section Transparent Erbium Doped Al_2O_3 (Er:Al_2O_3)

3.1. Introduction

The development of solid-state lasers with emission in the eye safe region of 1.5 μm is interesting for scientific and industrial purposes including laser cutting/manufacturing, communications and surgery. Here we present processing and characterization of erbium doped aluminum oxide (Er:Al_2O_3), a media with excellent thermomechanical properties that is promising for laser power scaling. The materials have high transparency at the emission wavelength, and absorption lines characteristic of Er^{3+}. Room temperature photoluminescence reveal broad emission peaks in the expected of ~1.5 μm corresponding to intra-4f transitions in Er^{3+} ($^4I_{13/2} \rightarrow {}^4I_{15/2}$ transition). The emission peaks are narrower at cryogenic temperatures (down to 10 K) revealing thermally broadened emission. In addition, ~ 1.5 μm emission has relatively long lifetimes that do not vary across a broad emission spectrum (1.5 - 1.6 μm), suggesting similar electronic environment of optically active Er sites. The emission cross sections derived from Fuchtbauer– Ladenburg relation is higher than that of Er:YAG which combined with its thermomechanical properties make Er:Al_2O_3 a potential an interesting gain medium for high-power laser applications.

As mentioned in Chapter 1.1 the development of Er doped gain media has been extensively studied over the last few decades because of the many benefits of light sources in the 1.5 – 1.6 μm range. The primary challenge to doping alumina with RE is the large ionic radii difference between REs and Al, the presumed substitutional dopant site. To date, RE:Al_2O_3 has been predominantly synthesized as

powders [1, 2] or in thin film form for optoelectronic applications using various deposition techniques [3 - 6]. Successful early work on Er:Al_2O_3 thin films by van den Hoven *et al* showed photoluminescence, PL, in the 1.5 - 1.6 μm range in Er ion implanted into alumina deposited on silicon [3]. Song *et al* [4] also observed PL ~ 1.5 μm in co-doped Er, Yb Al_2O_3 thin films. Instead of the most desirable, highly-thermally conductive α-Al_2O_3 phase, the films were found to be low crystallinity phases (θ-Al_2O_3 and γ-Al_2O_3), often found in nanoscale Al_2O_3. Highly crystalline Nd doped epitaxial α-Al_2O_3 films have been grown by Kumaran et al [5, 6] and these should be very useful for laser applications. However, thin epitaxial films are difficult to scale to dimensions necessary for high power application.

There have been significant advances towards ceramic Er:Al_2O_3 [7, 8]. In addition to the Er incorporation challenge, polycrystalline ceramics face the additional obstacle posed by birefringence scattering. Sanamyan *et al* fabricated Er:Al_2O_3 ceramics using Current Activated Pressure-Assisted Densification (CAPAD) [7]. They conducted a detailed spectroscopic study, identified the energy levels in the material, measured cross sections and emission lifetimes, clearly demonstrating that the material holds high promise as a lasing media if the transparency can be improved. Birefringent scattering can be minimized and thus transparency improved by producing ceramics with grain sizes smaller than the wavelength of light of interest [9-11]. As mentioned before, Drdlíková *et al* [8] fabricated highly transparent ceramics with fine grain sizes by sintering followed by hot isostatic pressing (HIP).

Recently we have demonstrated highly transparent RE:Al_2O_3 with PL in the visible [12] and optical gain at ~ 1 μm [13] fabricated using CAPAD. Here we

incorporate Er into Al_2O_3 through mechanical milling and further densification processing via CAPAD. We also report the laser-related spectroscopic properties of the resulting Er:Al_2O_3 with the aim of evaluating Er:Al_2O_3 as a next generation laser-gain media. We pay special attention to the typical pumping schemes that are including used for Er doped media in the visible near IR. These include exciting in the visible where there is a large absorption band (521 nm), in the 970 – 980 nm range because of the availability of reliable high power laser diodes and at the intraband ~ 1525 nm (so called resonant pumping) that has been previously shown to have high efficiency in other Er media. The samples have high transparency at the emission 1.5 μm, have sufficiently long emission lifetimes and high emission cross sections which is promising for laser application.

3.2. Experimental Materials and Methods

3.2.1. Powder Processing for synthesizing Er:Al_2O_3

Samples were processed using commercially available aluminum oxide powder (α-Al_2O_3, 99.99% purity, ~ 200 nm particle size, TM-DAR, Taimei Chemicals Japan) and Erbium Oxide, Er_2O_3 (99.5% purity, Inframat Materials, USA). The powders were weighed to achieve Er doping levels of 0.1 at. %. The powders were mixed for 12 hours by ball milling. Ultra-High Purity (UHP, 99.99% purity) water was used as a dispersant solution at a ratio of 10 grams of powder to 200 mL of UHP water. Alumina balls (99.9% density and purity, Performance Ceramics Co., Penninsula, OH USA) with 3 mm diameters were used as the milling media, at a 1:15 powder:ball weight ratio. After milling, the powders were sieved to separate from the milling media and then dried under vacuum at 70 °C for 24 hours in an oven. Dried

powders were subsequently planetary ball milled (PBM) with UHP water at 150 rpm for 6 hrs. Finally, the powders were sieved and dried under vacuum at 80 °C for 24 hours and kept dry until consolidation.

3.2.2. CAPAD Processing of Er:Al_2O_3

The Al_2O_3 + Er_2O_3 powders were densified using CAPAD [14]. In all cases, 0.330 g +/- 0.001 g of powder were placed into a graphite die with an outer diameter of 19 mm and inner diameter of 10 mm. The powder was secured between two graphite punches of the same outer diameter. A maximum vacuum of 2 x 10^{-2} Torr was achieved in all cases.

The powder was pre-pressed at 105 MPa for 5 minutes to create a dense green body. Afterwards, the pellet was subjected to an applied pressure of 120 MPa over a three-minute period in parallel with simultaneous heating to achieve and maintain temperatures of 1210 – 1250 °C. The samples were held at temperature for 5 minutes. Once our experiment was complete, the load was released. The sample temperatures are measured with an optical pyrometer, focused on a hole drilled in the graphite die located at the center point of the die height.

3.2.3. Microstructural and Optical Characterization of Er:Al_2O_3

Prior to characterization, samples were polished using diamond abrasive wheels followed by alumina paste on felt wheels to 1 µm. To characterize morphology, a Carl Zeiss Sigma 500 Field Emission Scanning Electron Microscope (FE-SEM) was used, with accelerating voltages ranging from 1 – 5 kV. Working distances in the system was approximately 5 mm**.** Micrographs of the fractured surface were used to estimate the average grain size of the bulk. X-Ray Diffraction patterns were attained using a

Phillips X'Pert Diffractometer (ModelDY1145), in point source mode system equipped with a copper source, with a step size of 0.01313 degrees and 3 seconds per step. Samples were pressed flat on a zero-background plate and measured with no stage rotation. A potential of 45 kV and a current of 40 mA was used for all measurements.

Optical transmission spectra were taken on an Agilent Technologies Cary 5000 spectrophotometer from 300 nm - 2500 nm. The bulk polished samples were placed at normal incidence to the beam path. The scans were obtained at a rate of 60 nm/min.

Photoluminescence data were taken on a modified PTI Horiba Spectrophotometer Quanta Master 8000 with spectrally filtered dual monochromators and using a Xenon Arc Lamp as a light source or a 980 nm laser diode. All measurements were taken in front face mode on polished bulk samples using a long pass 1050 nm cutoff filter. Excitation scans were taken between λ_{ex} = 300 nm - 1000 nm while monitoring the samples emission at λ_{em} = 1532 nm. Emission scans were taken between λ_{em} = 1400 nm - 1700 nm while pumping λ_{ex} = 980 nm as it was determined to be an effective pumping wavelength from the excitation spectra. All measurements were taken with varying integration times between 0.1 – 1 sec per nanometer and a varying step size of 0.1 - 1 nm.

For cryogenic measurements, the spectrophotometer was modified to integrates a closed-cycle helium cryostat (Advanced Research Systems, ARS-2HW) using a conductive cold finger within a windowed housing that enabled measurements from 8 K to 295 K. All measurements were performed at 45° angle of incidence (AOI) on

polished bulk ceramics and the PL spectra were collected from the specimen front face. The same varying integration times and step sizes were used for the cryogenic measurements.

PL lifetime measurements were collected using a pulsed tunable laser (Continuum Surelite EX nanosecond laser, coupled to a Horizon Optical Parametric Oscillator) as an excitation source with pulse widths of 6 ns. Exponentials were fit to the raw data and PL lifetimes were defined as the time required for the normalized intensity to decrease by 1/e.

3.3. Results and Discussion

Figure 3.1 are transmission measurements on samples with varying Er concentrations. The results show there is an observable effect on increasing doping concentration on the transmission of the samples. The densification temperature required to achieve full density is slightly different and increases with RE concentration. The maximum transmission of the sample doped with the highest decreases . The average grain size and relative density of across all samples are in close agreement to each other, at values for the grain size to be around 250 nm and 99% relative density. It is likely however that the decreased transmission is caused by increases scattering in the highest doped sample either from pores or larger grains (more birefringent scattering).

The absorption peaks in the 1450 to 1550 nm range become deeper with deeper as dopant concentration increases. The absorption at ~ 1450 nm, which is a

typical pumping band for resonant pumping for $^4I_{13/2} \rightarrow {}^4I_{15/2}$ transition is clearly observable in the 0.25, 0.35 and is most prominent in 0.5 at % Er^{3+}.

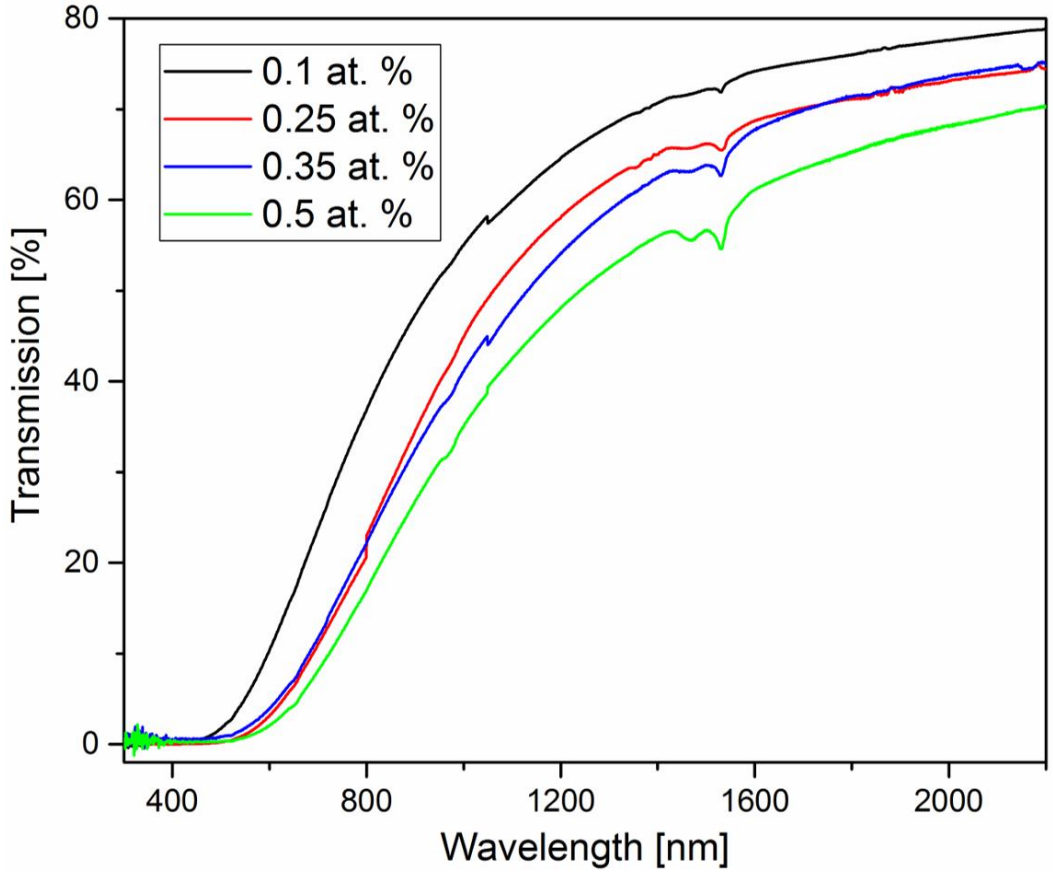

Figure 3.1. Transmission curves of all Er:Al_2O_3 processed samples, with varying dopant concentrations from 0.1 – 0.5 at.%.

Figure 3.2 depicts the excitation-emission pattern for the 0.1 at. % Er:Al2O3 bulk. It consists of one excitation band, which are located at ~ 975 – 985 nm and a single broadband emission band at ~ 1500 – 1580 nm. The peak of the emission band is found at 1532 nm. It is practically independent on excitation wavelength.

This excitation/emission band corresponds to the $^4I_{13/2} \rightarrow {}^4I_{15/2}$ transition. The excitation wavelength is scanned over the $^4I_{11/2}$ manifold. In this technique, the fluorescence intensity is recorded as a function of both excitation and emission

wavelengths. It is possible to get a clearer idea of the range the Er^{3+} ions have on $^4I_{13/2} \rightarrow {}^4I_{15/2}$ transition, especially at lower temperature. Figure 3.3 depicts the sample Er:Al_2O_3 ceramic characterized at 8 K. The excitation and emission band appear to be affected by the decrease in temperature. The emission band has narrowed to 1520 – 1560 nm. The most intense regions are highlighted with an excitation of ~ 980 nm and emission at ~ 1532 nm. It is likely that temperature dependent line broadening effects are affecting the emission structure of our ceramics. In order to fully investigate more of these effects, we perform more resolved PL analysis shown in Figure 3.5c and Figure 3.6a.

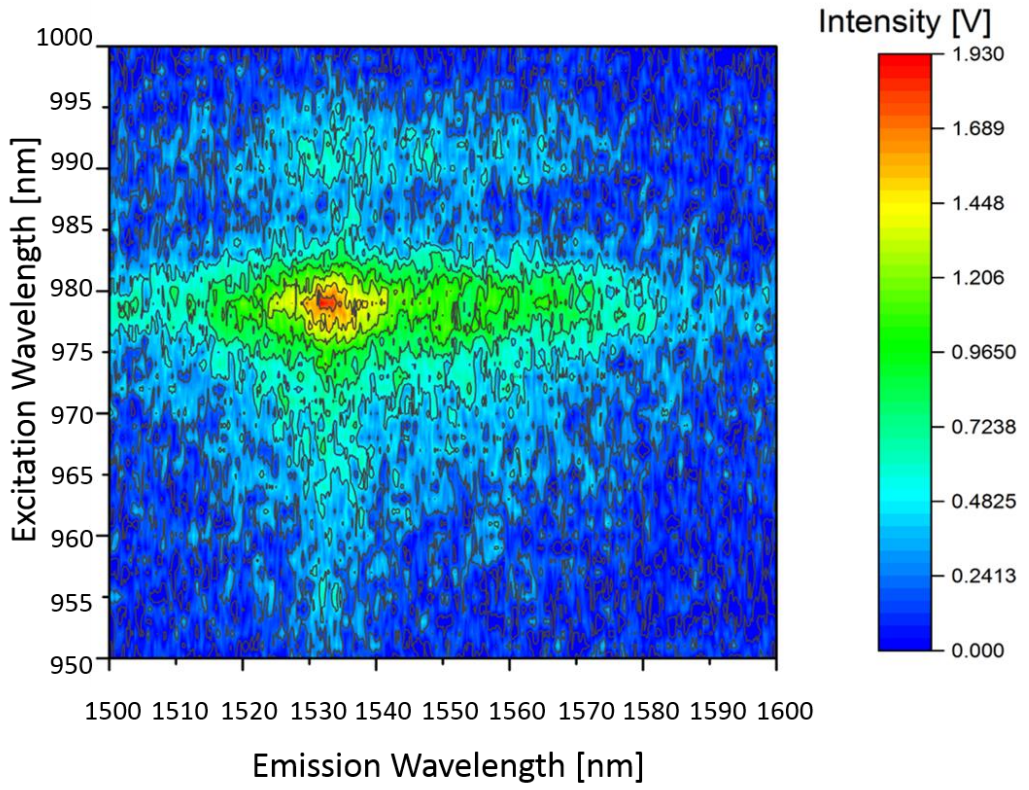

Figure 3.2. Emission map of 0.1 at. % Er_2O_3 + Al_2O_3. Excitation band of the $^4I_{13/2} \rightarrow {}^4I_{15/2}$ band centered at ~978 nm and emission at ~ 1532 nm at room temperature.

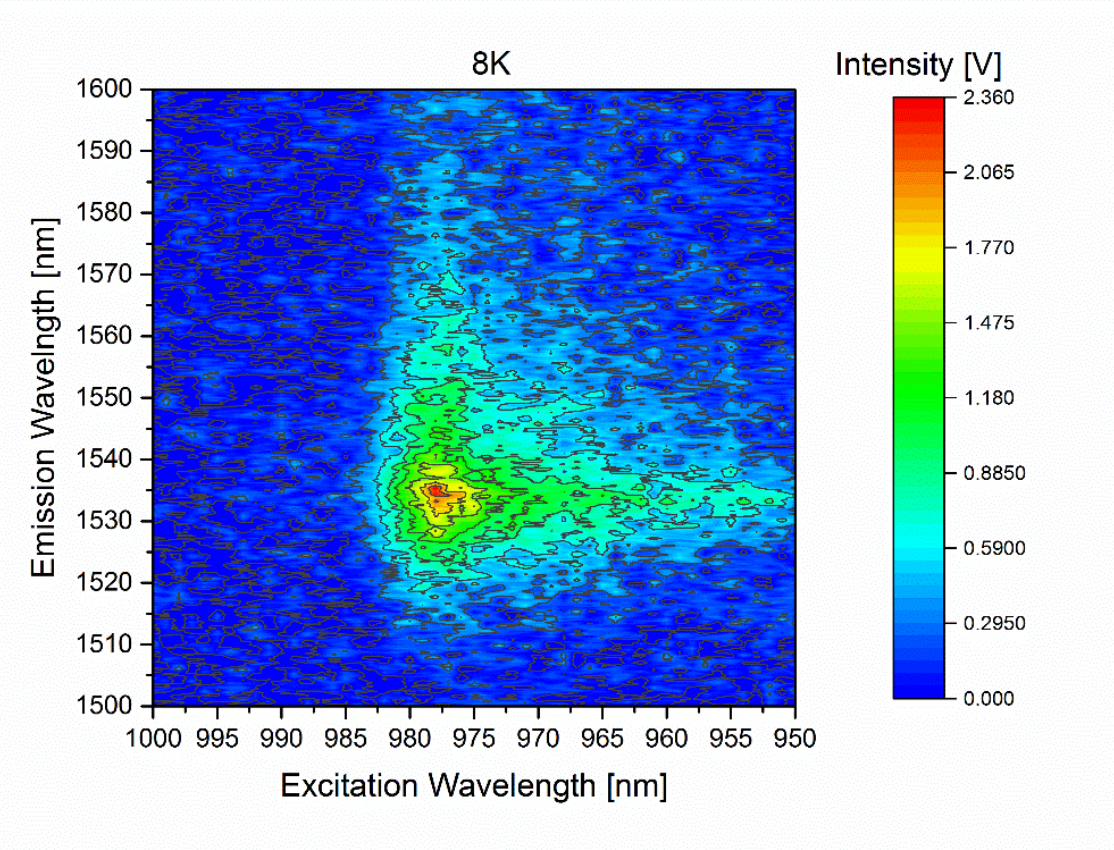

Figure 3.3. Emission map of 0.1 at. % Er_2O_3 + Al_2O_3. Excitation band of the $^4I_{13/2} \rightarrow {}^4I_{15/2}$ band centered at ~982 nm and emission at ~ 1532 nm at 8K.

Figure 3.4a shows SE micrographs of the processed 0.1 at. % Er_2O_3 + Al_2O_3 powder prior to densification, revealing relatively uniform sub-micron particle sizes (~ 200 nm). Fig. 3.4b shows SE micrographs of a fracture surface of the densified ceramic. The micrograph reveals a well densified sample, with fine equiaxed grains (average grain size is be ~ 250 nm). Relatively few very small pores (> 50 nm) can be identified in the samples.

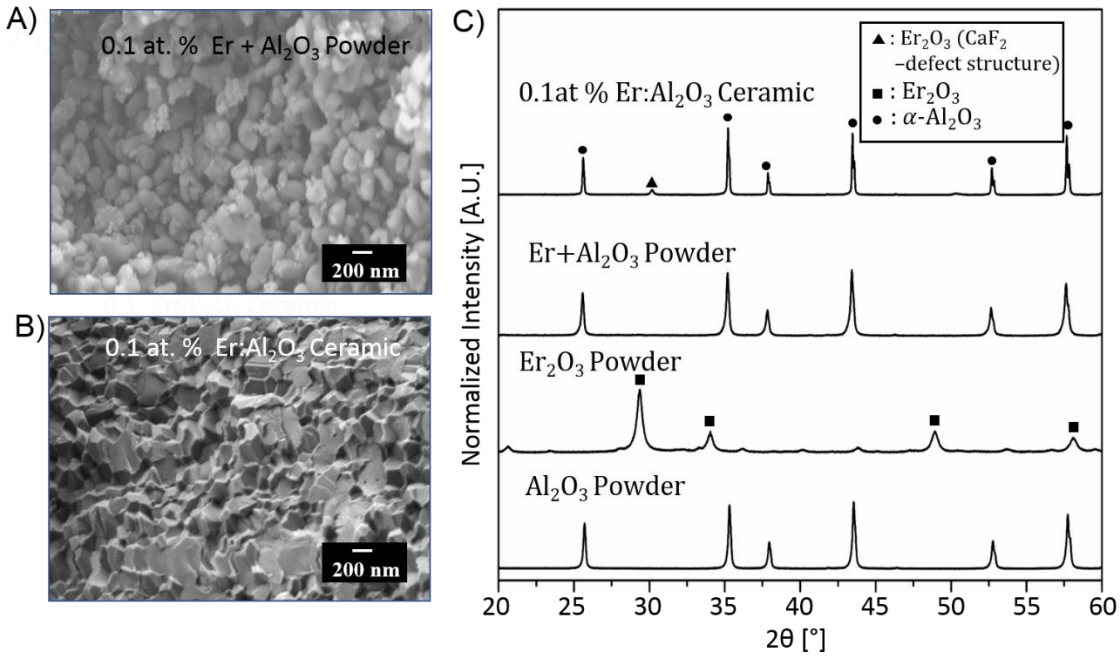

Figure 3.4. Microstructural characterization of $Er:Al_2O_3$. SE micrographs of a) the processed 0.1 at. % Er + Al_2O_3 powder prior to densification b) the fracture surface of the 0.1 at. % $Er:Al_2O_3$ densified ceramic. XRD profiles c) of Al_2O_3 powder, Er_2O_3 powder, Al_2O_3 + Er powders and 0.1 at. % $Er:Al_2O_3$ bulk ceramic after CAPAD processing. The ceramic bulk sample shows a clear secondary phase (indicated with a triangle).

Figure 3.4c also shows XRD profiles of constituent powders Al_2O_3 powder, Er_2O_3 powder, Al_2O_3 + Er_2O_3 powders after PBM and Al_2O_3 + Er_2O_3 bulk ceramic after CAPAD processing. XRD profile of the processed powder shows only peaks corresponding to Al_2O_3, suggesting that no secondary phase formed during the mechanical milling. The XRD spectra of the densified ceramic Figure 3.4c shows that the majority of peaks are attributable to the Al_2O_3. In addition, there is a minor peak centered at $2\theta = 30.7$ °, corresponding to the highest intensity peak for Er_2O_3 with a CaF_2 defect structure [15]. Since this peak was not present in the pre-densified

powder, we believe this phase likely formed through our high temperature (and high pressure) processing.

Figure 3.5a shows the transmission measurements of consolidated 0.1 at % Er: Al_2O_3, revealing high transparency, especially in the NIR region. Since the purpose of this study is the development of gain media for emission in the 1.5 μm region, high transparency is most important in the NIR region. The lower transparency at lower wavelengths can be partially explained by scattering caused by polycrystalline nature and birefringence of the trigonal alumina crystal leading to a Rayleigh-Gans Debye (RGD) type scattering. This is consistent with earlier work on other RE and transition metal doped alumina [13, 16]. In addition, there is optical loss due to absorption as expected from Er^{3+} ions. In order to confirm the presence of optically active Er in the ceramic matrix, we performed excitation scans of the sample Figure 3.5b monitoring a known Er emission peak near 1500 nm (1532 nm in this case). The excitation spectra reveal closely spaced absorption peaks located between 300 – 550 nm as well as distinct peaks at 650 and 980 nm. This is strong evidence that the Er^{3+} dopant is incorporated and is optically active in the Al_2O_3 matrix.

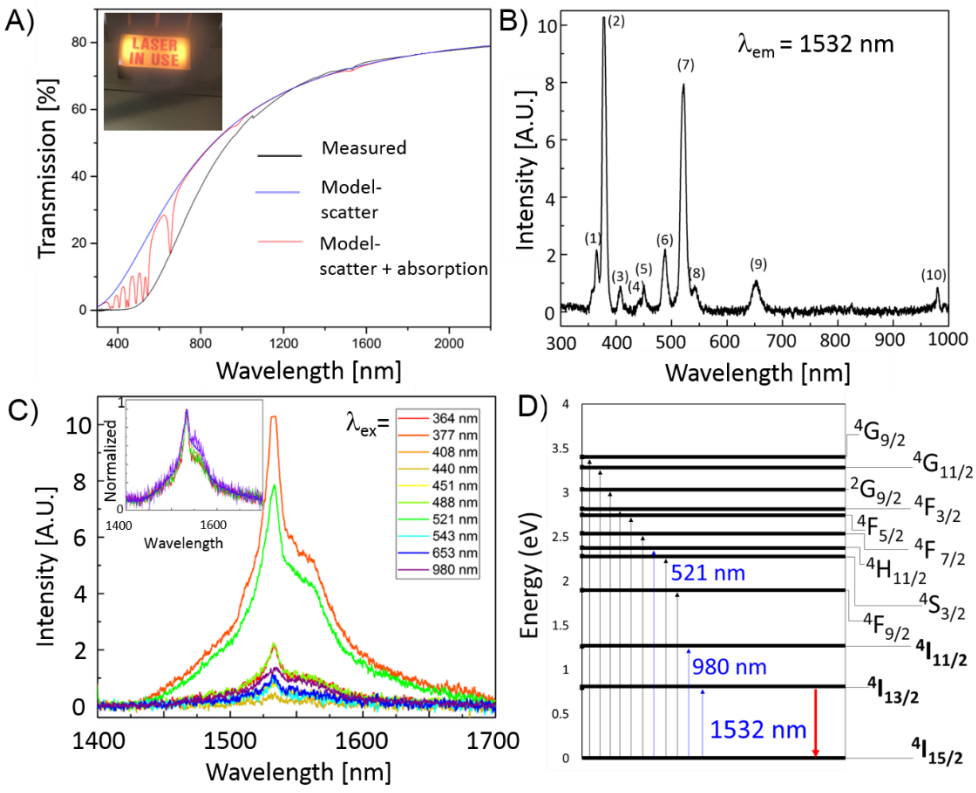

Figure 3.5. Spectroscopic characterization of the Er^{3+} bulk ceramic. a) transmission measurements of consolidated 0.1 at % Er: Al_2O_3. Using an RGD model to take account for scattering, a separate transmission curve was plotted with information about from our microstructural analysis, in order to reveal the effect of scattering by the polycrystalline nature and birefringence of the trigonal alumina crystal. Using the same model, we plotted another transmission curve, with known positions of absorption bands taken from our PLE spectra in (b) and from literature. In the inset, we hold the sample up against a lighted sign, which reveals a distinctive orange color, due to the various absorption bands in the blue-green region of the UV-Vis spectrum. The presence of optically active Er in the ceramic is shown with (b) PLE of the bulk ceramic, with all major peaks index from known Er transitions. c) PL emission spectra for the 0.1 at. % Er^{3+} ceramic excited at the absorption bands identified using the PLE spectra. The PL spectra reveal broad emission in all cases, attributable to transition from the $^4I_{13/2}$ manifold to the $^4I_{15/2}$ manifold, to further explain the (d) a proposed simplified energy diagram for Er:Al_2O_3 is constructed using the information from PLE and PL spectra.

The absorption peaks observed in the UV-Vis-NIR region (Fig. 3.2b) for the transparent sample are centered at λ_o = 364 nm, 378 nm, 408 nm, 440 nm, 451 nm, 488 nm, 521 nm, 543 nm, 653 nm, and 980 nm. These absorption bands are in

similar locations to those observed in previous reports of Er:Al_2O_3 [1] allowing us to attribute them to the $^4G_{9/2}$, $^2G_{11/2}$, $^2H_{9/2}$, $^4F_{3/2}$, $^4F_{5/2}$, $^4F_{7/2}$, $^2H_{11/2}$, $^4S_{3/2}$, $^4F_{9/2}$, and $^4I_{11/2}$ bands respectively. These energy bands along with their measured FWHM in Table 1**.** The existence of these optically active absorption bands gives the sample its distinctive orange color (see insert). We believe that distinct lines are not discernable in the transmission spectra because of they are closely spaced, relatively broad and in a region where there is significant scatter caused by birefringence in the polycrystalline alumina.

Table 1.1. Listed values of excitation peak locations and line breadth for Er:Al_2O_3.

Peak #	λ_o (nm)	Transition $\rightarrow {}^4I_{15/2}$	$\Delta\lambda$ (nm)
1	364	$^4G_{9/2}$	9.4
2	377	$^2G_{11/2}$	9.5
3	408	$^2H_{9/2}$	7.7
4	440	$^4F_{3/2}$	6
5	451	$^4F_{5/2}$	7.1
6	488	$^4F_{7/2}$	10.8
7	521	$^2H_{11/2}$	12.5
8	543	$^4S_{3/2}$	10.6
9	653	$^4F_{9/2}$	17.4
10	980	$^4I_{11/2}$	6.2

In order to confirm that the optical loss is due to Er^{3+} absorption as well as scattering, we applied a model we previously developed for transition metal (Cr^{3+}) dopants in alumina. The in-line transmission of a polycrystalline ceramic considering

scattering loss and absorption loss from multiple absorption lines can be written [16]:

$$T(\lambda) = \left[1 - 2\left(\frac{n-1}{n+1}\right)^2\right] exp\left[-l(\kappa + \sum_{i=1}^{j} g_i(\lambda)\alpha_i)\right] \qquad \text{(Eq. 3.1)}$$

where *n* is the refractive index, l is the thickness of the ceramic, *κ* is the scattering coefficient, *g*(λ) is the line shape function, *j* is the number of absorption lines and *α* is the absorption coefficient of each line. Assuming an RGD dominated scattering [16-18], $\kappa = d(\pi^2/\lambda^2)\Delta n^2 \chi$ where *d* is maximum grain size and χ is a parameter that depends on the degree of texturing in the ceramic. If there is no texture, *i.e.* the grains are randomly oriented, then χ = 0.28. The scattering model, using appropriate values for alumina, *n=1.76* and *Δn* = 0.008 and grain size of 250 nm, is shown in Figure 3.5a and overlaps well with the measured data at higher wavelengths confirming that scattering in samples is dominated by RGD type scattering similar to previous results of dense alumina [16]. The absorption line shape, assuming Lorentzian lines can be written $g(\lambda) = \left(\frac{(\Delta\lambda)^2}{4}\right)[(\lambda - \lambda_o)^2 + \left(\frac{\Delta\lambda}{2}\right)^2]^{-1}$ where *Δλ* is the full width of the line at half the maximum value. The model using scattering in addition to absorption with measured absorption line centers, λ_o values listed in Table 1 is also shown in Figure 3.5a. This model shows that the optical loss at wavelengths below ~ 800 nm can be explained by RGD type scattering and absorption is the sample caused by the closely spaces absorption lines due to Er^{3+} in the sample.

Figure 3.5c shows the PL emission spectra for the 0.1 at. % Er^{3+} ceramic excited at the absorption bands identified using the excitation scans Figure 3.5b. The

PL spectra reveal a broad emission in the 1500 - 1600 nm range in all cases, attributable to transition from the $^4I_{13/2}$ manifold to the $^4I_{15/2}$ manifold. As expected, the emission intensity depends on excitation band with the 377 and 521 nm band producing the most intense emission. However, the line shape of the emission remains similar as shown in the normalized emission with prominent peaks at 1532 and 1545 nm clearly visible in all cases. This suggest that the emission behavior is caused by very similar energy transitions regardless of the chosen pump band in 300 – 1000 nm range.

The line shape of the emission with the highest intensity (main) peak centered at 1532 nm and a side peak at 1545 nm is very similar to that observed in Er implanted alumina thin films [3]. The location of emission also closely resembles emission measured on Er:Al_2O_3 powders [1] and Er:Al_2O_3 ceramics at room temperature by Sanamyan et al [7]. They observed relatively broad emission between 1450 and 1600 nm with most intense emission peak is in the same location at 1532 nm. However, the line shape we observe is broader than Sanamyan et. al, likely due to the electronic environment near Er^{3+} in our samples being more disordered. Figure 3.5d is a proposed simplified energy diagram for Er:Al_2O_3 constructed using the excitation (Figure 3.5b) and emission scans (Figure 3.5c).

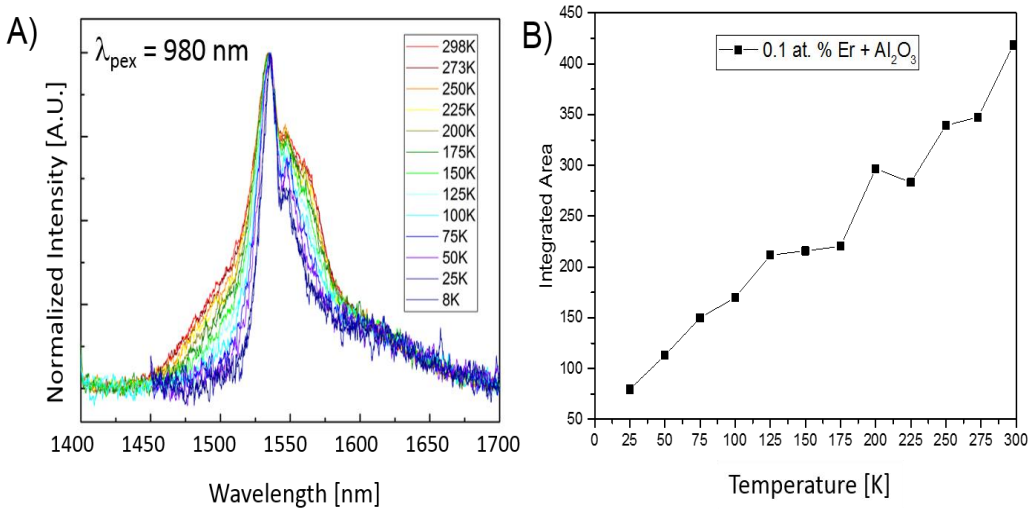

Figure 3.6. a) PL spectra of the $^4I_{13/2} \rightarrow {}^4I_{15/2}$ at varying temperatures, from 298 K to 8 K. The measurements show clear temperature broadening. Temperature broadening is shown more quantitatively in b) a plot of the integrated area of the PL intensity *vs.* measurement temperature. The integrated area is ~ 4× higher at room temperature compared to 25 K.

In order to better understand the nature of the broad emission of our Er:Al_2O_3, we performed cryogenic PL measurements. The sample was excited with a 980 nm diode laser, in order to investigate the $^4I_{13/2} \rightarrow {}^4I_{15/2}$ transition. Figure 3.6a, shows PL spectra at varying temperatures, from 298 K to 8 K. The measurements show clear temperature broadening; the location of the most intense peak does not change, but the shoulders on either side get considerably broader with increasing temperature.

Temperature broadening is shown more quantitatively in Figure 3.6b, a plot of the integrated area of the PL intensity *vs.* measurement temperature. The integrated area is ~ 4× higher at room temperature compared to 25 K. A similar temperature dependence was observed by Sanamyan et al [7]. At 77 K the lines observable in their emission cross section measurements were much more clearly discernable

compared to overlapping temperature broadened lines at room temperature. In inhomogeneously broadened materials, the spectral lines are expected to be independent of temperature, thus line broadening in our Er:Al_2O_3 is not exclusively caused by inhomogeneous broadening. However, even at low temperatures (8 K), we cannot resolve the individual thin lines are in our samples likely because of multi-site doping of Er^{3+} ions. Figure 3.7a shows the time dependent fluorescence of the $^4I_{13/2}$ to the $^4I_{15/2}$ transition monitoring 1532 nm (excited using 980 nm). The inset shows the decay curves plotted on a logarithmic scale. The linear dependence on a log scale suggest that the lifetimes are exponential consistent with previous work on low Er concentrations. The measured lifetime was 1.9 ms which is in the range of lifetimes reported for Er doped ceramics measured at this transition. Previous lifetime measurements range from 0.1 ms in Er:YAG, to 3.6 ms in Er:Y_2O_3 [19]. We believe these lifetimes are good approximations to the purely radiative lifetimes due to the low Er concentration in our ceramic which reduces the probability of upconversion and other concentration quenching processes [7].

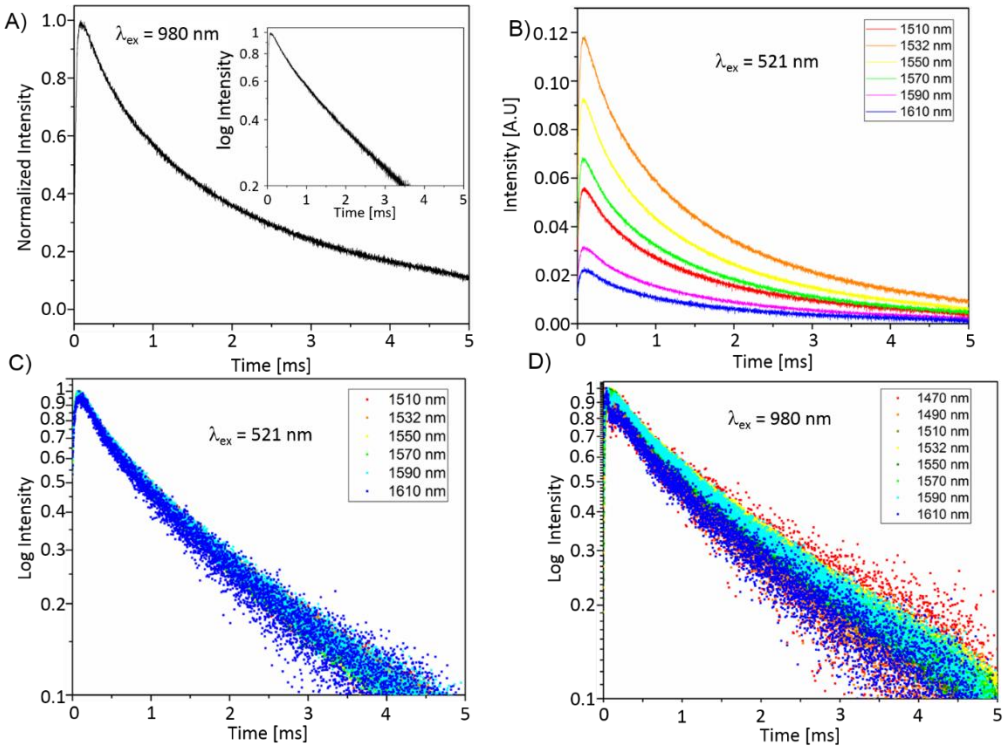

Figure 3.7. Analysis of the time dependent fluorescence of the bulk ceramic (a) the $^4I_{13/2} \rightarrow {}^4I_{15/2}$ transition, with the inset showing the decays plotted on a logarithmic scale. The measured lifetime was 1.9 ms, (b) decay curves taken using the same excitation wavelength, λ_{ex} = 521 nm, while monitoring emission across the emission bandwidth (λ_{em} = 1510 nm to 1610 nm). This is easily shown in (c) showing the same excitation (λ_{ex} = 521 nm) with normalized intensity plotted on a logarithmic scale. The data overlap confirming the same lifetime thus strongly indicating a similar nature of emission across the broad bandwidth. This was also confirmed, in (d) using an excitation of λ_{ex} = 980 nm, plotted on logarithmic scale showing similar emission behavior across the broad bandwidth (λ_{em} = 1470 nm to 1610 nm).

Given the very broad nature of the emission (Figure. 3.2c and 3.3a) it is interesting to see if the lifetime varies across the emission wavelength range. Figure 3.7b shows decay curves taken using the same excitation wavelength, λ_{ex} = 521 nm, while monitoring emission across the emission bandwidth (λ_{em} = 1510 nm to 1610 nm). As expected, the intensity of emission varies significantly with the monitored wavelength, consistent with the static emission measurements (Figure 3.2c). Interestingly, the lifetime shows very little variation across the very broad emission;

The measured lifetime of the single exponential fit ranges from τ = 1.4 to 1.9 ms (λ_{em} = 1470 nm to 1610 nm). This is more easily appreciated in Figure 3.7a, showing the normalized intensity plotted on a logarithmic scale. The data overlap confirming the same lifetime thus strongly indicating a similar nature of emission across the broad bandwidth. This would not be the case if the Er ions responsible for emission had a very different electronic environment. We also confirmed that the lifetimes are consistent when exciting with 980 nm, as shown in Figure 3.7d.

Having confirmed the high transparency in ceramic samples, with expected Er^{3+} transitions with reasonably long lifetimes we can now discuss the 0.1 at % Er as laser gain material by finding the absorption and emission cross sections. We again concentrate on the emission band at 1.53 μm arising from the $^4I_{13/2} \rightarrow {}^4I_{15/2}$ transition because it is useful for optical communication and IR laser applications at a relatively eye safe range.

We can obtain absorption cross section, σ_{abs} spectra by using the total Er^{3+} concentration in the expression, $\sigma_{abs} = \alpha/N$, where σ_{abs} is the, α is the absorption coefficient, and N is the volumetric concentration of Er^{3+} ions contributing to the absorption spectrum. α was measured estimated using the transmission measurement and N was assumed to be the initially added concentration of Er. In order to not overestimate the absorption coefficient (and cross section values), we considered only absorption observable below the scattering envelope. This analysis was performed and plotted for both the $^4I_{11/2}$ and $^4I_{13/2}$ manifold, shown in Figure 3.8a and 3.8b. The value of the absorption cross section, $\sigma_{abs} \sim 10^{-21}$ cm^2, is relatively low

in comparison to other erbium doped oxides with the given concentrations. We believe this is due to the conservative nature of our measurement scheme.

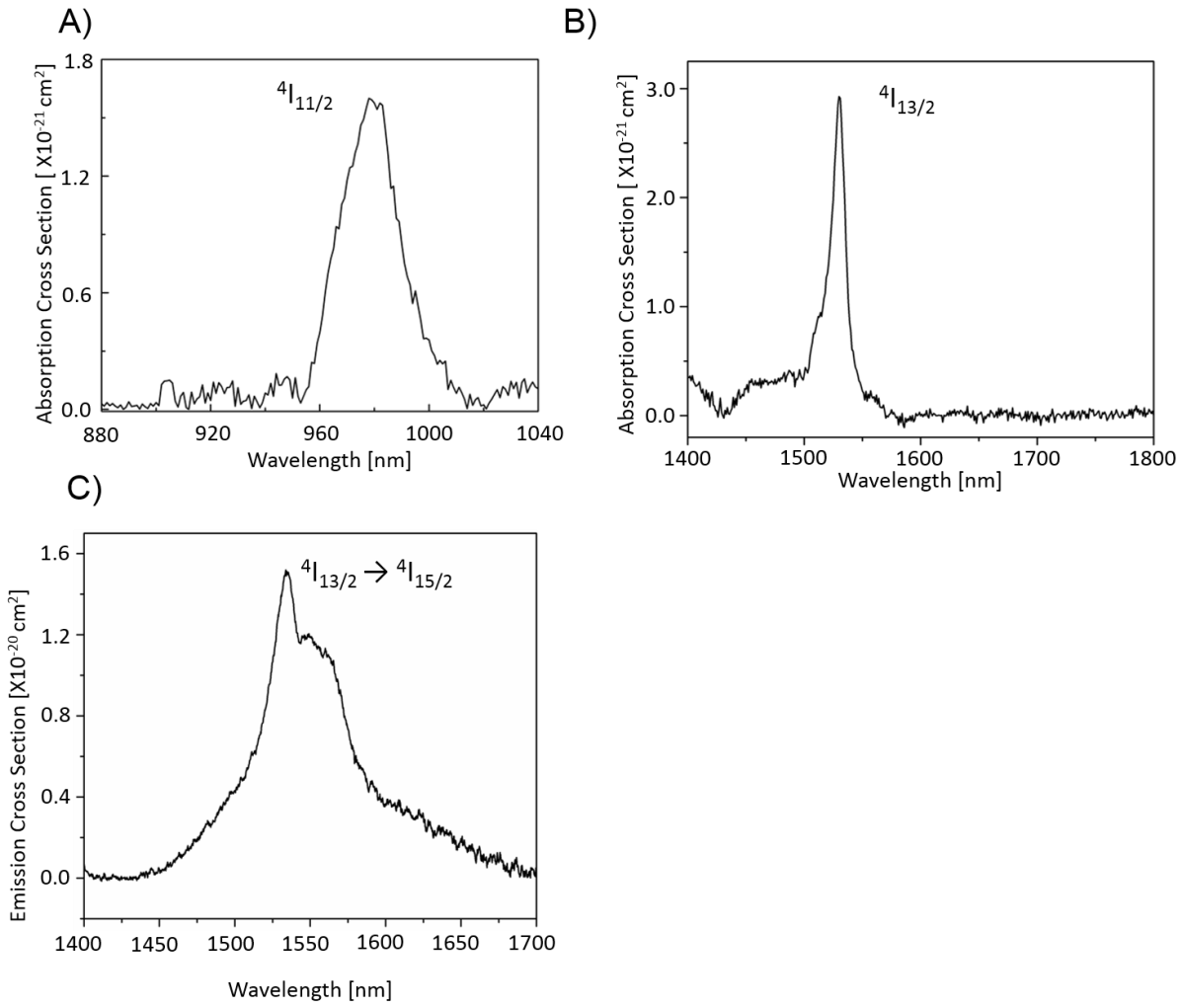

Figure 3.8. Absorption cross of the a) $^4I_{11/2}$ and b) $^4I_{13/2}$ transition and c) is stimulated emission cross section spectra of the $^4I_{13/2} \rightarrow {}^4I_{15/2}$ transition, at room temperature. The absorption cross sections were calculated from measured absorption spectrum and the stimulated emission cross section was calculated using the Fuchtbauer –Ladenburg Relation.

Emission cross sections in Er dopants are most often determined using the reciprocity method [20] and the Fuchtbauer – Ladenburg method (F-L Method) [21]. The reciprocity method is problematic for our samples due to the difficulty in separating pure absorption from scattering as discussed above. Thus, we estimated

the emission cross section σ_{em} from the measured room temperature fluorescence spectrum and the measured lifetime, using the Fuchtbauer – Ladenburg method, (F-L Method) [21]:

$$\sigma_{em}(\lambda) = \frac{\lambda^5}{8\pi n^2 c \tau_{rad}} * \frac{I(\lambda)}{\int \lambda I(\lambda) d\lambda} \qquad \text{(Eq. 3.2)}$$

where $I(\lambda)$ is the normalized fluorescence intensity, λ is the fluorescence wavelength, τ_{rad} is the fluorescence lifetime, *n* and *c* are the refractive index and the light velocity, respectively. Based on an assumption that in our samples, they exhibit a purely radiative lifetime decay, a nonradiative quenching process leads us estimate the quantum efficiency, η, of this transition to be close to 1. It is important to note that we have confirmed that the lifetimes are same over this range (Figure 3.8c, d), justifying the use (Eq. 3.2) integrating from 1400 - 1700 nm.

The emission cross section is shown in Figure 3.10c. The data show that the maximum cross section is our Er ceramic has an emission cross section value of, 1.5 × 10^{-20} cm^2. This value compares favorably with other Er doped media. It is similar to that previously reported by Sanamyan et al [7] in Er:Al_2O_3 ceramic. Most interesting perhaps is that it is it is higher than that observed in Er:YAG which is σ_{em}= 1.5 ×10^{-20} cm^2 [22], making the Er:Al_2O_3 ceramics a promising gain media.

As mentioned in Chapter 1.6, the effective stimulated-emission cross section (σ_{em}) and radiative lifetime (τ_{rad}) are two important parameters for the assessment of a laser crystal. We can calculate the product $\sigma\tau$ at the peak lasing wavelength as determined by the measured emission spectra of the differently doped media. With

our measured lifetime of 2.02 ms and the calculated emission cross section of 1.5 x 10^{-20} cm^2, we have a sigma tau product of 3.03 x10^{-20} cm^2*ms.

Another interesting parameter is the gain cross section gain that leads to an estimation of the probable operating laser wavelength. If *P* is the population inversion rate for $^4I_{13/2} \rightarrow {}^4I_{15/2}$ Er^{3+} laser transition, the gain cross section can be calculated using the following relation:

$$\sigma_{gain} = P * \sigma_{em}(\lambda) - \left(1 - P * \sigma_{abs}(\lambda)\right) \qquad \text{(Eq. 3.3)}$$

where σ_{em} and σ_{abs} are emission and absorption cross sections, respectively and P is degree of population inversion. A value of *P* = 1 signifies complete population inversion (all electrons are in excited state) and at *P* = 0, all electrons are in the ground state. The wavelength dependence of the gain cross section was calculated for different values of population inversion *P* (*P* = 0, 0.1, 0.2, . . . ,1) and are shown in Figure 3.9.

To achieve lasing at 1532 nm, $^4I_{13/2} \rightarrow {}^4I_{15/2}$, the population inversion rate is expected to be higher than 0.5. For a population inversion level of 0.6, the gain cross-section value is 1.2 x10^{-20} cm^2 at 1532 nm. This gain cross section is comparable to other proven gain media such as Er^{3+}:Sc_2O_3 with a reported $\sigma_{gain} = 2.47 \text{ x}10^{-21} \text{ cm}^2$ at 1534.4 nm [22]. The present results suggest that Er^{3+}:Al_2O_3 transparent ceramics could be a promising laser material operating near 1.53 μm.

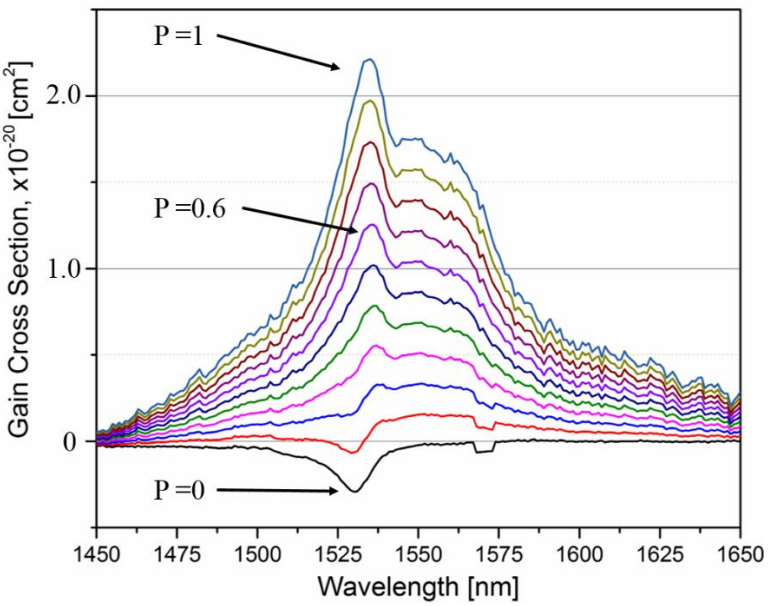

Figure 3.9. Gain cross section calculated for different values of *P* for $^4I_{13/2} \rightarrow {}^4I_{15/2}$ transition of Er^{3+} in Al_2O_3 transparent ceramic.

The gain cross section calculated for different values of *P* for $^4I_{13/2} \rightarrow {}^4I_{15/2}$ transition suggests that Er^{3+} doped in Al_2O_3 transparent ceramic could be good solid-state laser media, especially in the range of about 1.53 μm.

3.4. Summary

In summary, through the powder processing with ball milling and consolidation with CAPAD, a transparent Er^{3+} doped Al_2O_3 ceramic was fabricated. This work presents spectroscopic evidence of optically active trivalent Er^{3+} ions in Al_2O_3 host despite the significant ionic radius mismatch between dopant and host material. Room temperature photoluminescence revealed broad emission peaks in the 'eye-safe' region of ~ 1.5 μm, which corresponds to the known Er^{3+} $^4I_{13/2} \rightarrow {}^4I_{15/2}$ transition. When operating at cryogenic temperatures, as low as 10 K, the emission peaks are narrowed revealing thermally broadened emission. In addition, ~ 1.5 μm emission has relatively long lifetimes that do not vary across a broad emission spectrum (1.5 -

1.6 μm), suggesting similar electronic environment of optically active Er sites. The emission cross section was calculated from the derived Fuchtbauer– Ladenburg method, 2.69 x10^{-20} cm^2, which is particularly high for Er:Al_2O_3, at this transition. Detailed spectroscopic study of the ground state $^4I_{15/2}$ and the excited Er^{3+} $^4I_{13/2}$ manifold in Al_2O_3 can hopefully lead to future design to further improve the optical characteristics for the development of high power Er:Al_2O_3 lasers. It is of interest to us to eventually "resonantly" pumped our ceramic even though laser diodes at the relevant wavelengths (~ 1450 - 1530 nm) are considerably less efficient than those at ~ 980 nm. The spectroscopy at this transition is of interest as a possible laser design scheme and then be able to compare our works with others.

3.5. Acknowledgments

Funding for this work form the DE-JTO and the office ONR is gratefully acknowledged. Chapter 3, in part is currently being prepared for submission for publication of the material. Chapter 3 is coauthored with Elias Penilla, Matthew Wingert, Yasuhiro Kodera, and Javier Garay. The dissertation author was the primary investigator and author of this material.

3.6. References

[1] A. A. Kaplyanski, , A. B. Kulinkin, A. B. Kutsenko, S. P. Feofilov, R. I. Zakharchenya, and T. N. Vasilevskaya, "Optical spectra of triply-charged rare-earth ions in polycrystalline corundum," Physics of the Solid State Volume 40, Number 8 Aug (1998).

[2] X.J. Wang, "Phase structure and photoluminescence properties of Er^{3+}-doped Al_2O_3 powders prepared by the sol–gel method." Optical Materials 26 (2004) 247–252

[3] G. N. van den Hoven, E. Snoeks, and A. Polman, J. W. M. van Uffelen, Y. S. Oei, and M. K. Smit, “Photoluminescence characterization of Er-implanted Al203 films” Appl. Phys. Lett. 62, 3065 (1993).

[4] Q. Song, C-R. Li, J-Y. Li, W-Y. Ding, S-F. Li, J. Xu, X-L. Deng, C-L. Song, “Photoluminescence properties of the Yb:Er co-doped Al2O3 thin film fabricated by microwave ECR plasma source enhanced RF magnetron sputtering” Optical Materials 28 (2006) 1344–1349

[5] Kumaran, R., Webster, S. E., Penson, S., Li, W. Tiedje, T., P. Wei, and Francois Schiettekatte, “Epitaxial neodymium-doped sapphire films, a new active medium for waveguide lasers” Opt. Lett. 34, 3358–3360 (2009)

[6] Kumaran, R., Tiedje, T., Webster, S. E., Penson, S. & Li, W., “Epitaxial Nd-doped α- (Al1−xGax)2O3 films on sapphire for solid-state waveguide lasers”. Opt. Lett. 35, 3793–3795 (2010).

[7] T. Sanamyan, R. Pavlacka, G. Gilde, M. Dubinskii. Spectroscopic properties of Er^{3+}-doped α-Al_2O_3. Optical Materials 35 (2013) 821–826

[8] K. Drdlíková, R. Klement, D. Drdlík, T. Spusta, D. Galusek and K. Maca. “Luminescent Er^{3+}doped transparent alumina ceramics”. Journal of the European Ceramic Society 37 (2017) 2695–2703

[9]. S. R. Casolco, J. Xu and J. E. Garay, “Transparent/translucent polycrystalline nanostructured yttria stabilized zirconia with varying colors.” *Scripta Materialia* (2008) **58,** 516-519.

[10] J. R. Morales, N. Amos, S. Khizroev and J. E. Garay, “Magneto-optical Faraday Effect in Nanocrystalline Oxides,” Journal of Applied Physics (2011)109, 093110.

[11]. Y. Kodera, C.L. Hardin and J.E. Garay, “Transmitting, emitting and controlling light: Processing of transparent ceramics using current-activated pressure-assisted densification” *Scripta Materialia* (2013), **69**, 149–154.

[12] E. H. Penilla, Y. Kodera, J.E. Garay, Blue-green emission in terbium-doped alumina (Tb:Al_2O_3) transparent ceramics, Adv. Funct. Mater. 23 (48) (2013) 6036–6043

[13] E. H. Penilla, L. F. Devia-Cruz, M. A. Duarte, C. L. Hardin, Y. Kodera, and J. E. Garay, “Gain in Polycrystalline Nd-doped Alumina: Leveraging Length Scales to Create a New Class of High-Energy, Short Pulse, Tunable Laser Materials” *Light: Science & Applications.* (2018) **7.**

[14] J. E. Garay, Annu. Rev. Mater. Res., 2010, 40:445-68

[15] A.A. Kashaev, L.V. Ushchapovskii and A.G. Il’in, “Electron-diffraction and x-ray diffraction study or rare earth metal oxides in thin films” Sov. Phys. Crystallogr., Vol. 20. No. 1 (1973).

[16] E. H. Penilla, C. L. Hardin, Y. Kodera, S. A. Basun, D. R. Evans, and J. E. Garay, “The role of scattering and absorption on the optical properties of birefringent polycrystalline ceramics: Modeling and experiments on ruby ($Cr:Al_2O_3$).” Journal of Applied Physics 119, 023106 (2016).

[17] Apetz and M. P. B. Bruggen, J. Am. Ceram. Soc. 86, 480 (2003).

[18] C. Pecharroman, G. Mata-Osoro, L. A. D_ıaz, R. Torrecillas, and J. S. Moya, Opt. Express 17, 6899 (2009).

[19] T. Sanamyan, J. Simmons, M. Dubinskii, “Efficient cryo-cooled 2.7-μm Er3+:Y2O3 ceramic laser with direct diode pumping of the upper laser level” Laser Phys. Lett. 8 (2010) 569–572.

[20] S. A. Payne, L. L. Chase, L. K. Smith, W. L. Kway, and W. F. Krupke Infrared Cross - Section Measurements for Crystals Doped with Er3+, Tm3+, and Ho3+, IEEE JOURNAL OF QUANTUM ELECTRONICS, (28) 1992 p. 2619

[21] Aull, Brian F., Jenssen, Hans P. Vibronic Interactions in Nd:YAG Resulting in Nonreciprocity of Absorption and Stimulated Emission Cross Sections. *IEEE J. Quantum Electron.* QE-18(5), 925–929 (1982).

[22] C. Gheorghe, S. Georgescu, V. Lupei, A. Lupei, and A. Ikesue, “Absorption intensities and emission cross section of Er^{3+} in Sc_2O_3 transparent ceramics” JOURNAL OF APPLIED PHYSICS 103, 083116 (2008).

Chapter 4. Synthesis, Densification and Characterization of Transparent Co-doped Chromium Erbium Al_2O_3 (Cr:Er:Al_2O_3)

4.1. Introduction

Wavelength-tunable lasers have become an important scientific tool in areas of research such as spectroscopy and photochemistry [1]. Titanium-doped sapphire (Ti:Sapphire) is the most successful solid-state laser material in the near-infrared (NIR) wavelength range due to its high saturation energy, large stimulated emission cross-section, and broad absorption gain bandwidths. range, its successful operation requires high-power blue-green pump success [2, 3].

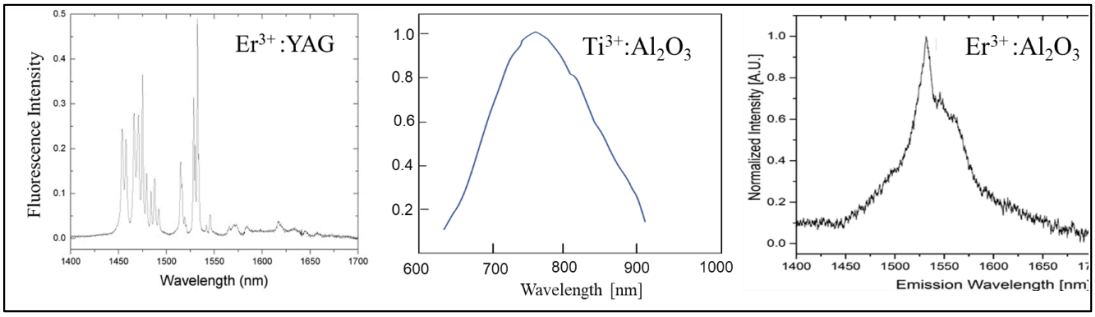

Figure 4.1. Comparison of emission bandwidth of 3 different gain media [4].

Transition metal ions like Ti^{3+} ion has a very large gain bandwidth (much larger than that of typical rare-earth-doped gain media, see Er:YAG in Fig. 4.1), allowing the generation of very short pulses and also wide wavelength tunability. The maximum gain and laser efficiency are obtained around 800 nm. The Ti^{3+} doping concentration has to be kept fairly low (e.g. 0.15% or 0.25%) because sapphire is an Al_2O_3 single crystal and crystal quality is will suffer as concentration increases. The therefore limited pump absorption usually enforces the use of a crystal length of several millimeters, which in combination with the small pump spot size (for high

pump intensity) means that a rather high pump brightness is required. The upper-state lifetime of Ti:Sapphire is short (3.2 μs) [5], and the saturation power is very high. This means that the pump intensity needs to be high, so that a strongly focused pump beam and thus a pump source with high beam quality is required [6].

With the development of nanopowder technology and vacuum sintering method, the optical quality of ceramics has been improved greatly and ceramic lasers can be obtained with a high efficiency that is comparable with that of single-crystal lasers [7]. As a result of their high thermal conductivity and feasibility of large-scale laser gain media, ceramic lasers have attracted much attention for the development of high-output-power and ultrashort-pulsed lasers, as an alternative to Ti:Sapphire lasers [8].

In this work, we propose Cr:Er:Al_2O_3 as a promising as a tunable near infrared laser gain material that can be pumped with 532 nm source, a wavelength commonly used for pumping Ti:Sapphire. Sensitizer ions different from the laser-active ion, can be added to a laser crystal to absorb additional energy from the pumping source and non-radiatively transfer excitation over to the active ion. A sensitizer of interest is chromium, Cr^{3+} (3d activator [9]) to solid-state media for function optical lighting applications. If the sensitizer ion induces broad, intense absorption bands in the crystal, then there can be a significant increase in pumping efficiency and, ultimately, laser efficiency.

Due to the three energy levels of the laser system and low absorption of Er^{3+} ions to the pump sources, it is difficult to increase the laser output efficiency.

Excitation of RE ions of Er, which originates from the f-f transitions which are forbidden and weak. In contrast to RE, excitation for Cr^{3+} are broad and intense bands arising from $^4A_{2g} \rightarrow {}^4T_{1g}$ and $^4A_{2g} \rightarrow {}^4T_{2g}$ transitions [10] and thus it has been widely used as a luminescent sensitizer for RE ions in order to obtain high excitation efficiency. If energy can be transferred from Cr^{3+} to the Er^{3+} ion, then intense near infrared (NIR) emission (~ 1.53 μm) can be obtained with excitation in the visible region.

In this study, we report on spectroscopic studies of Cr^{3+}:Er^{3+}:Al_2O_3 in order to identify how efficient the Cr^{3+} to Er^{3+} energy transfer is in Al_2O_3, to investigate it as a potential wide bandwidth NIR laser gain media. While co-doping with Cr and Er has been successfully demonstrated in YSGG [11, 12], RE doped α-Al_2O_3 has significantly higher thermal conductivity and fracture strength than state of the art gain media and can thus can potentially be used to significantly increase laser power output [13-15]. The NIR emission is important for several applications such as telecommunication [16] solar cell technologies [17], bio-imaging [18] and laser technologies [19]. The primary challenge to doping alumina with RE is the large ionic radii difference between REs and Al, the presumed substitutional dopant site. To date, co-doped RE:Al_2O_3 has been predominantly synthesized as phosphors [20] or in thin film form for optoelectronic applications using various deposition techniques [21]. Successful early work on Yb:Er:Al_2O_3 thin films by Song et. al [22] showed photoluminescence, PL, in the 1.5 - 1.6 μm range in Yb and Er ion implanted into alumina waveguide structures.

There have been significant advances towards ceramic Er:Al_2O_3 [23-25]. Recently, we have demonstrated highly transparent RE:Al_2O_3 with PL in the visible [26] and optical gain at ~1 μm [27] fabricated using Current Activated Pressure Assisted Densification (CAPAD). Here we incorporate Cr^{3+} and Er^{3+} into Al_2O_3 through mechanical milling and further densification processing via CAPAD. We also report the laser-related spectroscopic properties of the resulting Cr:Er:Al_2O_3 with the aim of evaluating Cr:Er:Al_2O_3 as a next generation laser-gain media. Intense pumping in the green spectral region will lead to intense emission at ~1.5 μm. The ceramic samples have high transparency at the emission 1.5 μm, sufficiently long radiative lifetimes and high absorption/emission cross sections which is promising for laser design.

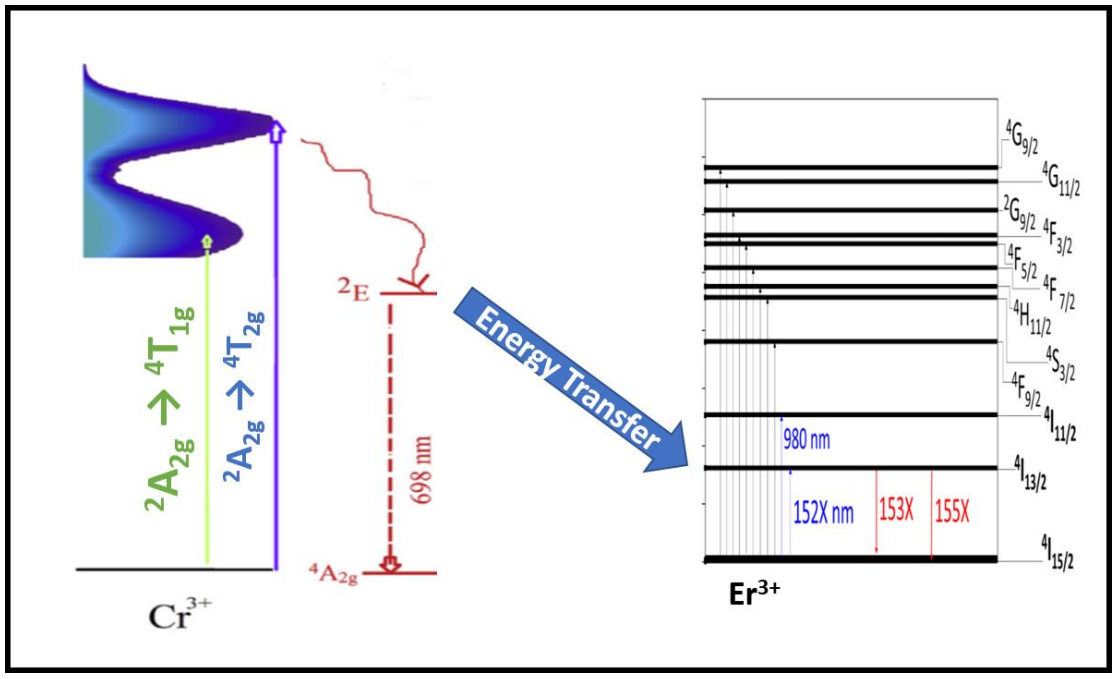

Figure 4.2. Mechanism of Cr^{3+} to Er^{3+} energy transfer in Cr^{3+}:E^{r3+}: Al_2O_3 bulk ceramic similar to [20].

Efficient pump absorption in Er bulk crystals are relatively difficult to achieve on the $^4I_{15/2} \rightarrow {}^4I_{13/2}$ transition, because the absorption cross sections are relatively small, and the doping concentration is limited by the need to avoid excessive quenching processes. Therefore, co-doping utilizes pumping options in the visible spectral region, other than at 980 nm. Chromium, Cr^{3+}, can absorb additional energy in the visible spectrum, due to the two broad absorption bands, $^4A_2 \rightarrow {}^4T_2$ around 550 nm and $^4A_2 \rightarrow {}^4T_1$ peaking around 400 nm, the blue and green spectrum, from a pump light source and partially transfer it to erbium ions [20]. Such media can be pumped with flash lamps, particularly when the absorption efficiency is optimized. The chromium ions can efficiently absorb pump radiation and then transfer the energy to erbium ions in the ground-state manifold, bringing them from $^4I_{13/2}$ to the $^4I_{15/2}$. From that level, the ions quickly decay into the upper laser level $^4I_{13/2}$, so that energy transfer back to sensitizer ion is suppressed, as shown schematically in Figure 4.2. There are various dopant concentration combinations, between the erbium and chromium, that have been explored, which depend on the host material used as well as the erbium transition of interest. For the ~ 1.5 μm emission, a combination of low concentration Er and Cr would be ideal for the gain media.

4.2. Experimental Materials and Methods

4.2.1. Synthesis of Co-doped Bulk Powders

All samples were processed from commercially available aluminum oxide powder (α-Al_2O_3, 99.99% purity, ~ 200 nm particle size, TM-DAR, Taimei Chemicals Japan) as received as well as doped with Erbium Oxide, Er_2O_3 (99.5% purity, Inframat Materials, USA) and chromium (III) nitrate nonahydrate, $Cr(NO_3)_3$* $9H_2O$,

(99.99% purity, Alfa Aesar Ward Hill, MA, USA). The powders were weighed to achieve Er^{3+} doping levels of 0.1, and 0.25 at. %. The erbia and alumina powders were mixed for 12 hours by low-energy ball milling. Ultra-High Purity (UHP, 99.99% purity) water was used as a dispersant solution at a ratio of 10 grams of powder to 200 mL of UHP water. Alumina balls (99.9% density and purity, Performance Ceramics Co., Peninsula, OH USA) with 5 mm diameters were used as the milling media, at a 1:15 powder: ball weight ratio. After milling, the powders were sieved to separate from the milling media and then dried under vacuum at 70°C for 24 hours in an oven. Dried powders were subsequently planetary ball milled (PBM) with UHP water at 150 rpm for 3 hours. The chromium nitrate was weighed to achieve Cr^{3+} doping levels of 0.1 and 0.25 at. %. The erbium doped alumina powder was mixed with the Alumina + $Cr(NO_3)_3$* $9H_2O$ powder for 3 hours via planetary ball milling using 10 mm silicon nitride milling media at 450 rpm and a 1:10 powder: ball weight ratio. After milling, the powders were sieved to separate them from the milling media and stored dry until densification.

4.2.2. Processing of Co-doped Bulk Ceramic

The Al_2O_3 with Er and Cr dopant precursors prepares according to powders were densified using the CAPAD technique [28]. In all cases, 0.330 g +/- 0.001 g of powder were placed into a graphite die with an outer diameter of 19 mm and inner diameter of 10 mm. The powder was secured between two graphite punches of the same outer diameter. The die, plunger, and powder were placed into the CAPAD and secured between two graphite spacers and copper electrodes. A maximum vacuum of 2×10^{-2} Torr was achieved in all cases.

The powder was pre-pressed at 105 MPa for 5 minutes to create a dense green body. Afterwards, the pellet was subjected to an applied pressure of 120 MPa over a three-minute period in parallel with simultaneous heating to achieve and maintain temperatures of 1250 – 1300 °C. The sample temperatures are measured with an optical pyrometer, focused on a hole drilled in the graphite die located at the center point of the die height. The samples were held at temperature for 5 minutes.

Structural characterization

Prior to characterization, samples were polished using diamond abrasive wheels followed by alumina paste on felt wheels to 1 μm. To characterize morphology, a Carl Zeiss Sigma 500 Field Emission Scanning Electron Microscope (FE-SEM) was used. X-Ray Diffraction patterns were attained using a Phillips X'Pert Diffractometer (ModelDY1145), in point source mode system equipped with a copper source. Samples were pressed flat on a zero-background plate and measured.

Optical characterization

Optical transmission spectra were taken on an Agilent Technologies Cary 5000 spectrophotometer from 300 nm - 2500 nm. The bulk polished samples were placed at normal incidence to the beam path. The scans were obtained at a rate of 60 nm min^{-1}.

Photoluminescence data were taken on a PTI Horiba Spectrophotometer Quanta Master 8000 with spectrally filtered dual monochromators and using a Xenon Arc Lamp as a light source. All measurements were taken in front face mode on polished bulk samples using a long pass 600 nm and 1050 nm cutoff filter to block

light scatter. Photoluminescence Excitation (PLE) scans were taken between λ_{ex} = 300 - 600 nm while monitoring the Cr^{3+} emission at λ_{em} = 694 nm. Also, excitations scan between λ_{ex} = 300 - 1000 nm while monitoring the Er^{3+} emission at λ_{em} = 1532 nm. Emission scans were taken for the Cr^{3+} bands between λ_{em} = 500 - 800 nm while pumping multiple absorption bands at λ_{ex} = 400, 532 nm for Cr^{3+} as it was determined to be effective pumping wavelengths from the excitation spectra. Scans for Er^{3+} emission were taken between λ_{em} = 1400 - 1800 nm while pumping multiple absorption bands for Cr^{3+} and Er^{3+} at λ_{ex} = 400, 532, and 980 nm. All measurements were taken with varying integration times between 0.1 – 1 sec per nanometer and a varying step size of 0.1 - 1 nm.

With the same experimental setup, PL lifetime measurements were collected using a Continuum Surelite EX nanosecond laser, coupled to a Horizon Optical Parametric Oscillator as a monochromatic excitation source with pulse widths of 6 ns. Exponentials were fit to the raw data and PL lifetimes were defined as the time required for the normalized intensity to decrease by 1/e. Similar wavelengths for the static luminescence measurements were used for the decay measurements across all samples, with the exception that 532 nm wavelength was used.

4.3. Results and Discussion

Figure 4.3 shows XRD profiles of Cr:Er:Al_2O_3 bulk ceramic after CAPAD processing. XRD profile of the processed ceramic shows peaks corresponding to Al_2O_3, as well as a minor peak centered at 2θ = 30.7 °, corresponding to the highest intensity peak for Er_2O_3 with a CaF_2 defect structure, as discussed in Chapter 3.3. Since this peak was not present in the pre-densified powder, we believe this phase

likely formed through our high temperature (and high pressure) processing. There is no trace of chromium formation with the incorporation of the chromium nitrate at either concentration.

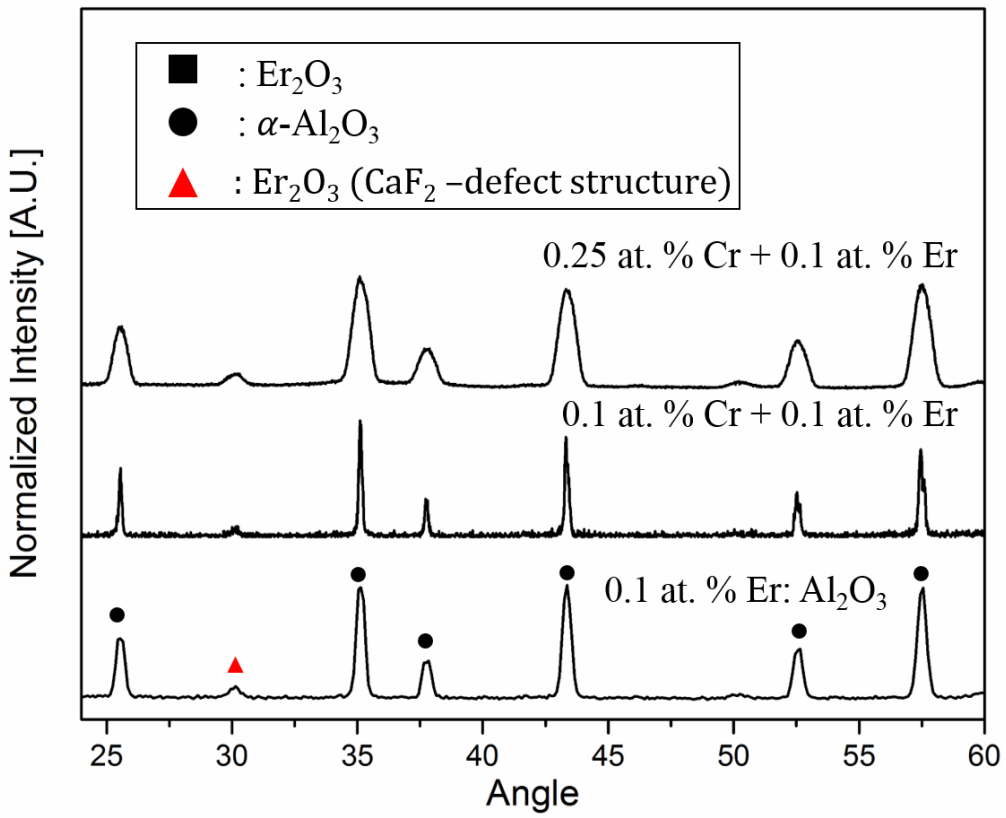

Figure 4.3. Microstructural characterization of Cr:Er:Al_2O_3. XRD profiles c) of Al_2O_3 powder, Er_2O_3 powder, Al_2O_3 + Er powders and 0.1 at. % Er:Al_2O_3 bulk ceramic after CAPAD processing. The ceramic bulk sample shows a clear secondary phase (indicated with a triangle).

Since the powder used for the planetary ball milling for mixing in the $Cr(NO_3)_3$, came from the ball milled powder of the Er_2O_3 + Al_2O_3 batch, it is not surprising that the same secondary phase is seen in the diffraction measurement. In Figure 4.4, we show UV-Vis-NIR transmission measurements of the single doped and co doped ceramics. Based on the transmission spectra, the singly Er^{3+} doped ceramic displayed the well-known, $^4I_{15/2}$ absorption band, as well as the various absorption

bands in the UV-Vis region, which cannot be discerned here, as discussed in Chapter 3.3. The co-doped samples display two Cr^{3+} absorptions bands centered around 400 and 550 nm which correspond to the $^4T_{1g}$, and $^4T_{2g}$. These absorption bands are evidence of incorporation of the Cr^{3+} ions in the Al_2O_3 matrix. There are also indications of Er^{3+} ions incorporated into this ceramic as there is the presence of absorption band centered around ~ 1.53 µm.

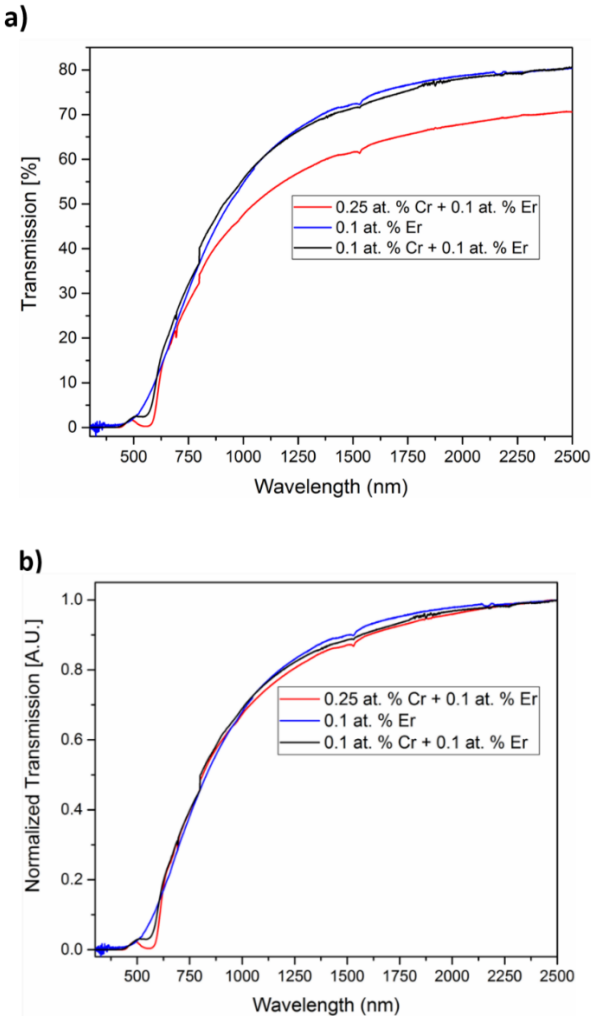

Figure 4.4. Transmission curves of (a) 0.1 at % Er:Al_2O_3, 0.1 at. % Cr + 0.1 at. % Er Al_2O_3 and 0.25 at. % Cr + 0.1 at. % Er: Al_2O_3. Data is plotted by (b) normalizing transmission in order to reveal the similar line trend despite the differences in transmission.

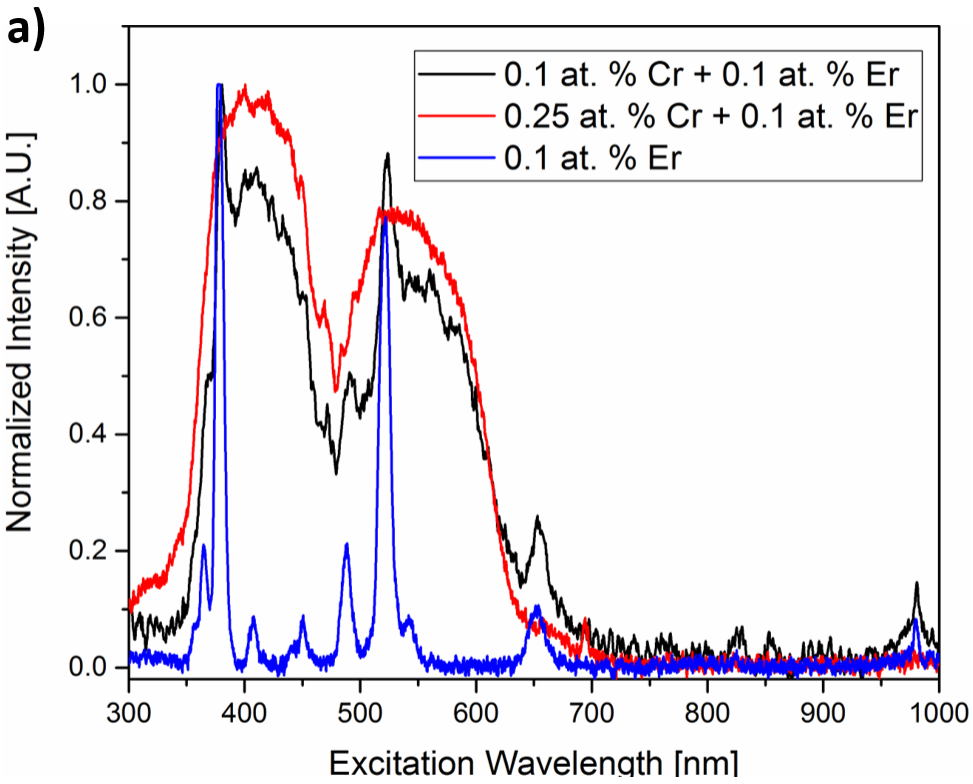

Figure 4.5. Spectroscopic PLE characterization of the Er^{3+} and Cr^{3+}:Er^{3+} co-doped bulk ceramic.

In order to confirm the presence of optically active Cr^{3+} and Er^{3+} ions in the ceramic, we performed excitation scans of the sample shown in Figure 4.5, monitoring emissions from a known Er^{3+} emission peak at centered around 1532 nm. While monitoring 1532 nm emission, the PLE spectra contains several weak narrow-line transitions due to f-f transitions of Er^{3+} super-imposed over the two broad Cr^{3+} bands centered around 450 and 550 nm. These bands appearing at 400 and 550 nm are the very similar as those observed for Cr^{3+}:Al_2O_3 as shown in our previous work [29]. These two bands can be assigned to the spin-allowed transitions $^4A_2$–$^4T_1$ and $^4A_2$–$^4T_2$ of Cr^{3+}, respectively. The excitation spectra also reveal closely spaced absorption peaks located between 300 – 550 nm as well as distinct peaks at 650 and

980 nm. This is strong evidence that the both Cr^{3+} and Er^{3+} ions are incorporated and are optically active in the Al_2O_3 matrix.

The PLE spectra for the 0.25 at. % Cr^{3+}:0.1 at. % Er^{3+}:Al_2O_3, exhibits similar behavior as the 0.1 at.% Cr^{3+}:0.1 at.% Er^{3+} ceramic, with intensities of the transitions varying. While monitoring emission at 1532 nm, the excitation spectra revealed two intense broad bands centered at 400 and 555 nm and a sharp band at 694 nm which correspond to the $^4A_{2g} \rightarrow {}^4T_{1g}$, $^4A_{2g} \rightarrow {}^4T_{2g}$ and $^4A_{2g} \rightarrow {}^2E$ ruby transitions. There are no clear signs of the various known Er^{3+} excitation transitions [30] as with the previous samples. The intensity of the Cr^{3+} excitation bands are shown to increase as the concentration is increased from 0.1 at. % to 0.25 at. %, as seen in Figure 4.5

This again is strong evidence that the both Cr^{3+} and Er^{3+} ions are incorporated and are optically active in the Al_2O_3 ceramic. Even though there are no signs of the Er^{3+} excitation transitions in the UV-Vis spectrum, there is no NIR emission at 1.5 μm without Er^{3+} ions being optically active.

Just as in the case with Er:Al_2O_3, there is a possibility that the electronic environment of the Er ion is slightly disordered, which can lead to a similar emission spectrum. However, the breadth and line shape of the emission spectra is different from what was presented in Chapter 3.3. There is more structure to the emission lines, there are peaks at 1469, 1490, 1553 and 1650 nm that are more pronounced than our Er^{3+} singly doped counterpart. This could mean that the energy dynamics of the emission process has been altered with the addition of the Cr^{3+} ions.

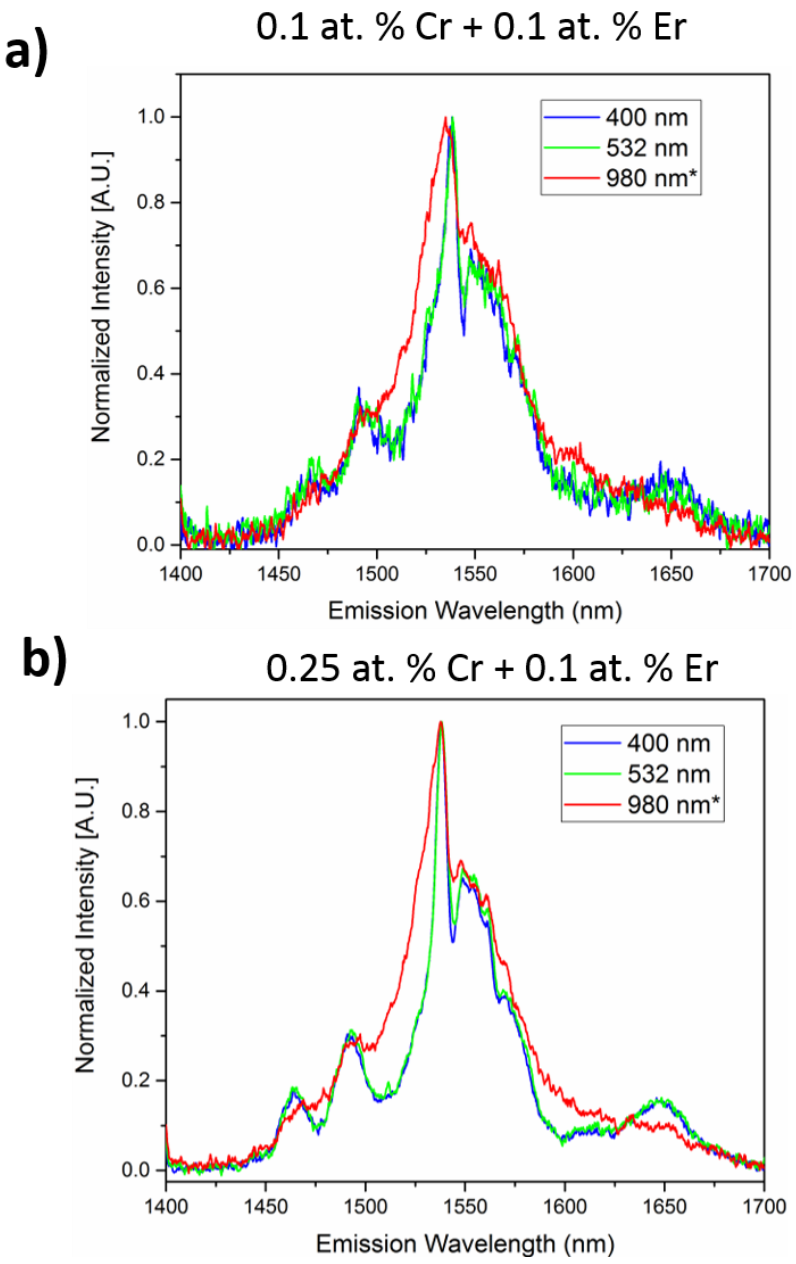

Figure 4.6. PL characterization of the Cr^{3+}:Er^{3+} bulk ceramics. PL emission spectra for the a) 0.1 at. % Cr^{3+}+ Er^{3+} and b) 0.25 at.% Cr^{3+} + 0.1 at.% Er^{3+} ceramic excited at the absorption bands identified using the PLE spectra. The PL spectra reveals broad emission in all cases, attributable to transition from the $^4I_{13/2}$ manifold to the $^4I_{15/2}$ manifold.

Figure 4.6 shows the emission spectra of our ceramic samples. The singly doped Er^{3+} ceramics display the same behavior in Chapter 3.3. The NIR emission originated from Er^{3+}:$^4I_{13/2} \rightarrow {}^4I_{15/2}$ transition can be clearly observed under the

excitation of Cr^{3+}:$^4T_{1g}$ and $^4T_{2g}$ energy levels, which can indicate an energy transfer from Cr^{3+} to Er^{3+} as discussed previously in Figure 4.4. Under 400 or 532 nm excitation, there would be no NIR emission in the ceramic without the Er^{3+}ions. For the co-doped ceramics, the intensities have been normalized and found to be very dependent on Cr^{3+} concentration. At a Cr^{3+} concentration of 0.1 at. %, the emission intensity is relatively low. As seen from the plots the signal-to-noise ratio is low. This can indicate that the energy isn't efficiently transferred from the Cr ions to the Er ions, however, at this stage, further analysis is needed to make that conclusion. When the Cr concentration is increased to 0.25 at.%, the transition at $^4I_{15/2}$ is shown, when exciting at various wavelengths, 400 and 532 nm, there is more observable emission structure than with our singly doped Er^{3+} ceramic. When both co-doped samples are pumped with 980 nm, they have similar emission structure as with the singly doped Er^{3+} ceramic. This is to be expected, as when the 980 nm pump light strikes the ceramic and excites the dopant.

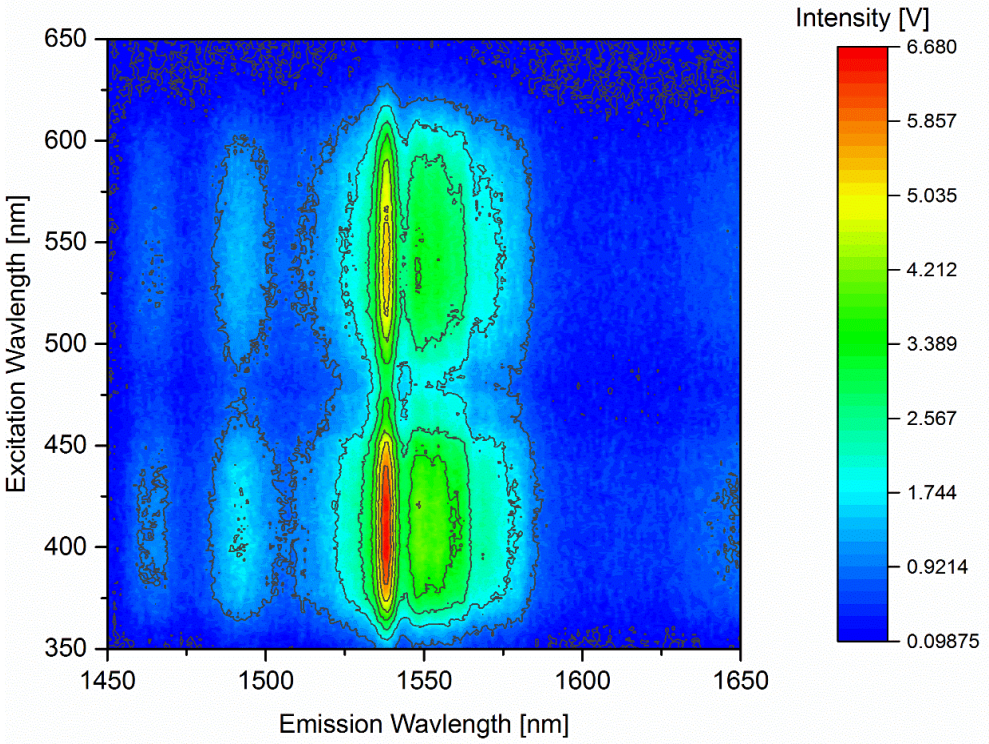

Figure 4.7 Emission Map of 0.25 at % Cr + 0.1 at. % Er: Al_2O_3 at room temperature. Two broadband excitation/emission bands are shown, arising from the $^4T_{1g}$ and $^4T_{2g}$ energy levels, to the $^4I_{13/2} \rightarrow {}^4I_{15/2}$ transition.

The emission map, shown in Figure 4.7, highlights the broadband emission of the 0.25 at % Cr + 0.1 at. % Er ceramic. As said before, the two chromium excitation bands are shown here, $^4T_{1g,}$ between ~ 375 – 460 nm and $^4T_{2g}$ which lies between ~ 480 – 620 nm, pump Er ions directly to $^4I_{13/2}$ energy level which then decay to the $^4I_{15/2}$ ground state. This gives that intense emission at ~ 1.53 um.

Again, 400 nm excitation does not lead to any emission in singly doped $Al_2O_3:Er^{3+}$. This emission is obtained only by f-f excitation around 980 nm or the other known Er^{3+} transitions [31], indicating that the emission described in Figure 4.6 is due to $Cr^{3+} \rightarrow Er^{3+}$ energy transfer. This is further substantiated by the excitation spectra shown in Figure 4.5. The energy transfer efficiency from $Cr^{3+} \rightarrow Er^{3+}$ can be

calculated based comparing the emission intensities of a ceramic with only Cr^{3+} ions present and another ceramic with both the Cr^{3+} ions and Er^{3+} ions. The concentration of Cr^{3+} ions are held constant for both ceramics. The efficiency of energy transfer can be based on the following expression [31, 32]:

$$\eta_{ET} = 1 - \left(\frac{I_s}{I_{so}}\right) \qquad \text{(Eq. 4.1)}$$

where η_{ET} is the energy transfer efficiency, I_s and I_{so} are the corresponding emission intensity of donor Cr^{3+} in the absence and the presence of the acceptor Er^{3+}, respectively. From data of Figure 4.8, η_{ET} for 0.25 at. % Cr^{3+}:0.1 at. % Er^{3+}:Al_2O_3 comes out to be ~ 15%.

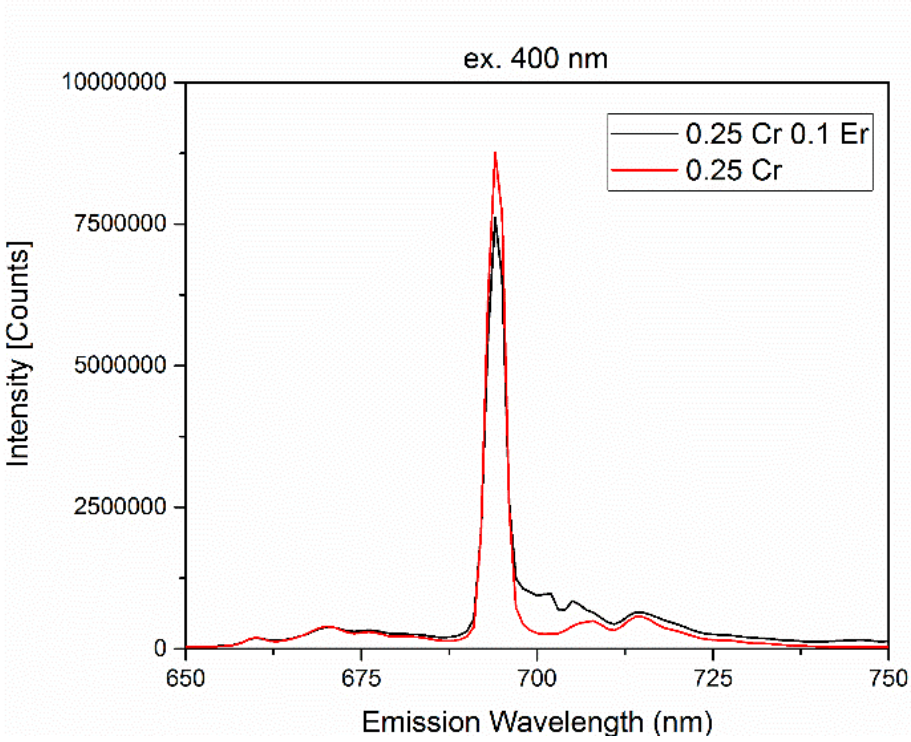

Figure 4.8. PL Emission spectrum of 0.25 at. % Cr^{3+}:Al_2O_3 with 400 nm excitation. This is overlaid on top of the emission spectrum of 0.25 at. % Cr^{3+}: 0.1 at. % Er:Al_2O_3.

From the data in Figure 4.8, energy transfer from Cr^{3+} to Er^{3+} is thus seen. This evidence comes from the decrease in Cr^{3+} emission intensity of Cr^{3+}:Al_2O_3 with addition of Er^{3+}.

Just like in Chapter 3, we show time dependent fluorescence of the $^4I_{13/2}$ to the $^4I_{15/2}$ transition and the $^4T_{2g} \rightarrow {}^4I_{13/2} \rightarrow {}^4I_{15/2}$ transition. Figure 4.9 shows the decay curves plotted on a logarithmic scale. After a prolonged rising time, there is a linear dependence shown on a log scale which suggests that the lifetimes are exponential and consistent with our previous work on low Er concentrations. The measured lifetime was 5.9 ms for the $^4T_{2g} \rightarrow {}^4I_{13/2} \rightarrow {}^4I_{15/2}$ transition and 6.01 ms for the $^4I_{13/2} \rightarrow {}^4I_{15/2}$ transition.

Given the very broad nature of the emission shown in Figure. 4.6, we again check to see if the lifetime varies across the emission wavelength range. Figure 4.10 shows decay curves taken using the same excitation wavelength, λ_{ex} = 532 nm, while monitoring emission across the emission bandwidth (λ_{em} = 1490 nm to 1570 nm). Just as with the singly doped Er^{3+}:Al_2O_3, the intensity of emission varies significantly with the monitored wavelength, consistent with the static emission measurements. The lifetimes again show little variation across the very broad emission. This is shown in Figure 4.10 b, showing the normalized intensity plotted on a logarithmic scale. The data overlap confirming the same lifetime thus strongly indicating a similar nature of emission across the broad bandwidth.

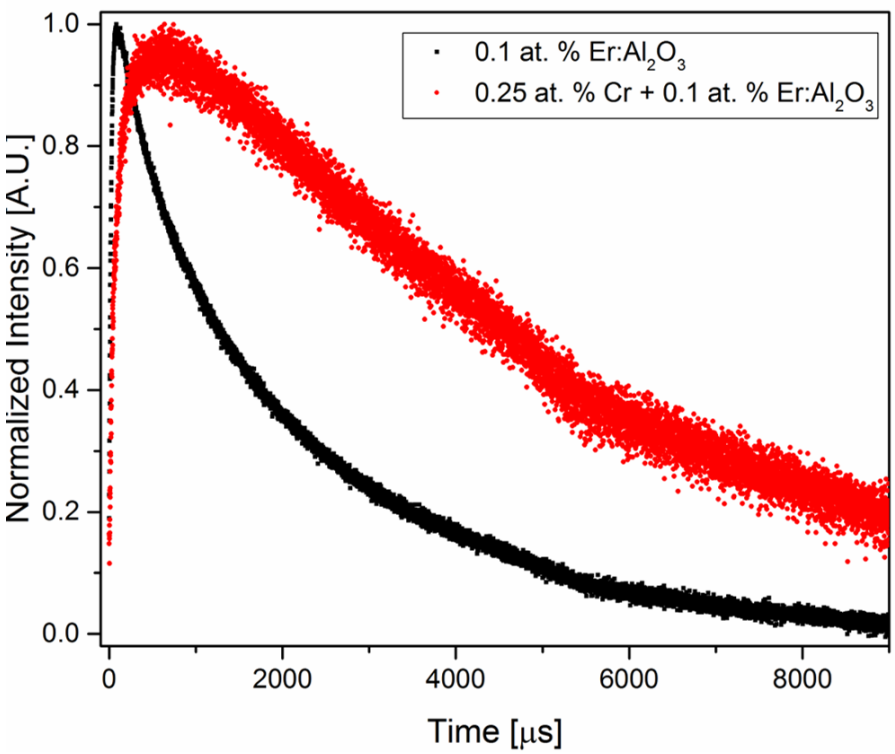

Figure 4.9. Analysis of the time dependent fluorescence of the bulk ceramic at the $^4T_{2g} \rightarrow {}^4I_{15/2}$ transition for the 0.25 at. % Cr + 0.1 at. % Er :Al2O3. The measured lifetime was 5.9 ms. Also plotted for comparison, the 0.1 at. % Er singly doped bulk ceramic.

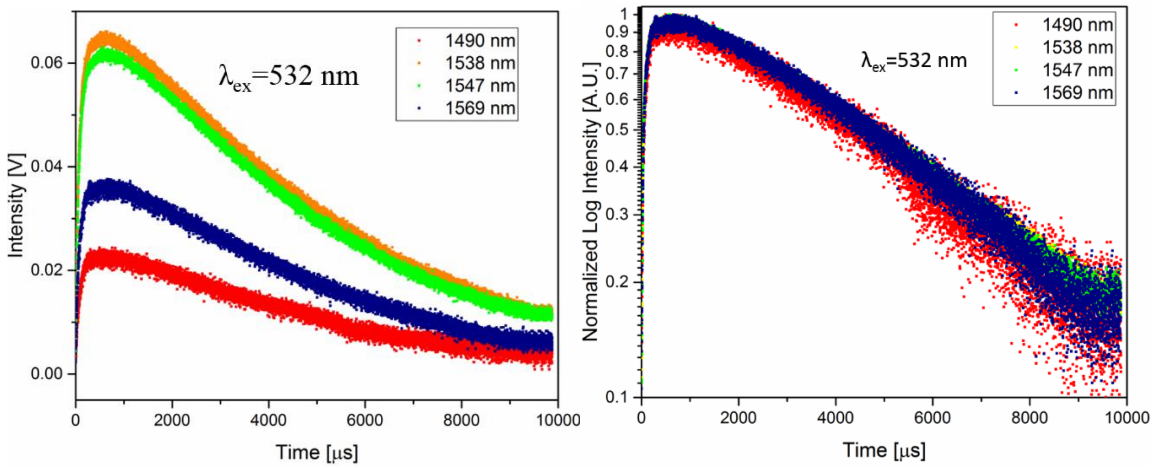

Figure 4.10. Decay curves taken using the same excitation wavelength, λ_{ex} = 532 nm, while monitoring emission across the emission bandwidth (λ_{em} = 1490 nm to 1610 nm). This is easily shown with normalized intensity plotted on a logarithmic scale. The data overlap confirming the same lifetime thus strongly indicating a similar nature of emission across the broad bandwidth.

However, as stated briefly, there is an observable rise time prior to the decay curves. It can be seen that the curves of Er:Cr:Al_2O_3 ceramics show a rise at the early times because the Er^{3+} ions can accept energy from Cr^{3+} ions through the direct energy transfer process from $^4T_{2g}$ level of Cr^{3+} to $^4I_{11/2}$ level of Er^{3+}. Along with the addition of Cr, more and more Cr^{3+} ions can act as donors to provide energy for Er^{3+} ions, so the rise processes will continue for longer time accordingly.

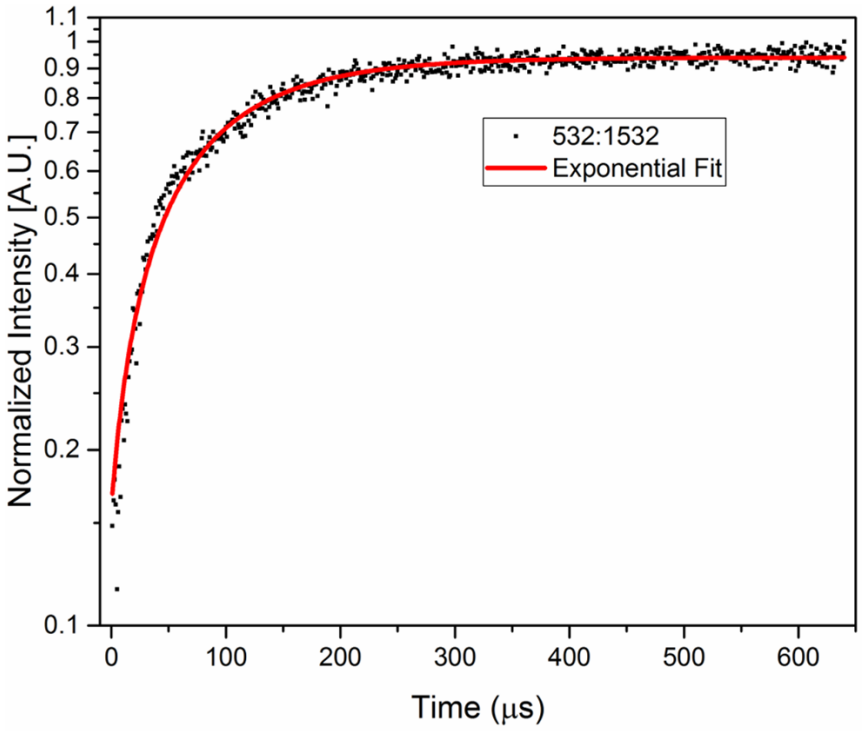

Figure 4.11. Analysis of the time dependent build up fluorescence at the $^4T_{2g} \rightarrow {}^4I_{15/2}$ transition for the 0.25 at. % Cr + 0.1 at. % Er :Al_2O_3.

We examined the 1532 nm build up and determined that a single-rate build up model provided a good fit to the data. Figure 4.11 shows the observed fluorescence build up signal and a model based on an exponential buildup. Since the 532 nm excitation source pumps the $^4T_{2g}$ level, one would expect that, in the absence of any pair interactions between Er^{3+} ions, excitation transfer, or excited-state absorption of

the pump the $^4I_{13/2}$ state could be excited in only two ways. One is directly from the $^4H_{11/2}$ level, and the other is from the $^4I_{11/2}$ level after that level is excited by an $^4T_{2g} \rightarrow {}^4I_{15/2}$ transition. Build up indicates that the $^4T_{2g} \rightarrow {}^4I_{15/2}$ transition occurs in less than a microsecond, and thus excitation of the $^4I_{13/2}$ level directly from the $^4H_{11/2}$ level must be negligible. Since we measured a lifetime for the $^4I_{13/2} \rightarrow {}^4I_{15/2}$ transition of approximately 2.02 ms, we could expect the same buildup time for 1532 nm fluorescence. The shorter observed buildup time shown in Figure 4.11 indicates that the excitation process for 1532 nm emission is more complex than simple decay of levels in an isolated Er^{3+} ion.

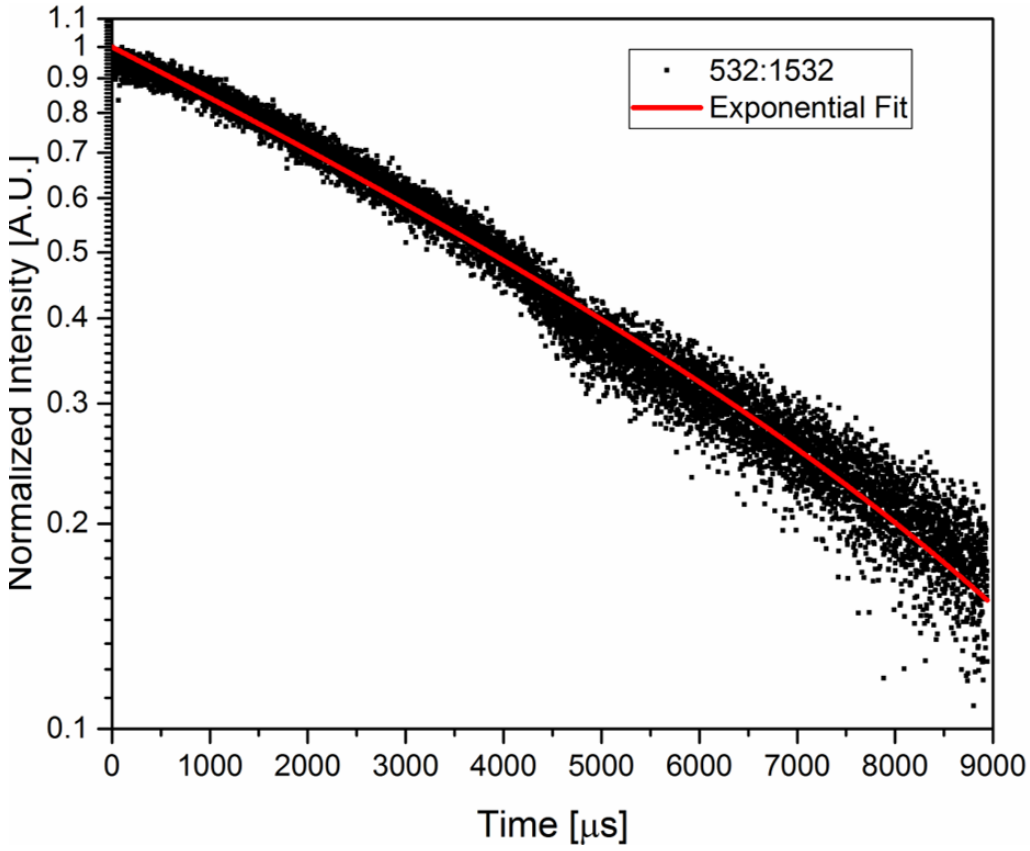

Figure 4.12. Analysis of the time dependent decay after build-up fluorescence at the $^4T_{2g} \rightarrow {}^4I_{15/2}$ transition for the 0.25 at. % Cr + 0.1 at. % Er :Al_2O_3.

Figure 4.12 shows the decay curves of the 0.25 at % Cr: 0.1 at. % Er:Al_2O_3 co-doped ceramics. For these measurements, the pumping wavelength was 532 nm and monitored at 1532 nm. The comparison of lifetimes between the two ceramics reveal that there is a longer decay of the co-doped ceramic in both concentrations. This is caused by energy transfer from Cr^{3+} to the Er^{3+} as shown schematically in Figure 4.2.

Just like in Chapter 3, the fluorescence lifetimes of Er^{3+}:$^4I_{13/2}$ manifold were fitted using Eq. 4.2 by monitoring 1.5 μm emission. For the $^4T_{2g} \rightarrow {}^4I_{15/2}$ transition, there was a rising stage and before it turned to fall in a multi exponential decay curves of $^4T_{2g} \rightarrow {}^4I_{15/2}$ transition as shown in Figure 4.9, which mainly resulted from the transition of $^4T_{2g} \rightarrow {}^4I_{15/2}$ with 532 nm pumping. Therefore, these decay curves were fitted by (Eq.4.2) with the influence of Cr^{3+}:Er^{3+}: $^4T_{2g} \rightarrow {}^4I_{15/2}$ transition taken into consideration:

$$Y = y_0 + A_1 e^{\left(-\frac{x-x_0}{t_1}\right)} + A_2 e^{\left(-\frac{x-x_0}{t_2}\right)} \qquad \text{(Eq. 4.2)}$$

where y_0, A_1, A_2, t_1 *and* t_2 are constants, the terms $e^{\left(-\frac{x-x_0}{t_1}\right)}$ and $e^{\left(-\frac{x-x_0}{t_2}\right)}$ both corresponded to the influence of Er^{3+}: $^4I_{11/2} \rightarrow {}^4I_{13/2}$ process and to fit the lifetime value t_{avg}, we used Eq. 4.3:

$$t_{avg} = \frac{(A_1 * t_1) + (A_2 * t_2)}{A_1 + A_2} \qquad \text{(Eq. 4.3)}$$

The listed values for all the fitted lifetimes for the Cr^{3+}:Er^{3+}: $^4T_{2g} \rightarrow {}^4I_{15/2}$ transition, for both single and double exponential fits are listed in Table 5. All the fitted data across the emission spectrum from 1490 – 1570 nm were analyzed.

Table 2.1. Single and Double Exponential Fits of time constants for the $^4I_{13/2} \rightarrow {}^4I_{15/2}$ transition in 0.25 at. % Cr + 0.1 at. % Er.

Excitation wavelength, λ_{ex}: 532 nm	Single Exponential Fit	Double Exponential Fit		
0.25 at.% Cr + 0.1 at. % Er	τ	t_1	t_2	t_{avg}
1490 nm	1.46	7.808	7.81	7.809
1538 nm	1.57	7.478	7.479	7.479
1547 nm	1.38	7.169	7.168	7.168
1569 nm	1.38	7.999	8.001	8.000

In general, non-radiative energy transfer processes occur via two major mechanisms, the Forster resonance mechanism and the Dexter exchange mechanism. The Forster resonance mechanism involves an electrostatic interaction between the sensitizer and acceptor. Such an interaction can occur over a long range, that is it does not require a very short contact between the donor and the acceptor. Energy transfer via the resonance mechanism may proceed over donor–acceptor distances as long as 50 – 100 Å.

In order for energy transfer to be efficient via the resonance mechanism, the energies of the donor and acceptor transitions must be nearly identical [34]. Nevertheless, the presence of phonons may provide assistance for energy transfer when small differences exist between the donor and the acceptor excited states. Such processes are called phonon-assisted energy transfer processes [34]. The energies of the phonons should be high enough to surmount the difference between the donor and acceptor excited states. However, too high phonon energies increase the likelihood of non-radiative de-excitation, which would take place before energy transfer can take place [34].

The Dexter exchange mechanism involves a direct contact between the donor and the acceptor ions. The exchange interaction between the donor and the acceptor

ions involves a transition state with a distance that is close to the sum of the gas-kinetic collision radii of donor and acceptor ions, respectively [reference35]. Therefore, information about the energy transfer mechanism can be gained by structural studies of the system under consideration. If the critical distance is short (normally < 5 Å) then the exchange mechanism is the more likely, but if the critical distance is long (> 5 Å) then the re resonance mechanism would be more likely.

The critical distance R_c for energy transfer from the Cr^{3+} to Er^{3+} ions were calculated using the concentration quenching method. The critical distance R_c between Cr^{3+} and Er^{3+} can be estimated by the following formula suggested by Blasse [31, 32]:

$$R_c \approx 2\left[\frac{3V}{4\pi x_c N}\right]^{\frac{1}{3}} \qquad \text{(Eq 4.2)}$$

where N is the number of molecules in the unit cell, V is the unit cell volume and x_c is the critical concentration. For Al_2O_3 host, N = 12, V = 254.092 $Å^3$ and the critical concentration is about 0.001 and 0.0025 from the total concentration of Cr^{3+}. According to (Eq. 4.2), the critical distance of energy transfer for the critical concentration of 0.001 and 0.0025 is estimated to be about 34.33 Å and 25.294 Å, respectively.

This is much larger than 5 Å which is typical of Dexter's exchange interaction [35]. Thus, it is possible that energy transfer mechanism in this system is governed by the electric multipolar interaction. However, this method of energy transfer is under the assumption that the location at which the donor and acceptor ions sit on the lattice sites and not mixed in the grain boundary. As is shown here, there is no

clear indication that fully incorporated dopants in the lattice, which would mean that all the energy transfer cannot be determined through this method.

We obtained approximate absorption cross section spectra by using the total Cr^{3+} concentration in the usual expression, $\sigma_{abs} = \alpha/N$, where σ_{abs} is the absorption cross section, α is the absorption coefficient, and N is the concentration of Cr^{3+} ions contributing to the spectrum. This analysis was performed and plotted for both the $^4T_{1g}$ and $^4T_{2g}$ manifold, shown in Figure 4.13. The value of the absorption cross section, $\sigma_{abs} \sim 10^{-19} cm^2$. This value is relatively high in comparison to other erbium doped oxides with similar concentrations.

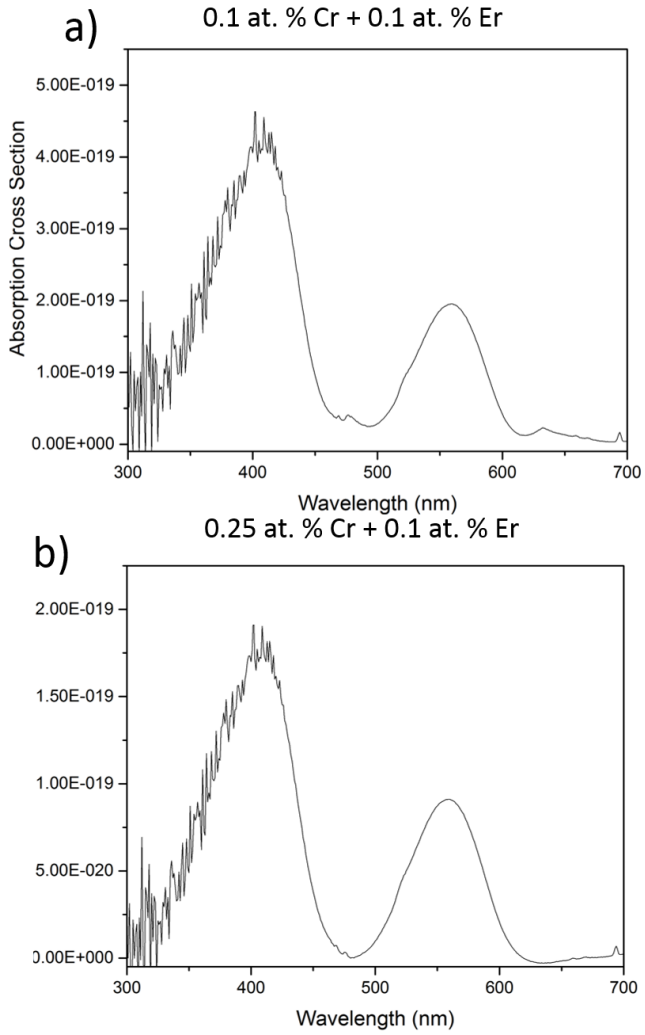

Figure 4.13. Absorption cross of the a) 0.1 at. % Cr + 0.1 at. % Er:Al_2O_3 and b) 0.25 at. % Cr + 0.1 at. % Er:Al_2O_3 bulk ceramic. The absorption cross sections were calculated from measured absorption spectrum.

As in Chapter 3, the emission cross sections in the are determined using the Fuchtbauer – Ladenburg method (F-L Method) [36]. Based on the success and accuracy of our previous results, we estimated the emission cross section σ_{em} from the measured room temperature fluorescence spectrum and the measured lifetime, using the (F-L Method) [36]:

$$\sigma_{em}(\lambda) = \frac{\lambda^5}{8\pi n^2 c \tau_{rad}} * \frac{I(\lambda)}{\int \lambda I(\lambda) d\lambda} \qquad \text{(Eq. 4.3)}$$

where λ is the fluorescence wavelength, *I* is the fluorescence intensity, τ_{rad} is the radiative lifetime, *n* and *c* are the refractive index and the light velocity, respectively. Based on an assumption that in our samples, they exhibit a purely radiative lifetime decay, a nonradiative quenching process leads us estimate the quantum efficiency, η, of this transition to be close to 1. It is important to note that we have confirmed that the lifetimes are same over this range (Figure 4.10), justifying the use Eq. 4.3 integrating from 1400 to 1700 nm.

The emission cross section is shown in Fig 4.14. The data show that the maximum cross section is our 0.25 at. % Cr:0.1at % Er ceramic has an emission cross section value of, 7.58×10^{-21} cm^2. This value compares favorably with other Er doped media.

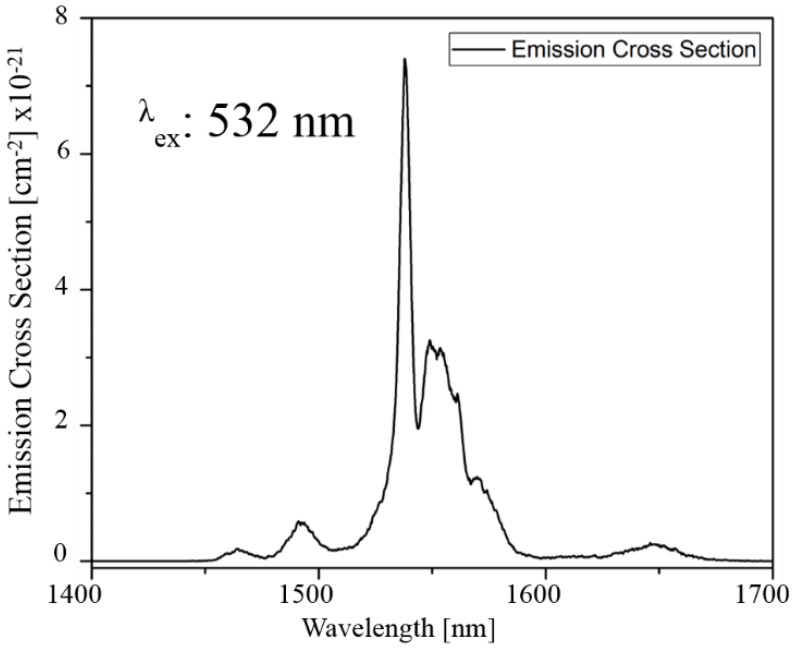

Figure 4.14. Stimulated emission cross section spectra of the $^4T_{2g} \rightarrow {}^4I_{15/2}$ transition, The stimulated emission cross section was calculated using the Fuchtbauer – Ladenburg Relation.

4.4. Summary

In summary, through the powder processing with ball milling and consolidation with CAPAD, a transparent co-doped Cr^{3+}:Er^{3+}:Al_2O_3 ceramic was fabricated. With chromium acting as our sensitizer, broad band excitation in the visible region and emission around 1.5 μm make these laser gain media are attractive for applications such as green pumped tunable NIR lasers. Using Cr Er energy transfer, it is possible to design Al_2O_3 based NIR emitting laser gain media. The technology for other Al_2O_3 based lasers technology is already established. The results presented here indicate the possibility of extending this technology to optoelectronic in the NIR region around 1.5 μm. Some quantitative details of the energy transfers are summarized below. Luminescence in transparent Cr:Er:Al_2O_3 has been reported for the first time. Critical distances for 0.1 at. % and 0.25 at. % Cr/Cr is estimated to be 34.33 Å and 25.294 Å, respectively. Efficiency of energy transfer is estimated to be 15% for Cr/Er. Mechanisms for Cr/Er energy transfer are suggested. The values for the absorption and emission cross section, suggests that this material has the potential to be an efficient green pumped gain media.

4.5. Acknowledgments

Funding for this work form the DE-JTO and the office ONR is gratefully acknowledged. Chapter 4, in part is currently being prepared for submission for publication of the material. Chapter 4 is coauthored with Elias Penilla, Matthew Wingert, Yasuhiro Kodera, and Javier Garay. The dissertation author was the primary investigator and author of this material.

4.6. References

[1] J. Duarte and D. R. Foster, in *Encyclopedia of Applied Physics* (G. L. Trigg, Ed.), Vol. 8, pp. 331-352, VCH, New York (1994).

[2] V. S. Letokhov, in *Dye Lasers: 25 Years* (M. Stuke, Ed.), pp. 153-168, Springer-Verlag, Berlin (1992).

[3] J. E Roch, G. Roger, P. Grangier, J. M. Courty, and S. *Reynaud, Appl. Phys. B* 55, 291 (1992).

[4] M.T. Asaki, C.Huang, D. Garvey, J. Zhou, H.C. Kapteyn, and M.M. Murnane, "Generation of 11-fs pulses from a self-mode-locked Ti:Sapphire Laser," OPTICS LETTERS, Vol. 18, No. 12. June 1993.

[5] P. F. Moulton, "Spectroscopic and laser characteristics of Ti:Al_2O_3," J. Opt. Soc. Am. B 3, 125-133 (1986).

[6] A. Sanchez, R. E. Fahey, A. J. Strauss, and R. L. Aggarwal, "Room-temperature continuous-wave operation of a Ti:Al_2O_3 laser," Opt. Lett. 11, 363-364 (1986).

[7] Ikesue, A., Aung, Y. Ceramic laser materials. *Nature Photon* **2,** 721–727 (2008).

[8] K. Kincade, Laser Focus World, 73, August (1996).

[9] G. Rani, P.D. Sahare, Structural and photoluminescent properties of Al_2O_3: Cr^{3+} nanoparticles via solution combustion synthesis method, Adv. Powder Technol. 25 (2014) 767 - 772.

[10] J.A. Aramburu, P. Garcia- Fernandez, J.M. Garcia Lastra, M.T. Barriuso, M. Moreno, "Colour due to Cr^{3+} ions in oxides: a study of the model system MgO:Cr^{3+}", J. Phys. Condens. Matter 25 (2013) 175501.

[11] A. Högele G. Hörbe, H. Lubatschowski, H. Welling, W. Ertmer " CrEr:YSGG laser with high output energy and FTIR-Q-switch," Opt. Commun. 125(1–3), 90–94 (1996).

[12] M. Tempus ; W. Luthy ; H.P. Weber ; V.G. Ostroumov ; I.A. Shcherbakov., "2.79 μm YSGG:Cr:Er laser pumped at 790 nm," IEEE J. Quantum Electron. 30(11), 2608–

2611 (1994).

[13] Z. Fang, D. Sun, J. Luo, H. Zhang, X. Zhao, C. Quan, M. Cheng, Q. Zhang, and S. Yina “Influence of Cr3+ concentration on the spectroscopy and laser performance of Cr,Er:YSGG crystal” Optical Engineering 56(10), 107111 (October 2017)

[14] P. Albers V G Ostroumov, A. F. Umyskov, S. Shnell and I. A. Shcherbakov, “Low threshold YSGG:Cr:Er laser for the 3 μm range with a high pulse repetition frequency,” Sov. J. Quantum Electron. 18(5), 558–559 (1988).

[15] M. Pollnau, J. D. B. Bradley, “ Optically pumped rare-earth-doped Al2O3 distributed-feedback lasers on silicon,” Vol. 26, No. 18. Sep 2018. OPTICS EXPRESS 24165.

[16] Jean-Claude G. Bunzli, Steve Comby, Anne-Sophie Chauvin, D. Caroline, B. Vandevyver, New opportunities for lanthanide luminescence, J. Rare Earths 25 (2007) 257-274.

[17] M.B. de la Mora, O. Amelines-Sarria, B.M. Monroy, C.D. Hernandez-Perez, J.E. Lugo, Materials for downconversion in solar cells: perspectives and challenges, Sol. Energy Mater. Solar Cells 165 (2017) 59-71.

[18] Y. Min, J. Li, F. Liu, P. Padmanabhan, K. Edwin, L. Yeow, B. Xing, “Recent advance of biological molecular imaging based on lanthanide-doped upconversion-luminescent nanomaterials”, Nanomaterial 4 (2014) 129-154.

[19] J. Zhu, Z. Xia, Q. Liu, ”Synthesis and energy transfer studies of $LaMgAl_{11}O_{19}:Cr^{3+}$, Nd^{3+} phosphors”, Mater. Res. Bull. 74 (2016) 9-14.

[20] P.K. Tawalare, V.B. Bhatkar, S.K. Omanwar, S.V. Moharil, “Cr^{3+} sensitized near infrared emission in Al_2O_3:Cr,Nd/Yb phosphors” Journal of Alloys and Compounds 790 (2019) 1192-1200

[21] M. Tuomisto Z. Giedraityte M. Karppinen M. Lastusaari, “Photon up-converting $(Yb,Er)_2O_3$ thin films by atomic layer deposition” Rapid Research Letter Volume 11, Issue 6 June 2017.

[22] Q. Song, C-R. Li, J-Y. Li, W-Y. Ding, S-F. Li, J. Xu, X-L. Deng, C-L. Song,

“Photoluminescence properties of the Yb:Er co-doped Al2O3 thin film fabricated by microwave ECR plasma source enhanced RF magnetron sputtering” Optical Materials 28 (2006) 1344–1349.

[23] T. Sanamyan, R. Pavlacka, G. Gilde, M. Dubinskii. Spectroscopic properties of Er^{3+}-doped α-Al_2O_3. Optical Materials 35 (2013) 821–826

[24] K. Drdlíková, R. Klement, D. Drdlík, T. Spusta, D. Galusek and K. Maca. “Luminescent Er^{3+}doped transparent alumina ceramics”. Journal of the European Ceramic Society 37 (2017) 2695–2703

[25] B. Wang, C. Li, B. Dong, L. Zhang, W. Xu "Application to temperature sensor based on near-infrared emissions of Nd3+:Er3+:Yb3+ codoped Al2O3," Optical Engineering 48(10), 104401. October 2009

[26] E. H. Penilla, Y. Kodera, J.E. Garay, Blue-green emission in terbium-doped alumina (Tb:Al_2O_3) transparent ceramics, Adv. Funct. Mater. 23 (48) (2013) 6036–6043

[27] E.H. Penilla, L.F.Devia-Cruz, M.A. Duarte, C.L Hardin, Y. Kodera, J.E. Garay, “Gain in Polycrystalline Nd-doped Alumina: Leveraging Length Scales to Create a New Class of High-Energy, Short Pulse, Tunable Laser Materials” Light Science Applications, April 2018.

[28] J. E. Garay, Annu. Rev. Mater. Res., 2010, 40:445-68

[29] E. H. Penilla, C. L. Hardin, Y. Kodera, S. A. Basun, D. R. Evans, and J. E. Garay, “The role of scattering and absorption on the optical properties of birefringent polycrystalline ceramics: Modeling and experiments on ruby (Cr:Al_2O_3).” Journal of Applied Physics 119, 023106 (2016).

[30] A. A. Kaplyanski, , A. B. Kulinkin, A. B. Kutsenko, S. P. Feofilov, R. I. Zakharchenya, and T. N. Vasilevskaya, Optical spectra of triply-charged rare-earth ions in polycrystalline corundum, Physics of the Solid State Volume 40, Number 8 Aug (1998).

[31] G. Blasse and A. Bril, Energy transfer from trivalent rare earth ions to Cr3, *Phys. Lett. A* 25(1), 29 (1967).

[32] A. Die, A. J.Faber, G. Blasse, W.F.Van Der We, “Energy transfer in Cr^{3+}, Nd^{3+}-codoped borate glass,” Journal of Physics and Chemistry of Solids Volume 47, Issue 11, 1986, Pages 1081-1084.

[33] P.I. Paulose, G. Jose, V. Thomas, N.V. Unnikrishnan, M.K.R. Warrier, Sensitized fluorescence of Ce3+/Mn2+ system in phosphate glass, J. Phys. Chem. Solids 64 (2003) 841-846.

[34] M.A. Omary, H.H. Patterson, “Luminescence, Theory,” University of Maine, Orono. Elsevier 2017.

[35] Dexter D 1953 J. Chem. Phys. 21 836

[36] Aull, Brian F.; Jenssen, Hans P. Vibronic Interactions in Nd:YAG Resulting in Nonreciprocity of Absorption and Stimulated Emission Cross Sections. *IEEE J. Quantum Electron.* QE-18(5), 925–929 (1982).

Chapter 5. Summary and Conclusion

By applying the ideas of non-equilibrium synthesis and processing techniques including high energy planetary ball milling and CAPAD processing, along with careful rare earth dopant source selection, significant progress has been made in the development of Al_2O_3 as a high thermal conductivity laser gain material. Non-equilibrium doping was made possible with our well-studied synthesis and processing routes. We have demonstrated above equilibrium concentrations of Er, Er and Cr dopant in transparent polycrystalline bulk alumina for the first time. The Er:Al_2O_3 ceramics show a broad emission spectrum centered around 1530 nm. With a relatively high gain cross section the Er doped alumina ceramic has potential to be an efficient laser gain media. When introducing the chromium as a sensitizer, the broadband visible absorption, lead our alumina ceramic to have different electronic emission mechanics and the potential to be an efficient gain media.

5.1. Future directions

From this study, with a better understanding on optimal doping concentrations and processing, we can develop other combinations of RE systems to see efficient laser actions at different wavelengths.

With all the potential that both these material systems possess, to further realize their development, integration in a laser system is required. There have been recent efforts in our group as how to integrate our gain media. Building a basic Fabry-Perot Cavity, in order to prove that our material is efficient and capable of high powers. We have also been fabricating waveguides from our media, whether it be,

channel waveguide, ribbed waveguides or cladded, we have ideas to integrate our material to ensure laser action is realized.